



Title	LATTICE DEFECTS IN METALS AND ALLOYS IRRADIATED IN HIGH VOLTAGE ELECTRON MICROSCOPE
Author(s)	吉田, 直亮
Citation	大阪大学, 1973, 博士論文
Version Type	VoR
URL	<a href="https://hdl.handle.net/11094/332">https://hdl.handle.net/11094/332</a>
rights	
Note	

*The University of Osaka Institutional Knowledge Archive : OUKA*

<https://ir.library.osaka-u.ac.jp/>

The University of Osaka

LATTICE DEFECTS IN METALS AND ALLOYS  
IRRADIATED IN HIGH VOLTAGE  
ELECTRON MICROSCOPE

NAOAKI YOSHIDA

February 21, 1973

## Synopsis

Lattice defect formation in gold, iron, aluminum and aluminum-zinc alloys by the electron irradiation in the 3MV electron microscope has been studied. In gold, interstitial type dislocation loops and small vacancy type defects are formed successively at room temperature. Permanent sinks for interstitials, such as specimen surfaces and dislocations, prevent the formation of interstitial type defects and enhance the formation of vacancy clustered defects. A rapid formation of vacancy type defects and the simultaneous shrinkage of interstitial type loops take place after the cessation of the irradiation. Kinetics analysis of the point defect movement quantitatively explained all the observed phenomena as the competing processes between the vacancy and interstitial movement. The irradiation intensity dependence of the density of interstitial type defects shows that the di-interstitials are their stable nuclei. Observed variety of the growth rate of the loops is ascribed to the influence of the permanent sinks to the interstitial accumulation.

The defect formation in iron, aluminum and an aluminum alloy is also observed and explained in a similar way. In aluminum, preferential nucleation of loops takes place on quenched-in faulted dislocation loops. The irradiation produced defects in the Al-Zn alloy are much less than those in pure aluminum. The growth and shrinkage behaviour of the vacancy type dislocation loops and helical dislocations in aluminum and its alloy suggests the long range attractive interaction between the dislocation and interstitials and also the trapping of interstitials by solute atoms.

## Contents

### Chapter I. Introduction

I-1.	Lattice Defects in Metals	1
I-2.	Point Defect Formation by Radiation Damage with Fast Electrons	2
I-3.	Recovery Process of Electron Irradiated Gold	4
I-4.	Radiation Damage Experiment using HVEM	7
I-5.	Purpose of the Present Work	10

### Chapter II. Experimental Procedures

II-1.	Specimens	11
II-2.	Electron Irradiation and Observation	12

### Chapter III. Experimental Results and Discussions

III-1.	Gold	
III-1-1.	Experimental Results	13
III-1-1-1.	Nature of Dislocation Loops	13
III-1-1-2.	Formation of Dislocation Loops	14
III-1-1-3.	Formation of Black spot Defects	17
III-1-1-4.	Behaviour of Pre-existing Defects	20
III-1-2.	Discussions	
III-1-2-1.	Nature of Dislocation Loops	
	—Interstitial Type Dislocation Loops	21
III-1-2-2.	Model Analysis	
	—Formation of Dislocation Loops	22
III-1-2-2-1.	No clustering case	26
III-1-2-2-2.	Clustering case I (Di-interstitial)	29
III-1-2-2-3.	Clustering case II (Tri-interstitial)	36

III-1-2-2-4. Mobility of interstitials	38
III-1-2-3. Vacancy Clustered Defects	39
III-1-2-4. Condition for Formation of Vacancy	41
Clustered Defects During Irradiation	
III-2. Iron	
III-2-1. Experimental Results	42
III-2-2. Discussions	43
III-3. Aluminum	
III-3-1. Experimental Results	45
III-3-2. Discussions	46
III-4. Aluminum-Zinc Alloy	47
 Chapter IV. Summary	 50
 Acknowledgement	 53
 References	 55
 Figure Captions	 56

## Chapter I. Introduction

In this chapter of introduction, firstly a brief review of lattice defects will be given, a special interest being focused to the roles of the point defects in the change of properties of materials. Secondary, the method of the fast electron irradiation to produce point defects and a brief survey of the history of radiation effect study will be shortly described, followed by the discussions on the unsolved important problems concerning the point defects in gold. The main purpose of the paper will be summarized to the last in this chapter.

### I-1. Lattice Defects in Metals

Studies concerning the lattice imperfections have revealed that the real crystals are not perfect but contain various kinds of lattice defects, i.e., the grain boundaries, stacking faults, dislocations, interstitial atoms, lattice vacancies, etc., and they have important effects on the physical properties of crystals even if their amount is very small. The point defects in metals play an important role on their mechanical properties such as hardening, internal friction and other anelastic properties, since the interaction between the point defects and dislocations may cause the pinning of dislocations. Another important role of point defects is seen in the phenomena such as the ordering of alloys, recrystallization and sintering, which include the diffusion process. It is commonly accepted that an atom in pure metals moves only when it can move into a vacancy which has come to an adjoining site.

Upon recognition of the importance of the point defects, studies which aim the quantitative description and understanding

of their properties were desired, and numerous studies in this field have been performed in recent twenty years. Nevertheless, in spite of the extensive studies, some of the basic properties of lattice defects such as atomic configuration and dynamical properties of interstitials are not known enough at present.

There are several methods to introduce a high concentration of point defects in a specimen; they are for instance, radiation with energetic particles<sup>1)</sup>, quenching from high temperature<sup>2)</sup>, plastic deformation<sup>3)</sup>, vacuum deposition on a substrate at low temperature<sup>4,5,6)</sup>. The electron irradiation, which was employed in the present work, is believed to be most useful method for the production of interstitials and vacancies. The irradiation with high energy electrons is suitable for the study of the nature of point defects, because the configuration of the defects produced directly by the electrons is rather simple compared to that produced by fast neutrons or deuterons.

The study of the lattice defects produced by radiation damage is practically important since the defects may cause the serious problems in reactor materials.

## I-2. Point Defect Formation by Radiation Damage with Fast Electrons

The interaction between the incident particles and constituent atoms in solids leads to the recoiling of atoms from their lattice sites. If the recoil is sufficiently energetic, at least one interstitial-vacancy pair (Frenkel pair) may be formed. Ordinarily the collision can be treated as a two-body collision. In the case of energetic electron this problem must be treated as the scattering of electron by the

nuclear charge, and calculated by using the relativistic quantum theory.

As well known, the recoil energy of an atom,  $T$ , by Rutherford scattering is given by

$$T = 2E(E + 2m_0c^2) \sin^2(\theta/2) / Mc^2,$$

where  $E$  is the bombarding energy of an electron,  $m$  is the rest mass of the electron,  $M$  is the mass of the recoil atom,  $c$  is the light velocity and  $\theta$  is the scattering angle. Putting  $\theta = \pi$  in the equation the maximum possible recoil energy  $T_m$  is

$$T_m = 2E(E + 2m_0c^2) / Mc^2,$$

and the values for several elements are shown in Fig. 1. When  $T_m$  exceeds the displacement threshold energy,  $T_d$ , Frenkel pair can be produced. In table I the experimentally determined  $T_d$  and corresponding electron energy  $E_d$  are given for several metals. It is apparent that most of metals are damaged by electrons with energies less than 1.5 MeV. When  $T_m$  exceeds the displacement threshold energy the production rate  $P$  of displaced atoms can be calculated from the primary displacement cross section  $\sigma_p$  by

$$P = \sigma_p N \phi$$

where  $\phi$  is the electron flux per unit time (or irradiation intensity) and  $N$  is the total number of displaced atoms by one primary knock-on. Oen<sup>7)</sup> carried out the numerical calculation of  $\sigma_p$  and  $N$  by using the method of Mott<sup>8)</sup>. Figure 2 shows one of the examples of his calculation for various threshold energies. The solid and dotted lines express the primary displacement cross section  $\sigma_p$  and the total cross section  $\sigma_p N$  respectively. In the present work, his data of the displacement cross section were used for the estimation of the production rate of displaced atoms.

### I-3. Recovery Process of Electron Irradiated Gold

When a metallic specimen is irradiated with fast electrons at very low temperature such as 4.2 K, most of the produced point defects are accumulated in the lattice. Upon warming the point defects become mobile by thermal agitation, and will annihilate by recombining with the opposite type defects, will form their clusters or will be trapped by impurity atoms and other kinds of imperfections in the course of migration. In the isochronal annealing these reactions give rise to so called annealing stages, which depend on the activation energy of migration of the point defects, the type of reaction, the initial distribution of mobile defects and sinks and their interaction potentials. Since Kauffman's first study<sup>9)</sup>, extensive works concerning the annealing process of radiation damaged gold have been reported and revealed the existence of recovery stages in isochronal annealing. The characters of each recovery stage of gold are contained in Table I with those of other fcc metals.

By now most workers agreed on the major outlines of annealing process of the low temperature part of stage I, which obeys first order annealing, and ascribed the substages of that part to the close Frenkel pair recombination. However, the assignment of the other recovery stages to the migration and annihilation of various point defects is still a matter of controversy.

Concerning the recovery process of irradiated fcc metals two confront models have been proposed:

(1) One interstitial model (or vacancy model)

This model was proposed by Koehler's school. The subpeak at or near the end of stage I which shows the second order

reaction is ascribed to the long range three dimensional migration of interstitials to vacancies, impurity atoms, interstitial clusters, surfaces, grain boundaries or dislocations. Though this stage has been clearly observed in the recovery process of aluminum and copper, no distinct stage corresponding to this has been found in that of gold. It is supposed that at stage II, interstitials which have been trapped by impurity atoms during irradiation or during the stage I annealing are released and annihilate at vacancies or sinks of other types. Stage III is ascribed to the migration and annihilation of vacancies. The evidence of this model for gold is mainly based on the fact that the activation energy observed in stage III annealing is the same as that in the annealing of a specimen quenched from certain high temperature like 700°C. The activation energy observed in the gold specimen with 99.9999% purity by Lee and Koehler<sup>10)</sup> for 3MeV electron irradiation at 100 K was

$$E_{III} = 0.85\text{eV} \pm 0.02\text{eV}$$

and for fast quenched specimens of the same purity

$$E_V^m = 0.86\text{eV} \pm 0.02\text{eV}$$

They also pointed out that the activation energy of stage III recovery process decreases with purity of the specimen. When the purity of the specimen is 99.999%,  $0.82 \pm 0.04\text{eV}$  was obtained for the activation energy of stage III<sup>11)</sup>

Shimomura<sup>12)</sup> observed with an electron microscope that interstitial type dislocation loops produced by the irradiation at 100K shrank at the stage III temperature range. The results strongly suggest that vacancies can migrate at stage III.

## (2) Conversion two interstitial model

Bauer, Seeger and Sosin<sup>13)</sup> proposed another model for explaining the recovery stages of irradiated fcc metals. In the model each stage is reasoned as follows:

(i) The substages at the end of stage I, i.e., stage  $I_D$  and  $I_E$  are ascribed to the one dimensional long range migration of metastable crowdion interstitials. Some of them would annihilate by combining with vacancies and the others would convert to interstitial with stable configuration by encountering with other interstitials or impurity atoms. However, some investigators claimed that in the case of gold no evidence existed for the long range migration of crowdions at the end of stage I.

(ii) Stage III is ascribed to the migration of the interstitials. Vacancies become mobile at higher temperature than those of stage III.

As above described, in spite of the extensive works, even the basic problem whether the interstitials become mobile below 40K or at about 300K is unsolved yet. One of the main reasons which lead to this confusion seems to arise from the method used for the detection of the recovery process. For example, the electrical resistivity measurement which have been used in the most experiments in this field, could reveal the existence of the recovery stages and could determine the activation energy and the order of reaction of each recovery stage, but the method is not suitable for the identification of the type of defects responsible for each stage. A similar situation arises in the measurements of the stored energy, density, length and lattice parameters. In order to settle

the above mentioned discussion the experiment using the method such as field ion microscopy and electron microscopy which can determine directly the type of the defects should be performed.

#### I-4. Radiation Damage Experiments Using High Voltage Electron Microscope

Electron microscopes with high acceleration voltage (HVEM) which have been developed in the last decade have many advantages as follows for the studies in various fields such as metallurgy, solid state physics biology and so on.

(1) Since electron penetration efficiency increases in accordance with the increase of acceleration voltage, thick specimens can be used for observation. For example, it is possible at the acceleration voltage of 2MV to obtain the transmission image of dislocations in an aluminium foil as thick as  $20\mu^{14}$ ). This thickness is 12 to 14 times of that observable with an 100kV electron microscope. (2) Because the wave length of electron decreases with acceleration voltage it becomes possible to obtain the higher resolution of images and (3) to determine the structure of microcrystals by using the selected area diffraction from a very small region. Though HVEM has these advantages, it involves an essential difficulty for some purposes. Namely, most of the crystals are inevitably damaged by the highly accelerated electrons, since they can give a sufficient energy to atoms to displace themselves from their lattice sites. In the cases of investigations of the properties sensitive to lattice defects such as mechanical properties and

diffusion controlled processes, radiation induced lattice defects may cause the additional effects. For making use of HVEM for such investigations effectively, it is urgently necessary to study the radiation damage in HVEM during observation.

There exist three aspects in the radiation damage in HVEM. One is concerned with the production of point defects, including the problem of threshold energy for atomic displacement and of the crystallographic orientation and acceleration voltage dependence of the displacement cross section. The second is the accumulation and clustering of these point defects in the specimen. This phenomenon strongly depends on the properties of the radiation induced point defects, production rate of the defects and thickness of foil for observation. The third is the influence of these defects on the physical properties.

For the study of electron radiation damage, HVEM have many advantages. They are, for instance, the in situ observation of defect structures during irradiation, the easy setting of the accurate crystallographic orientation of specimens, the easy control of the irradiation intensity including such a strong intensity as  $10^{20}$  electrons/cm<sup>2</sup>sec, the easy selection of desired energy of electrons with a high stability, and so on.

Several reports showed the complication of the formation of point defect clusters by the irradiation in HVEM at the temperature at which some kinds of point defects can move freely. Makin<sup>15)</sup> observed the formation of dislocation loops in copper at room temperature in an electron microscope with 600kV. The number of the loops reached its maximum at the early stage of irradiation and decreased gradually. The total area surrounded by the loops increased with the irradiation time. These loops

were identified to be the interstitial type by Ipohorski et al.<sup>16)</sup>. At a higher temperature such as 200°C, they also observed vacancy type stacking fault tetrahedra in a thin part of a foil in addition to the interstitial type dislocation loops<sup>17)</sup>. In aluminum, vacancy type dislocation loops were observed at 20°C by Shiraishi et al.<sup>18,19)</sup> with 1000kV electron microscope but not at 70°C. Urban<sup>20)</sup> showed in nickel the simultaneous formation of interstitial and vacancy type defect clusters in an intermediate temperature range above and below only the interstitial type defect clusters formed. Norris<sup>21,22)</sup> irradiated thin foils of nickel at 450°C in a HVEM and observed that interstitial type dislocation loops formed in the thin area grew in proportion with the irradiation time. He also observed the formation of voids in the specimen at 480°C which had been irradiated by argon before irradiation with electrons, and observed a constant increase of their number. The formation of the dislocation loops in cobalt irradiated with electrons in a HVEM was studied by Howe<sup>23)</sup>. The density of dislocation loops increased rapidly in the first few minutes and saturated. The size of loops increased with the square root of the irradiation time.

The above various observations clearly show that the formation of point defect clusters is essentially related to the irradiation temperatures, migration rates of each kind of point defects, the binding among themselves and so on.

Makin<sup>24)</sup> developed a simple theory of homogeneous nucleation of interstitial clusters which fitted the experimental data on copper<sup>15)</sup>. The theory was used to predict the time dependence of cluster growth, the width of the denuded zone close to interfaces, the apparent variation in the threshold energy for

cluster formation with the foil thickness and temperature, the interstitial and vacancy concentrations and their enhanced diffusion.

#### I-5. Purpose of the present Work

The main purpose of the present work is to obtain the knowledge of point defects in metals and alloys especially that of interstitial atoms. For this purpose, the accumulation of point defects directly produced by irradiation and the clustering process of these point defects should be examined experimentally, and overall process should be analyzed quantitatively. As the result of the analysis the problems such as the identification of the stage III recovery and the behaviours of interstitials including their mobility should be solved.

At the time when a great future possibility of the HVEM has been expected in wide fields of the natural science, one should realize that the damage of the structure of materials by electron irradiation is an unavoidable phenomenon. Though the damage itself would often prevent the straightforward progress of each field of the studies, the accumulation of the accurate knowledge of the nature of damage such as given in the paper would supply the ways to effective application of the HVEM in these studies.

## Chapter II. Experimental Procedures

### II-1 Specimens

Gold of nominal purity of 99.999% was cold rolled to the thickness of  $40\mu$  and was annealed in air for one hour at  $800^{\circ}\text{C}$ . The average grain size was about  $0.2\text{mm}$  and the density of dislocations inside the grains was less than  $1 \times 10^5/\text{cm}^2$ . Some of the rolled thin foils were heated to  $900^{\circ}\text{C}$  and subsequently quenched into water kept a little above the room temperature to introduce large stacking fault tetrahedra and dislocation loops of the Frank sessile type. Some others were plastically deformed 30% by cold rolling in order to introduce high density of dislocations. The average dislocation density in these deformed specimens was about  $10^{10}/\text{cm}^2$ . The specimens for irradiation and observation in HVEM were prepared by usual electropolishing in a cyanide bath.

Pure aluminum specimens with faulted vacancy type dislocation loops were prepared by quenching aluminum foils of 99.999% purity from  $550^{\circ}\text{C}$  into water at room temperature. The average size and density of the dislocation loops were  $1000\text{\AA}$  and  $10^{13}/\text{cm}^3$  respectively.

An aluminum alloy with 6.5 at% zinc with well developed helical dislocations were also prepared by quenching from  $550^{\circ}\text{C}$  into water at  $80^{\circ}\text{C}$ . The alloy specimens were electropolished in perchloric acid and ethanol solution.

Iron foils of 99.9% purity were annealed in vacuum of  $3 \times 10^{-5}\text{Torr}$  at  $700^{\circ}\text{C}$  for 2 hours, and then thinned by bath jet electropolishing and normal electropolishing methods.

## II-2. Electron Irradiation and Observation

A high voltage electron microscope HU-2000, which was installed in Osaka University in 1972 as shown in Fig. 3, was used for irradiation and simultaneous observation at several acceleration voltages between 1.5MV and 2.5MV. In some cases the acceleration voltage was lowered to 1.0MV or less to avoid the production of lattice defects by radiation damage. Some of the specimens were reobserved after irradiation with an electron microscope HU-11A with 100kV to see the annealing effects.

The irradiation was performed at room temperature. Though the temperature of the specimens were not measured in the present experiment, it was assured by other investigations the temperature rise during irradiation and observation was less than 10 degrees<sup>25)</sup>. The electron beam density of individual case was measured with a Faraday cage located at a position between the projection lens and the florescent screen. The maximum density of electrons was about  $3 \times 10^{19}$  electrons/cm<sup>2</sup>. The irradiation and recording on photographic films was made usually under the same illumination of electron beam to avoid the change of accumulation behaviour of the point defects by changing the irradiation intensity.

### Chapter III. Experimental Results and Discussions

The formation of visible defects by the room temperature electron irradiation in the HVEM varied widely from metal to metal and <sup>was</sup> modified by the conditions such as the specimen thickness, presence of pre-existing defects, irradiation rate and dose and so on. In this chapter the experimental results for gold, iron, aluminum and aluminum-zinc alloy will be described. The interpretation of the results and discussions also be accompanied.

#### III-1. Gold

##### III-1-1. Experimental Results

Thin foils of pure gold were irradiated by the electrons above 2.0 MeV in the HVEM. In general, dislocation loops appeared at a very early stage of irradiation and grew large by successive irradiation. When the irradiation intensity was high enough, another type of defect clusters which are called the black spot defects gradually appeared besides the dislocation loops. The formation of these defects were strongly affected by pre-existing defects.

##### III-1-1-1. Nature of Dislocation Loops

When the specimen was thicker than about  $500 \text{ \AA}$ , a large number of dislocation loops appeared and grew during electron irradiation. Figure 4 (a) and (b) shows one of the examples of these loops in a specimen irradiated for 110 and 240 seconds respectively with 2.5 MeV electrons of the intensity of  $6.4 \times 10^{18}$  electrons/cm<sup>2</sup>sec. The loops had the typical images of dislocation loops, and some of the loops showed well defined hexagonal shape as marked with H in the figures. The hexagonal loop

had fringe contrast rising from a stacking fault as in Fig. 5, when they were observed at an orientation far from exact Bragg condition of low indices. Therefore, the hexagonal shaped dislocation loops must be faulted type with the Burgers vector,  $\mathbf{b} = a[111]/3$ . The dislocation loops as A and B in Fig. 4 became irregular in shape and did not show any contrast of stacking fault after they had grown up extensively by the prolonged irradiation with high intensity of electrons. This means that the loops which once nucleated as the faulted loops were converted to the perfect type loops with  $\mathbf{b} = a[110]/2$  during their growth. On the other hand, it is not certain whether there was any loop which originally nucleated as perfect type.

Two difficulties were encountered in the course of the determination of the sense of the Burgers vector of these loops from their image contrast. One arose from the fact that so many diffracted waves were simultaneously excited in the high voltage electron microscopy, and consequently the loop image became complicated. The second difficulty came from the growth and shrinkage behaviour of the loops as will be described in the following. Actually one case was found in which the change of the loop size was stabilized and stopped even when the irradiation was stopped. Nevertheless, the dislocation loops were determined to be of interstitial type, judging from various phenomena explained hereafter.

### III-1-1-2. Formation of Dislocation Loops

Each series of micrographs in Fig. 6 shows the growth behaviours of the dislocation loops for two different irradiation intensities and Fig. 7 shows the variation of the areal density

of dislocation loops with the irradiation time counted in an area of about  $2000 \text{ \AA}$  in thickness. Though each loop became larger and larger, their density saturated within a very early stage of irradiation, less than 1 second, and decreased in a later stage by slipping out to the specimen surfaces or their mutual coalescence.

In an experiment for the determination of the irradiation intensity dependence of the formation of the dislocation loops, all the conditions other than the intensity should be kept unchanged. This could be satisfied when the comparison was performed within a narrow vicinity of the flat tapered edge of polished specimen with the same thickness gradient and same foil orientation. Actually, these conditions were fulfilled for the pictures in Fig. 6. Fig. 8 shows a comparison of the loop numbers for three different irradiation intensities made at the same total electron dose. The number of dislocation loops was plotted against the distance from the edge of a smoothly tapered specimen. The corresponding thickness in the figure was estimated from the width of slip traces appeared in a vicinity of the irradiated areas. It was found that no loop appeared in a thin area under a certain limit of thickness. The number of the loops increases gradually above this critical thickness and in the area where thickness is large enough it increased linearly with thickness. These observed distribution of loops indicates that the dislocation loops were formed uniformly in the foil except in the surface denuded layers of dislocation loops. The thickness of the denuded layer may be defined as the half of the limiting thickness which is obtained by extrapolating the linear part to zero as shown by the dotted

lines in Fig. 8. It is apparent from the figure that the thickness of the layer decreased with the irradiation intensity. These layers were subtracted from the actual thickness in the estimation of the loop densities shown in Fig. 9. The figure shows that the saturated density of the loops increased with the square root of the irradiation intensity.

Large angle grain boundaries and dislocations play similar roles as specimen surfaces for the formation of dislocation loops. Grain boundaries were observed to be accompanied with denuded area of the loops of about  $1500 \text{ \AA}$  in width as in Fig. 10. When an area with a high density of dislocations was irradiated even with an intensity and integrated dose strong enough to introduce dislocation loops of high density in the dislocation free area, only a few dislocation loops were observed as in Fig. 11. Especially, no loops were formed in the region where dislocations highly tangled. These facts suggest clearly that not only the specimen surfaces but also the large angle grain boundaries and dislocations act as the effective sinks for the point defects forming the dislocation loops and consequently suppress their cluster formation.

The growth rate of dislocation loops formed by irradiation was fast in the early stage of their formation, and it slowed down later. The diameter of the majority of the loops observed in fairly thick area of a foil increased with the cube root of the irradiation time as A and B in Fig. 12. A few loops were found to increase their size linearly with irradiation time at the beginning and slowed down to grow in the later stage as C and D in Fig. 12. The growth manner of the dislocation loops appeared in a thin foil area irradiated strongly was a

little more complicated and was informative about the behaviour of the radiation induced point defects. Fig. 13 shows an example of the specimen having the tapered edge. Four sets of the composite photographs in the lower part of the figure are the enlarged photographs of individual areas marked as A, B, C and D. The times indicated in the figures are the irradiation times. In contrast with the simple growth of the loop A in a thick area, the loops B and C formed in thinner areas stopped their growth and began to shrink in the later stage of the irradiation. The loops formed in the thinner area went into the stage of shrinkage earlier. Accompanied by the shrinkage of loops, another type of defects of higher density appeared gradually as clearly seen in D.

### III-1-1-3. Formation of Black Spot Defects

As described briefly in the last paragraph, after a few minutes irradiation with very high intensity as  $10^{19}$  electrons/cm<sup>2</sup>sec the black spot defects became visible preferentially at the thin area of a foil and increased their size and number during continuous irradiation. Further irradiation lead to the appearance of the defects in a thicker area. Typical example of the formation of the black spot defects are shown in Fig. 14 (a), (b) and (c). The area shown in this figure was irradiated by 2.0MeV electrons of  $0.55 \times 10^{19}$  electrons/cm<sup>2</sup>sec and its thickness estimated from the width of slip traces was about 500 Å. The black spot defects appeared at about 100 sec and its density reached as high as  $3.5 \times 10^{16}$  cm<sup>2</sup> at 300 sec. The variation of the density of black spot defects, their average diameter and that of dislocation loops in Fig. 14 are shown in Fig. 15 (b),

(c) and (a) respectively. It is apparent from the figure that the time of the cessation of the growth of dislocation loops had a good coincidence with that of the appearance of the black spot defects. The irradiation was stopped at 310 sec and then the damage area was observed again with a very short illumination of electrons to prevent the additional damage after some room temperature aging. The micrographs (d) and (e) in Fig. 14 and the picture in the middle of Fig. 15 show the behaviours of the both kinds of the defects during the aging. The behaviours of both defects after irradiation showed a clear interrelation, namely whereas the dislocation loops continued to shrink, the black spot defects which had appeared during irradiation grew further and its diameter reached twice of that immediately before stopping the irradiation. Additional defect clusters scarcely nucleated during the annealing. After aging for 300 sec the area was irradiated again. As shown in the micrograph (f) in Fig. 14 and right hand of Fig. 15, the size of dislocation loops increased again but that of black spot decreased.

The concentration of the point defects in the foil which will form the black spot defects was estimated from the amount of growth of the black spot defects during the aging. Assuming that all the defects are absorbed to the black spot defects until 300 sec, and the black spots are dislocation loops, the total concentration of the point defects in the foil immediately after stopping the irradiation was about  $1.7 \times 10^{-4}$ , and its one half annihilates within a minute as shown in Fig. 16.

It was revealed by the stereoscopic observation using 100kV electron microscope that the black spot defects exist uniformly through the foil. The stereo pair photographs are shown in

Fig. 17.

All the above observed results strongly suggest that the black spot defects are the clusters of radiation induced point defects and have a nature opposite to that of dislocation loops.

Formation of the black spot defects was affected by the dislocations. A foil containing a high density of tangled dislocations was irradiated with a very high intensity as  $3.2 \times 10^{19}$  electrons/cm<sup>2</sup>sec. Though all the area shown in Fig. 18 should have been covered with a large number of dislocation loops if there were no tangled dislocations, only a few loops were observed. However, by prolonged irradiation many black spot defects appeared preferentially in the area of higher dislocation density as in Fig. 18 (b) and (c). The variation of areal density of black spot defects in areas of low and high dislocation density are shown in Fig. 19. Though the nucleation of the black spot defects in the former area was delayed, the density of black spot defects saturated at the same level as that of the latter. It should be noticed that the roles of dislocations on formation of dislocation loops and of black spot defects was opposite; namely, formation of the former was suppressed and that of the latter was enhanced by them. As will be discussed in III-1-2-2, the phenomena can be understood by considering the role of dislocations in the accumulation of radiation induced lattice defects.

A prolonged irradiation with a high intensity caused the appearance of the black spot defects even in an area which had been originally free from any pre-existing defects such as large angle grain boundaries, specimen surfaces and dislocations. Fig. 20 shows the formation of black spot defects in a well

annealed specimen irradiated by 2.0 MeV electrons of  $3.2 \times 10^{19}$  electrons/cm<sup>2</sup>sec. The variation of the density of black spot defects are plotted against irradiation time in Fig. 21. It was clear from these figures that black spot defects appeared preferentially inside large dislocation loops, which had nucleated in the early stage of the irradiation, and they were larger in size and higher in number compared with those outside the loops. But at the later stage of irradiation, the density in the latter approached to that of the former. As will be discussed in the next section, the observed behaviour of the black spot defects suggests high accumulation of vacancies along the growth path of the dislocation loops.

#### III-1-1-4. Behaviour of Pre-existing Defects

Stacking fault tetrahedra formed in a quenched specimen were observed to be converted into faulted dislocation loops by electron irradiation. The conversion was rapid even for a comparatively low illumination intensity as in Fig. 22. The loops which had been converted from stacking fault tetrahedra shrank during the further irradiation, presumably absorbing interstitials and they became irregular in shape during the shrinkage as in Fig. 23. The average shrinkage rate was about  $1 \text{ \AA}/\text{sec}$  at about a few ten seconds.

As shown in Fig. 18 dislocations moved through the specimen and rearranged their configuration. It seemed that their movement was caused not only by the stress arising from the local thermal expansion and contamination by irradiation but also by the absorption of point defects. The development of the helical dislocation marked as H in the figure strongly suggests

that the dislocation can absorb the point defects.

### III-1-2. Discussions

The image contrast and three dimensional distribution of the clusters produced in the foil by the electron beam irradiation suggest that they were the result of the clustering of point defects primarily produced by the irradiation of electrons. A variety of the observed phenomena can be understood as the results of the competition process of interstitials and vacancies under various circumstances. In order to understand the phenomena, a kinetics analysis based on the chemical rate theory was performed, and it lead us to some conclusions on the basic properties of lattice defects and the formation of point defect clusters.

#### III-1-2-1. Nature of Dislocation Loops

##### - Interstitial Type Dislocation Loops

For the determination of the nature of the dislocation loops there is a direct method which utilizes their image contrast. There is an indirect method for the same purpose to use the behaviour of their clustering process. When one attempts to use the indirect method, it is necessary to know the mobility of interstitials at room temperature. In this respect Fig. 23 is quite suggestive. The vacancy type dislocation loops shrank with the rate of about  $1 \text{ \AA}/\text{sec}$  by absorbing interstitials produced by radiation damage. If the mobility of interstitials at room temperature is assumed to be less than 1 jump/sec as proposed in the conversion two interstitial model, the shrinkage of the loop will occur only when interstitials are

produced in the area very close to the dislocation loops. As the production rate of interstitials was about  $10^{-4}$ /sec, the expected shrinkage rate in this case will be two or three orders smaller than the observed rate. Therefore it is not appropriate to assume that the mobility of interstitial is as small as 1 jump/sec. On the other hand, the observed rate can be explained by assuming the appreciable mobility of interstitials as will be fully discussed in III-1-2-2-2. These strongly suggest that interstitials have high mobility at room temperature<sup>26)</sup> and the observed dislocation loops were their clusters. The validity of this interpretation will be discussed again in III-1-2-2-4.

### III-1-2-2. Model Analysis--Formation of Dislocation Loops

To know the accumulation of point defects and their clustering during irradiation, the kinetics analysis for the processes was performed. In general, the formation of the defect clusters depends on the concentration of point defects, their migration rate and binding energy between them. The mobility of vacancies at room temperature must be 0.1 jumps/sec judging from the quenching experiment<sup>2)</sup>, and standing on the above mentioned discussion it seems natural to assume that the mobility of interstitials is extremely large compared with that of vacancy. Therefore, even in the early stage of irradiation, during which the accumulation of vacancies and interstitials are not so high, interstitials must easily form their clusters and the formation of vacancy clusters will be reasonably neglected in the following analysis of the early stage of the irradiation. The later stage of irradiation in

which the effect of the motion of highly accumulated vacancies becomes appreciable will be treated in the latter half of the section.

The fraction of atomic sites at which the primary damage can take place is  $1-C_V$ , where  $C_V$  is the concentration of vacant lattice sites, and knocked-on atoms remain as interstitials only when they do not jump into spontaneous recombination sites around a vacancy. Then the interstitials will be produced with the rate of  $P(1-C_V)(1-Z_1C_V)$  in a crystal with vacancies, where  $P$  is the production rate in a perfect crystal and  $Z_1$  is the number of the spontaneous recombination sites around a vacancy. These interstitials annihilate by migrating to their sinks such as vacancies, specimen surfaces, dislocations, and other interstitials. In the present analysis, the efficiency of these sinks are assumed as follows.

i) Vacancies: An interstitial which reaches near a vacancy will be captured and annihilate with it. The rate of the decrease of the interstitial concentration  $C_I$  through this process is  $M_I Z_1 C_V C_I$ , where  $M_I$  denote the migration rate of an interstitial. If the oscillation frequency of the defect is  $\nu_0$ ,  $M_I$  would be expressed as:  $M_I = \nu_0 \exp(-E_m^I/kT)$ , where  $E_m^I$  is the activation energy for interstitial migration,  $k$  the Boltzmann constant and  $T$  the specimen temperature. The majority of interstitials and vacancies produced by radiation damage will annihilate by this mechanism, except during the very early stage of the irradiation, and except in the case in which the concentration of sinks is extremely high.

ii) Specimen surfaces and other permanent sinks: Specimen

surfaces, grain boundaries and dislocations may act as effective sinks for interstitials and they will greatly modify the accumulation of point defects and accordingly will result the variation in the formation of their clusters. For simplicity these sinks are assumed to be homogeneous in a foil, and then the efficiency of these sinks can be represented in the kinetics analysis as a constant sink concentration  $C_S$ . In the case of the surfaces being sinks, random walk theory suggests that  $C_S$  is about  $(a/h)^2$  at the center of a foil, where  $a$  and  $h$  are atomic distance and foil thickness respectively. For dislocations,  $C_S$  should be taken as a quantity proportional to the dislocation density, and so forth. The rate of the decrease of the interstitial concentration through this process is  $M_I C_S C_I$ .

iii) Interstitials and their clusters: An interstitial which reaches near another interstitial will combine and form a di-interstitial. The formation rate of di-interstitials will be

$$\frac{dC_{I2}}{dt} = Z_2 M_I C_I^2 \quad (1)$$

where  $Z_2$  and  $C_{I2}$  denote the number of the spontaneous combination site of this reaction and concentration of di-interstitials respectively. Because the configuration and size of the stable nucleus of interstitial cluster are not known at present, as a first trial, a di-interstitial is assumed to be the stable nucleus of an interstitial cluster. Then the above formation rate of di-interstitials is also the nucleation rate of the interstitial clusters. The case of a tri-interstitial as a stable nucleus of the interstitial cluster will be treated later, and, as will be clarified, only the di-interstitial case

will show a good agreement with experimentally observed interstitial cluster density and its irradiation intensity dependence. When the defects formed by the clustering of interstitials are dislocation loops as those observed in the present work, the concentration of the sinks of these loops for interstitials is approximated to be proportional to the total length of their dislocations. Using the integrated concentration  $C_{IL}$  of interstitials which have been already used to form the loops of the concentration  $C_L$  of (number. of loops/number of atomic sites), the rate of the accumulation of interstitials to the loops becomes

$$\frac{dC_{IL}}{dt} = Z_3 M_I (C_L - C_{IL})^{1/2} C_I \quad (2)$$

where  $Z_3$  is a numerical factor to represent the capture cross section for interstitials around a dislocation line. If the loop is approximated by a circle  $Z_3 = 2\sqrt{\pi} Z'_3$  where  $Z'_3$  is the number of spontaneous combination sites of the process per one atomic site on the dislocation. The size of the interstitial loops was supposed to be uniform, which is justified both from the experimental results showing the early cessation of the cluster nucleation and from the following analysis which will also show that the nucleation ceases rapidly by the decrease of the interstitial concentration.

All the above factors being considered, the variation of the interstitial concentration during the irradiation with a constant rate will be given by

$$\begin{aligned} \frac{dC_I}{dt} = & P(1-C_V)(1-Z_1 C_V) - Z_1 M_I C_V C_I - M_I C_S C_I - 2Z_2 M_I C_I^2 \\ & - Z_3 M_I (C_L - C_{IL})^{1/2} C_I \quad (3) \end{aligned}$$

The corresponding variation of the vacancy concentration will be

$$\frac{dC_V}{dt} = P(1-C_V)(1-Z_1C_V) - Z_1M_I C_I C_V \quad (4)$$

Here the effect from the migration of vacancies was neglected for the reason mentioned before.

### III-1-2-2-1. No clustering case

The case, in which the clustering of interstitials do not occur is considered at first as the simplest case. During a very early stage of the irradiation,  $C_I$  and  $C_V$  and consequently all the minus terms in eq.(3) are so small that both kinds of point defect will be accumulated in the specimen, and

$$C_I = C_V = Pt \quad (5)$$

Accompanied with the increase of  $C_I$  the annihilation rate of interstitials increases, and when there is no permanent sink, i.e.,  $C_S=0$ , they are held at constant  $C_I=C_V=(P/Z_1M_I)^{1/2}$  after  $t=(Z_1M_I P)^{-1/2}$  by the balance of production rate and annihilation rate.

When  $C_S$  is not zero but small, though the majority of continuously introduced interstitials annihilate at vacancies and consequently suppresses the vacancy accumulation, the same amount of vacancies as that of interstitials which disappeared at surfaces should be accumulated in the specimen. Therefore the accumulation rate of vacancies is expressed by

$$\frac{dC_V}{dt} = P \frac{C_S}{C_V Z_1 + C_S}$$

after  $(Z_1M_I P)^{-1/2}$ .

If  $C_S \ll Z_1C_V$ , the equation is approximated as

$$\frac{dC_V}{dt} = P \frac{C_S}{C_V Z_1}$$

Hence

$$C_V = \left\{ \frac{2PC_S t}{Z_1} - 2 \left( \frac{C_S^2 P}{Z_1^3 M_I} \right)^{1/2} + \frac{P}{Z_1 M_I} \right\}^{1/2} \quad (6)$$

where the initial condition  $C_V = (P/Z_1 M_I)^{1/2}$  at  $t = (Z_1 M_I P)^{-1/2}$  was used. As vacancies are dominant sinks for interstitial at this stage and as the rate of the accumulation is much smaller than  $P$ ,

$$\frac{dC_I}{dt} = P - M_I Z_1 C_V C_I = 0$$

or

$$C_I = \frac{P}{M_I Z_1 C_V} \quad (7)$$

Interstitial concentration is given from (6) and (7) as

$$C_I = \frac{P}{M_I Z_1} \left\{ \frac{2PC_S t}{Z_1} - 2 \left( \frac{C_S^2 P}{Z_1^3 M_I} \right)^{1/2} + \frac{P}{M_I Z_1} \right\}^{-1/2} \quad (8)$$

for

$$t > (Z_1 M_I P)^{-1/2}$$

Therefore,  $C_I$  and  $C_V$  are held constant at  $(P/Z_1 M_I)^{1/2}$  until  $1/2 M_I C_S$  at which  $2PC_S t/Z_1$  exceeds  $P/M_I Z_1$  and then they vary after then as

$$C_V = \left( \frac{2PC_S}{Z_1} \right)^{1/2} t^{1/2} \quad (9)$$

and

$$C_I = \left( \frac{P}{2M_I^2 Z_1 C_S} \right)^{1/2} t^{-1/2} \quad (10)$$

When  $C_S$  is large, typical for the case of a thin foil, the rate of escape of interstitials to surfaces become soon comparable with the production rate at first at about  $1/M_I C_S$ . After then, because of the balance of these two rates,  $C_I$  is held constant at  $C_I = P/M_I C_S$ . On the other hand, vacancies increase with Pt until interstitial-to-vacancy annihilation term  $M_I Z_1 C_V C_I$  exceeds interstitial-to-surface term  $M_I C_S C_I$ , which occurs at  $t = C_S/Z_1 P$ . After then, though the majority of the continuously introduced interstitials annihilate at vacancies and consequently suppresses the vacancy accumulation, the same amount of vacancies as that of interstitials which annihilated at surfaces should be accumulated in the specimen, and then

$$\frac{dC_V}{dt} = P \frac{C_S}{Z_1 C_V + C_S} \doteq \frac{C_S}{Z_1 C_V}$$

Hence,

$$C_V = \left\{ \frac{2PC_S}{Z_1} t - \left( \frac{C_S}{Z_1} \right)^2 \right\}^{1/2} \quad (11)$$

where the initial condition  $C_V = C_S/Z_1$  at  $t = C_S/Z_1 P$  was used. As the vacancies are dominant sinks, the relation between  $C_I$  and  $C_V$  also may be expressed by eq.(7) during this stage and putting it in eq.(11),

$$C_I = \frac{P}{Z_1 M_I} \left\{ \frac{2PC_S}{Z_1} t - \left( \frac{C_S}{Z_1} \right)^2 \right\}^{-1/2}$$

for  $t > C_S/Z_1 P$ . After the irradiation for long time

$$C_V = \left( \frac{2PC_S}{Z_1} \right)^{1/2} t^{1/2} \quad (13)$$

and

$$C_I = \left( \frac{P}{2M_I^2 Z_1 C_S} \right)^{1/2} t^{-1/2} \quad (14)$$

Vacancy and interstitial concentrations of "no clustering case" obtained from the computer simulation using eqs.(1), (2), (3) and (4) are shown in Fig. 25 for various sink efficiencies  $C_S$  of permanent sinks. As a typical case in the present experiment, the numerical value used in each parameters were;  $P=10^{-4}/\text{sec}$ , which corresponds to the case of the irradiation intensity of  $1 \times 10^{18}$  electrons/cm<sup>2</sup>sec with 2MeV as discribed in I-1,  $M_I=3 \times 10^{10}$  jumps/sec which is the jump frequency of interstitials at 300K with the activation energy of migration of 0.15eV. The constant  $Z_1$  was taken as 84. Its absolute value does not affect the following discussions even when it is changed within the same order of magnitude. In the present experiment of gold, such a simple case of on clustering is not realized. It should be pointed out that such a typical simple case of no clustering would be realized at a high temperature where clustering of interstitials and vacancies are difficult because of the strong thermal agitation. The case in which the clustering of interstitials is taken into account will be treated in the next section.

### III-1-2-2-2. Clustering case I (Di-interstitial)

The formation of the interstitial clusters will be discussed in the following two typical cases of thin and thick foil.

(i) Thin foil case ( $P/M_I C_S < (P/Z_1 M_I)^{1/2}$ )

Because vacancies and foil surfaces are the dominant

sinks for interstitials, the accumulation of vacancies and interstitials obey the eqs.(5), (6) and (8) as 'no clustering thin foil' case. Therefore, one can obtain the concentration of interstitial loops from the eqs.(1), (5), (6) and (8) as,

$$C_L = \frac{1}{3} Z_2 M_I P^2 t^3 \quad (15a)$$

for  $t < 1/M_I C_S$ ,

$$C_L = \frac{Z_2 P^2}{M_I C_S^2} t - \frac{2}{3} \frac{Z_2 P^2}{M_I C_S^3} \quad (15b)$$

for  $1/M_I C_S \leq t < C_S/Z_1 P$  and

$$C_L = \frac{P Z_2}{M_I C_S Z_1} \left\{ 1 + \frac{1}{2} \ln \left( \frac{2 P Z_1}{C_S} t - 1 \right) \right\} - \frac{2}{3} \frac{Z_2 P^2}{C_S^3 M_I^2} \quad (15c)$$

for  $t \geq C_S/Z_1 P$ . For larger  $t$ , the density of the loops is approximated by

$$C_L = \frac{P Z_2}{2 M_I C_S Z_1} \ln \frac{2 P Z_1}{C_S} t \quad (16)$$

The accumulation manner of  $C_I$  and  $C_V$  for  $C_S=10^{-4}$  and  $10^{-5}$  are shown schematically in Fig. 25 by dotted line and solid line respectively, and the results of corresponding computer calculation are shown in Fig. 26. Interstitial cluster concentration  $C_L$  estimated from eqs.(15a) (15b) and (15c) for  $C_S=10^{-4}$  is also shown in Fig. 27 by a dotted line with the corresponding results of computer calculation of solid line. The analytically obtained results show good agreement with that of exact calculation using computer except the transient regions. The other parameters such as  $M_I$ ,  $Z_1$ , and  $P$  are the same as those

used in Fig. 25. For the observation with an electron microscope the lower limit of the observable density of defects is around  $5 \times 10^{12}/\text{cm}^3$ , which is  $10^{-10}$  by the present notation of  $C_I$ . The critical condition for the formation and observation of the interstitial clusters for  $P=10^{-4}$  is estimated to be  $C_S=10^{-5} \sim 10^{-4}$ , which corresponds to the foil thickness of about 500Å. The magnitude of the observed limiting thickness and the width of the denuded zone along a grain boundary was in this order.

The growth rate of an interstitial loop is given by

$$\frac{dr}{dt} = aZ_3M_I C_I \quad (17)$$

where  $r$  is the radius of the loop and  $a$  is the growth distance by the absorption of one interstitial. The radius of a loop increases with

$$r = \frac{aZ_3^P}{C_S} t \quad (18)$$

for  $1/M_I C_S < t < C_S/Z_1 P$ , and putting (14) into (17) one can obtain the radius after long time irradiation,

$$\frac{dr}{dt} = \left( \frac{a^2 Z_3^2 P}{2Z_1 C_S} \right)^{1/2} t^{-1/2} \quad (19a)$$

$$r = \left( \frac{2a^2 Z_3^2 P}{Z_1 C_S} \right)^{1/2} t^{1/2} \quad (19b)$$

This expected behaviour of the loop growth in a thin part of a foil initially in proportion to  $t$  and finally to  $t^{1/2}$  has not been observed clearly, because highly accumulated vacancies in the later stage of irradiation may change the phenomenon even with a small mobility at room temperature. However, the loops C and D in Fig. 12 whose radii increased in proportion

to  $t$  at the early stage of irradiation and then it increased in proportion to  $t^{1/2}$  or with a smaller power must be an example of this case.

(ii) Thick foil case

In the case of smaller  $C_S$ , which corresponds to the case of thick specimen foil and also free from other structural permanent sinks such as grain boundaries and dislocations, interstitials accumulate in the early stage of irradiation to a higher level than in the case of large  $C_S$ . At the beginning of the irradiation both  $C_I$  and  $C_V$  increase with  $Pt$  until  $t = (Z_1 M_I P)^{-1/2}$  at which the vacancy-interstitial annihilation term becomes comparable with the production rate  $P$ . At this time interstitial concentration reaches its maximum value  $(P/Z_1 M_I)^{1/2}$ .

As the interstitial concentration increases with  $Pt$  until the maximum, the integrated concentration of interstitial clusters during the above initial stage of irradiation is estimated from eq.(1) as

$$C_L = \frac{1}{3} \left( \frac{Z_2^2 P}{Z_1^3 M_I} \right)^{1/2} \quad (20)$$

At this time of the maximum of interstitial concentration, vacancies should have reached their concentration to the same level as interstitials. For small  $C_S$ , which satisfies the condition  $M_I C_S C_I < Z_3 M_I (C_L C_{IL})^{1/2} C_I$  at this stage, the accumulation of vacancies after this point can be expressed as follows because the same amount of vacancies as that of interstitials consumed to form the loops will be accumulated in the specimen.

$$\frac{dC_V}{dt} = P \frac{Z_3 (C_L C_{IL})^{1/2}}{Z_1 C_V}$$

for  $t > (Z_1 M_I P)^{-1/2}$ . Considering that the amount of vacancies

accumulated further from this stages is equivalent to the amount of interstitials absorbed to interstitial loops,  $dC_{IL}/dt=dC_V/dt$ , and  $C_{IL}$  becomes nearly equal to  $C_V$  after long time irradiation, at which the amount of  $C_{IL}$  accumulated before  $(Z_1 M_I P)^{-1/2}$  becomes negligibly small compared with those accumulated after that time. And then,

$$\frac{dC_V}{dt} = P \frac{Z_3}{Z_1} \left(\frac{C_L}{C_V}\right)^{1/2} \quad (21)$$

The exact feature of the increase of  $C_L$  was obtained from the computer simulation of the eqs. (1), (2), (3) and (4), and the result of a typical case for  $C_S=10^{-8}$  is shown in Fig. 27 with the variations of  $C_I$  and  $C_V$ . One can see that the nucleation of interstitial type clusters quickly slows down after the maximum of interstitial concentration. This also agrees with the experimentally observed nature of their nucleation. Therefore  $C_V$  can be estimated from the assumption of constant  $C_L$ , and given by

$$C_V = \left(\frac{2}{3}\right)^{2/3} \left(\frac{P Z_3 C_L^{1/2}}{Z_1}\right)^{2/3} t^{2/3} \quad (22)$$

Considering that the majority of interstitials which is continuously introduced with the rate  $P$  are disappeared to vacancies,  $C_I$  is given as

$$C_I = \left(\frac{2}{3}\right)^{2/3} \frac{P^{1/3}}{Z_1^{1/3} Z_3^{2/3} M_I C_L^{1/3}} t^{-2/3} \quad (23)$$

The concentration of dislocation loops for a long time irradiation after the maximum of the interstitial concentration can be obtained by integrating eq.(1) with eq.(23) using eq.(20) as the initial condition;

$$C_L = \left\{ 5 \left( \frac{2}{3} \right)^{4/3} \frac{Z_2}{Z_1^{1/2} Z_3^{4/3}} + \left( \frac{1}{3} \right)^{5/3} \frac{Z_2^{5/3}}{Z_1^{5/2}} \right\}^{3/5} \frac{P^{1/2}}{M_I^{1/2}} \quad (24)$$

It should be noted here that  $C_L$  for long time irradiation is proportional to  $P^{1/2}$ .

Although the assumptions of the constant  $C_L$  in the estimation of  $C_V$  and of the sharp change in the analytical expression at the maximum of the interstitial concentration made in the above analysis leave some doubts in the exact absolute value of  $C_L$ , the fact that the integrated density of the interstitial cluster both before and after the maximum have the same intensity dependence confirms at least the total density to be proportional to  $P^{1/2}$ . The interstitial cluster density in the computer simulated results in Fig. 28 are plotted against the irradiation intensity in Fig. 29, and they showed the exact dependence proportional to  $P^{1/2}$  at various irradiation time.

The experimentally observed intensity dependence of the interstitial cluster density agreed well with the above result which stands on the free migration of interstitials with a high mobility and on the di-interstitials as the stable nucleus of dislocation loops. The experimentally observed interstitial cluster density was order of  $10^{15}/\text{cm}^3$  for the irradiation intensity of  $2 \times 10^{18}$  electrons/ $\text{cm}^2$ sec, which correspond to the production rate of  $P=10^{-4}$ /sec. The jump frequency  $M_I$  of interstitials which can explain the result estimated from eq. (24) is about  $3 \times 10^{10}$ /sec, and this yields to the activation energy of the motion of interstitials to be about 0.15 eV.

The growth rate of interstitial loop is given by putting eq. (23) into eq. (17),

$$\frac{dr}{dt} = \left(\frac{2}{3}\right)^{2/3} a \left(\frac{Z_3 P}{Z_1 C_L}\right)^{1/3} t^{-2/3}$$

and hence

$$r = a \left(\frac{12 Z_3 P}{Z_1 C_L}\right)^{1/3} t^{1/3} \quad (25)$$

for large  $t$ . Using numerical values as  $a=2.0\text{\AA}$ ,  $Z_1=Z_3$ ,  $P=10^{-4}/\text{sec}$  and  $C_L=10^{-8}$ , one can obtain the loop radius at  $t$

$$r \doteq 100 \cdot t^{1/3} \quad (\text{\AA})$$

Both the functional dependence of the size of dislocation loops on the irradiation time and its absolute value agreed well with the observed results described in the previous section.

The shrinkage rate of vacancy loops introduced by quenching can be also expressed by eqs. (19) and (25) for the thin foil and thick foil respectively. From these equations one can obtain the shrinkage rate of the order of  $1 \text{\AA}/\text{sec}$  at 100 seconds using the appropriate value of each parameter for the present experimental conditions. It should be noticed here that the value agrees well with the observed rate.

It should be emphasized here that all the above discussions which could explain the experimental results are standing on the model of the free three dimensional migration of interstitials near room temperature.

The accumulation behaviour of vacancies and interstitials in the thick foil of  $C_S=10^{-7}$  described by eqs. (5), (22) and (23) is shown schematically in Fig. 25 by a chain line. Where the following numerical value was used for each parameter which corresponded to the experimental conditions, namely  $M_I=3 \times 10^{10}$

jumps/sec (i.e.  $E_m^I = 0.15$  eV,  $\nu_0 = 10^{13}$ ,  $T = 300$  K),  $P = 10^{-4}$ ,  $Z_1 = Z_2 = 84$  and  $Z_3 = 40$ . The accumulation of vacancies in the foil of  $C_S = 10^{-7}$  retarded one or half order compared with that in the thin foil of  $C_S = 10^{-4}$ . Fig. 28 is the results of computer calculation for the foil of  $C_S = 10^{-8}$ , which shows the production rate dependence of the accumulation of vacancies and interstitials and nucleation of interstitial loops. It should be noted that even the weak irradiation of  $P = 10^{-6}$ /sec, the interstitial concentration at 1 second is  $7 \times 10^{-12}$ , so that the arrival rate of interstitials to dislocations,  $Z_3 M_I C_I$ , is as large as 1 atom/sec per one atomic site on a dislocation. On the other hand, vacancy concentration reaches  $10^{-5}$  by the irradiation of  $P = 10^{-4}$ /sec for 10 sec. Even if intensity is lowered to  $P = 10^{-6}$ /sec, which is the minimum intensity by which one can observe the image on the fluorescence screen, vacancy concentration reaches  $10^{-5}$  after 1000 seconds irradiation. When the foil is thinner or has more permanent sinks for interstitials the accumulation of vacancy is more enhanced. When the HVEM is used for the studies of the lattice defect sensitive properties of metals such as plastic deformation and diffusion controlled phenomena, these defects will cause additional effects, so that great attention for the irradiation effect must be paid for the studies of these fields.

### III-1-2-2-3. Tri-interstitial case II (Tri-interstitial)

If the binding energy of di-interstitial is small the di-interstitial concentration maintain equilibrium with interstitials, and then

$$C_{I2} = \frac{Z_2}{Z_4} C_I^2 \exp\left(\frac{B}{kT}\right) \quad (26)$$

where  $Z_4$  is the number of ways of the dissociation of a di-interstitial and  $B$  is the binding energy of the di-interstitial. Therefore, the nucleation rate of tri-interstitials, which corresponds to arrival rate of an interstitials to the di-interstitials, is given by,

$$\frac{dC_{I3}}{dt} = Z_5 M_I C_{I2} C_I = \frac{Z_2 Z_5}{Z_4} M_I \exp\left(\frac{B}{kT}\right) C_I^3 \quad (27)$$

where  $Z_4$  is the number of the spontaneous combination sites of the reaction. If the binding energy of the tri-interstitial is high enough to suppress of dissociation before the next interstitial arrives to it, this rate implies the rate of nucleation of interstitial clusters.

The intensity dependence of the saturated density of interstitial clusters for this tri-interstitial case would be obtained by the similar analysis as the case of di-interstitials

$$C_L = \frac{Z_2 Z_5}{Z_1^{3/2} Z_4 C_S M_I^{3/2}} \exp\left(\frac{B}{kT}\right) P^{3/2} \quad (28)$$

for a thin foil, and

$$C_L = 0.54 \left( \frac{Z_2^2 Z_5^2}{Z_1 Z_3^4 Z_4^2 M_I^3} \right)^{1/4} \exp\left(\frac{B}{2kT}\right) P^{3/4} \quad (29)$$

for a thick foil. These intensity dependences of the cluster density do not explain the observed results, and it can be inferred that larger clusters, if supposed as the stable nucleus, would result much more deviated results from the observation. A di-interstitial, which serves as the stable nucleus, is stable at least until the next interstitial reaches and form a tri-interstitial. The life time estimation of this process implies that the binding energy of the di-interstitial is more

than 0.4eV.

The diameter of the interstitial loop in a later stage in a thick foil should be proportional to  $t^{1/3}$ .

#### III-1-2-2-4. Mobility of interstitials

The results of experimental observation and kinetics analysis for the formation of dislocation loops are summarized in Table III, which shows that the experimental results agreed well with the calculated results for di-interstitial case assuming that the stable nucleus of the loop is a di-interstitial and the migration rate of interstitials is as high as  $10^{10}$  jumps/sec at room temperature.

The width of the denuded surface layer of dislocation loops, the growth rate of dislocation loops and the shrinkage rate of a quenched in vacancy type dislocation loop also agreed with the experimental results when  $M_I = 3 \times 10^{10}$  jumps/sec. As clearly seen from eq.(24), the loop concentration increase with activation energy of migration of interstitials. For example, when the activation energy is 0.3eV, 0.45eV or 0.55eV the corresponding concentration of dislocation loops will be  $1 \times 10^{-7}$ ,  $3 \times 10^{-6}$  or  $3 \times 10^{-5}$  respectively. Therefore, if the interstitial had a large activation energy as 0.8eV which was proposed in the conversion-two-interstitial model, the density of dislocation loops would be extremely high and it would become impossible to explain the observed growth rate of interstitial type dislocation loops and the shrinkage rate of vacancy type loops. Of course if the larger cluster of interstitials is assumed to be the stable nucleus of dislocation loop for explaining the observed density of

dislocation loops, the production rate dependence of the density does no longer obey  $P^{1/2}$  as typically shown in the tri-interstitial case.

It can be concluded that an interstitial in gold have extremely high mobility of the order of  $10^{10}$  jumps/sec at room temperature and di-interstitial is the stable nucleus of the dislocation loops.

### III-1-2-3. Vacancy Clustered Defects

Under the conditions for the appearance of the black spot defects, the interstitial type dislocation loops hardly nucleate or at least they shrink even once have grown to an observable size. This shows that the black spot defects have the opposite nature to that of the interstitial clusters, namely they are vacancy clusters. All the other various observed behaviours of the black spot defects strongly suggest that the defects are formed by the clustering of the lattice vacancies.

Although the clustering of vacancies is delayed during the irradiation by the fast moving interstitials, the clustering can easily takes place after the cessation of irradiation because the interstitials disappear very rapidly as soon as the irradiation is stopped. During the aging, some of the vacancies will annihilate at the vacancy clusters, interstitial clusters and surfaces, and the others will form divacancies. When the concentration of vacancies is high as in the present case, the latter process is dominant except in the final part of the recovery process. As soon as divacancy is formed it would annihilate at above mentioned sinks, since their

mobility is fairly high at room temperature. Therefore, the vacancy clusters (black spot defects) must be the major sinks in the present case. In such a situation, the reaction which controls the process should be the formation of divacancies, and the annihilation rate of vacancies is equal to the growth rate of vacancy cluster.

$$\frac{dC_V}{dt} = - \frac{dC_{BV}}{dt} = -Z_6 M_V C_V^2 \quad (30)$$

where,  $C_{BV}$  is the concentration of vacancies aggregated as the vacancy clusters during the aging,  $M_V$  the migration rate of vacancy,  $Z_6$  the number of combination sites of the formation of a divacancy. Hence,

$$C_V = \frac{C_V(0)}{Z_6 M_V C_V(0)t + 1} \quad (31)$$

where  $C_V(0)$  is the initial concentration of vacancies.

Putting the observed half decay time, initial concentration of vacancies and the aging temperature into eq.(31) one can obtain about 0.80eV for activation energy of vacancy migration. Since the value shows a good agreement with the activation energy of so called stage III in the heavily irradiated specimen, the black spot defects formation is considered to correspond to the stage III recovery. Consequently, it should be concluded that the stage III is the stage of the vacancy annihilation.

Observed preferential formation of the black spot defects in the area of high permanent sink density, such as in a thin foil, in a deformed specimen and the area with high density of interstitial type of loops, can easily understood

as the result of the high accumulation of vacancies by the extra escape of interstitials to the permanent sinks. For example of a typical case in Fig. 26, in a thin foil of the thickness of  $300\text{\AA}$  vacancies of  $10^{-4}$  in concentration will be accumulated by a few minutes of irradiation, whereas those in a thick foil of  $3000\text{\AA}$  will reach only to  $10^{-5}$ .

#### III-1-2-4. Condition for Formation of Vacancy Clustered Defects During Irradiation

During a continued irradiation vacancies will be accumulated while interstitials decrease in a foil specimen for several reasons described already in III-1-2-2. At a certain stage the arrival rate of vacancies to a defect cluster exceeds that of interstitials, namely

$$Z_V M_V C_V > Z_I M_I C_I \quad (32)$$

where  $Z_V$  and  $Z_I$  mean the number of spontaneous combination sites around the defect for a vacancy and for an interstitial respectively. In a later stage of irradiation, in which the majority of point defects introduced by irradiation are continuously annihilated, and also at room temperature at which vacancies cannot migrate fast, the simple approximation of eq.(7) can be used to obtain the relation between  $C_I$  and  $C_V$ . The condition (32) for the growth of vacancy type clusters becomes

$$C_V > \left( \frac{Z_I P}{Z_I Z_V v_0} \right)^{1/2} \exp\left(\frac{E_m^V}{2kT}\right) \quad (33)$$

or the critical temperature above which the vacancy type defects can be formed is

$$T_c = \frac{E_m^V}{k \ln \left( \frac{Z_I Z_V v_o C_V^2}{Z_{IP}} \right)} \quad (34)$$

It should be noted here that  $T_c$  depends on the activation energy of vacancy migration but does not depend on that of interstitials. The relation between  $T_c$  and  $E_m^V$  for various  $C_V$  are shown in Fig. 30. Since  $Z_V$  and  $Z_I$  depend on the interaction energy between the point defects and the cluster, they will differ according to the type of the defect clusters. Although the values of  $Z_V$  and  $Z_I$  are different from each other and vary with the type of the defects, depending on the interaction energy between each kind of point defects and the cluster,  $Z_V = Z_I$  was assumed for simplicity in the figure. Supposing that  $E_m^V$  is about 0.8eV, the growth of the vacancy type cluster during irradiation at room temperature is possible only if the vacancy concentration reaches to a value as high as  $10^{-3}$ .

### III-2. Iron

#### III-2-1. Experimental Results

Although only a preliminary experiment was performed on iron in this work without giving great care upon the specimen purity, some interesting results were obtained as follows.

In Fig. 31 are shown small dotted defects of extremely high density which have grown up by the irradiation with 2.0MeV electrons. Even in a thin edge region of the specimen thinner than a few hundreds Angstrom the defects could be observed. It should be noted that the layer free from the

defect clusters was much thinner than that observed in gold. The defects grown by a long irradiation caused the distortion of the lattice large enough to remove the equal thickness fringes. The irradiation intensity dependence of formation of the clusters was examined. Fig. 32 shows the comparison of the defect densities for three different intensities i.e.,  $0.5 \times 10^{18}$ ,  $1.7 \times 10^{18}$ , and  $4.7 \times 10^{18}$  electrons/cm<sup>2</sup>sec. The density of the defects counted at the areas of the same thickness (3000Å) which was estimated from the equal thickness fringes are plotted in Fig. 33 against the total dose. It was evident from these figures that the density of the defects saturated during the early stage of irradiation and that the saturated values varied with the irradiation intensity. Fig. 34 shows that the density increased with the square root of the irradiation intensity as observed in gold.

### III-2-2. Discussions

As discussed in III-1-1-2, the irradiation intensity dependence of the cluster formation suggests that the nucleus of the observed defects is the cluster of two point defects. The jump frequency  $M_I$  of the defects forming the observed defect clusters, which was estimated from eq.(24) is the order of  $10^7$ /sec and this yields the activation energy of the motion of the defect of about 0.25eV.

The recovery of pure iron irradiated at low temperature have several distinct recovery stages and one of them, which appeared near 80K with activation energy of 0.25eV has been ascribed by some investigators<sup>27)</sup> to the free migration of <110> split type interstitial. When we accept these

interpretation, the observed defects can be assigned to be the aggergation of interstitials.

Because the specimen used in the present experiment was not of high purity, the role of the impurity atoms on the formation of the defect cluster should be taken into account. As an extreme case, it is assumed that only the impurity atoms become the centers of the interstitial clusters and the binding energy between an impurity and an interstitial atom is large. As the discussion in III-1-1-2, if the migration rate of interstitials is large, the accumulation rate of vacancies for large  $t$  is given by

$$\frac{dC_V}{dt} = P \frac{Z_7 C_{Im}}{Z_1 C_V} \quad (35)$$

hence

$$C_V = \left( \frac{2Z_7 P C_{Im}}{Z_1} \right)^{1/2} t^{1/2} \quad (36)$$

where  $C_{Im}$  is the concentration of impurity atoms and  $Z_7$  is the number of sites of interstitial-impurity atom combination.

From eq.(36) and (7)

$$C_I = \left( \frac{P}{2M_I^2 Z_1 Z_7 C_{Im}} \right)^{1/2} t^{-1/2} \quad (37)$$

The nucleation rate of the defect cluster is

$$\frac{dC_C}{dt} = M_I Z_7 C_I C_{Im} = \left( \frac{Z_7 P C_{Im}}{2Z_1} \right)^{1/2} t^{1/2} \quad (38)$$

where  $C_C$  is the concentration of the defect clusters. At the early stage of irradiation where  $C_{Im}$  is essentially constant,

$$C_C = \left( \frac{2Z_7 P C_{Im}}{Z_1} \right)^{1/2} t^{1/2} \quad (39)$$

Although the concentration of interstitial clusters compared at the same irradiation time depends on  $P^{1/2}$ , they increase with  $t^{1/2}$  and will gradually saturate at the level of  $C_{Im}$  after a long time irradiation. The observed defects concentration saturated at the level much lower than that of the impurity concentration, and the assumption of the nucleation at an impurity atom should be denied. It is reasonable to neglect the role of impurity atoms in the discussion of the assignment of the defect cluster described above.

### III-3. Aluminum

#### III-3-1. Experimental Results

Quenched aluminum containing a number of large vacancy type dislocation loops was irradiated by 2.5 MeV electrons of  $1.0 \times 10^{19}$  electrons/cm<sup>2</sup>sec. The incident beam was nearly normal to (100) plane. As shown in Fig. 35 the defect clusters became visible after irradiation for 40 seconds, and then increased their size. The time needed for the growth to reach the visible size is much longer than that in gold which was less than 1 second.

After grown large, the defects showed the typical images of dislocation loops of four kinds. This suggests that these loops were dislocation loops lying on four {111} planes, which have been already reported by Shiraishi et al.<sup>18)</sup>. Fig. 36 shows that the growth rate of the loop slows down gradually with the irradiation time. The dislocation loops formed inside a large quenched-in vacancy type loop in Fig. 37 showed somewhat different growth features compared with those formed in the matrix. They have grown up to the observable size within 10 seconds, and their growth rate after this fast growth was

rather slow compared with other loops formed in the matrix. The growth manner of the loop is also shown in Fig. 36.

As illustrated in Fig. 38 the quenched-in loops shrank by absorbing interstitials formed by irradiation. It is interesting that the shrinkage rate at the corner is smaller than that at the middle of the straight edge of the loop.

### III-3-2. Discussions

Small dislocation loops formed by the irradiation were identified as the vacancy type by Shiraishi et al.<sup>18)</sup> and kinetics analysis described in III-1-2-3 also supports their assignment. As the activation energy of vacancy migration in aluminum obtained from the quenching experiment is  $0.64\text{eV}^{28)}$ , according to eq.(33) vacancy cluster will be formed when vacancies accumulate above  $8 \times 10^{-5}$ . In the case of Fig. 35 the concentration of vacancies is expected to reach this level by irradiation of a few ten seconds from the kinetics analysis. This time agreed well with the observed time necessary for the appearance of the clusters.

In order to understand the shrinkage of large quenched-in loops during the growth of smaller radiation induced loops of the same type, the flow of point defects around the dislocation loops was considered. The migration of interstitials, which have much smaller activation energy of migration than vacancies, is naturally more affected by the presence of strain field gradient. It is well known that the strain field of a large dislocation loop can be approximated by that of a straight dislocation line and is in inverse proportion to the distance from the dislocation, while that of a small loop is in inverse

proportion to the square of the distance as the results of the contributions from the whole parts of the loop. Therefore, the large loops introduced by quenching have more extended strain field compared with that of a small loop. This causes more absorption of interstitials by a large loop, and consequently its shrinkage.

Since the interaction between an interstitial and a vacancy type dislocation loop is attractive at the inside of the loop but repulsive at the outside, the interstitials inside the loop should be absorbed preferentially by it. This local decrease of interstitials gives rise to an additional accumulation of vacancies inside the large shrinkage loop, and these vacancies enhance the nucleation of vacancy type loops as shown in Fig. 37. At the corner of the hexagonal dislocation loop the attractive interaction in the loop is smaller than that of the straight part and repulsive one out the loop is stronger, so that the shrinkage rate at the former must be slow compared with that at the latter as shown in Fig. 38.

The interstitial clusters must be formed at the early stage of irradiation as gold, however the mobility of a vacancy is fairly large in aluminum, interstitial clusters can not grow large enough for the observation through the electron microscope, and they will disappear after vacancies accumulated highly.

#### III-4. Al-6.5 at% Zn

Figure 39 is an example of irradiation of the alloy, in which helical dislocations and vacancy type dislocation loops had already been introduced by quenching. The formation of

the new loops by the electron irradiation of this alloy was found to be much slower and fewer in number compared with the case of pure aluminum. For instance the last stage in Fig. 39 had undergone the more irradiation time with a stronger intensity compared with the last stage of pure aluminum in Fig. 35. In spite of this strong irradiation, much fewer number of loops were observed in the alloy. Especially the formation of the loops were suppressed near the quenched-in dislocation loops and helical dislocations.

Vacancy type helical dislocations were observed to increase their radii of turn and a straight dislocation located in the upper right part of the figure had developed into helix. The direction of the turn of this newly developed helix was confirmed with the aid of stereoscopic observation to be the same as those introduced by quenching. All the loops introduced by quenching were observed to grow by irradiation. The amount of the growth of helical dislocation, quenched-in loops and newly formed dislocation loops are plotted against the irradiation time in Fig. 40. The growth of newly appeared dislocation loops is a little larger than that of the other defects. The growth of the quenched-in vacancy type defects in Al-Zn alloy is in contrast to the shrinkage of large vacancy type loops observed in pure aluminum in section III-3. The growth can not be explained directly from the change in the vacancy behaviour, because the slower formation of new loops in the alloy is suggesting the suppression of the vacancy reaction. The reason for the difference between this alloy and pure aluminum, therefore, should be sought in the change in the interstitial behaviour. If the interstitials are trapped

by solute atoms, as often proposed in the analysis of the recovery of low temperature irradiation induced defects, the arrival rate of interstitials to loops and helices would be overcome by that of the vacancies.

## Chapter IV. Summary

The formation of defects by the aggregation of interstitials and vacancies introduced in various metals by the irradiation of 2.0~2.5 MeV electrons at room temperature was continuously traced in the high voltage electron microscope.

### Gold

- 1) The aggregation of interstitials generally precedes that of vacancies and the extent of the two processes are greatly modified by the existence of dislocations, grain boundaries and specimen surfaces.
- 2) The defects formed by the aggregation of interstitials are initially hexagonal dislocation loops with stacking fault and finally grow into the perfect dislocation loops of irregular shapes.
- 3) The defects formed by the aggregation of vacancies are observed as black spots.
- 4) In an area close to the permanent sinks, no clustering of interstitials takes place, and preferential clustering of vacancies occurs as the result of the extra accumulation of vacancies survived the annihilation.
- 5) When the irradiation is interrupted, the growth of the black spot defects and shrinkage of interstitial type dislocation loops are observed.
- 6) Stacking fault tetrahedra introduced by quenching are converted into dislocation loops and then shrank.

- 7) Kinetics analysis of the point defect behaviour in foils assuming the random motion and reaction of interstitials and vacancies explains all the various behaviours of the point defects clusters.
- 8) Experimentally observed square root dependence of the interstitial cluster density on the irradiation intensity is interpreted by the assumption that the di-interstitials are the stable nuclei for the clusters.
- 9) The diameters of the majority of the loops formed by irradiation increase with a proportional relationship to the cube root of the irradiation time. The deviation from the relationship is due to the difference of the interstitial accumulation influenced by permanent sinks.
- 10) The activation energy of migration of vacancies and interstitials which fit to explain the observed results are 0.80 eV and 0.15 eV respectively. This leads to the conclusion that the stage III recovery arises from the vacancy migration.

#### Iron

- 11) The defect formation is proportional to the square root of the irradiation intensity.
- 12) The activation energy of migration of the point defects which form the observed clusters is 0.25 eV. This suggests that the irradiation-produced interstitials migrate and form the clusters.

#### Aluminum and aluminum-zinc alloy

- 13) In aluminum there is preferential nucleation of irradiation

induced small dislocation loops on the thermally introduced large faulted loops.

14) The shrinkage of large dislocation loops of vacancy type in aluminum with the simultaneous growth of small loops of the same type shows the existence of the attractive interaction between the dislocations and interstitials.

15) The shrinkage rate of a hexagonal dislocation loop at its corner is slower than that at the straight part. It can be attributed to the difference of the strengths of the strain field at these parts.

16) The formation of defect clusters in Al-Zn alloys by electron irradiation is much less compared with that in pure aluminum.

17) The comparison of the growth and shrinkage of large vacancy type defects between pure aluminum and Al-Zn alloy leads to the conclusion of interstitials trapping by solute atoms.

### Acknowledgment

The author wishes to express his gratitude to Professors E. F. Fujita and M. Kiritani for their continuing guidance, discussions and encouragement. He wishes to express his thanks to Messrs. Y. Yamaguchi and H. Takata for their assistance in the experiment. The cooperation of the HVEM groups in Osaka University and the members of Hitachi Central Laboratory is greatly appreciated. He also wishes to express his hearty thanks to Miss M. Ishii for her great help in typewriting the paper.

## References

- 1) M.W.Thompson: Defects and Radiation Damage in Metals  
(Cambridge University Press, 1969)
- 2) R.M.J.Cotterill et al.:"Inter. Conf. Lattice Defects in  
Quenched Metals" Argonne 1964 (Academic Press, 1965)
- 3) H.I.Dawson: Acta Met. 13 (1965) 453.
- 4) K.Yamakawa, M.Nakao and F.E.Fujita: Japan. J. Appl. Phys.  
9 (1970) 1045.
- 5) N.Yoshida, R.Oshima and F.E.Fujita: J. Phys. F2 (1972) 237.
- 6) N.Yoshida, J.Hatakeyama, M.Kiritani and F.E.Fujita: J. Phys.  
Soc. Japan 33 (1972) 858.
- 7) O.S.Oen: USAEC unclassified report ORML-3818 (1965).
- 8) N.F.Mott: Proc. Roy. Soc (London) A124 (1929) 426, A135  
(1932) 429.
- 9) J.B.Ward and J.W.Kauffman: Phys. Rev. 123 (1961) 90.
- 10) C.Lee and J.S.Koehler: Phys. Rev. 176 (1968) 813.
- 11) W.Bauer and A.Sosin: Phys. Rev. 136 (1964) A474.
- 12) Y.Shimomura: Phil. Mag. 19 (1969) 773.
- 13) W.Bauer, A.Seeger and A.Sosin: Phys. Letter 24A (1967) 195.
- 14) H.Fujita, T.Tabata, K.Yoshida, N.Sumida and S.Katagiri:  
Japan. J. Appl. Phys. 11 (1972) 1522.
- 15) M.J.Makin: Phil. Mag. 18 (1968) 637.
- 16) M.Ipohorski and M.S.Spring: Phil. Mag. 20 (1969) 937.
- 17) M.Ipohorski and M.S.Spring: Phil. Mag. 22 (1970) 1279.
- 18) K.Shiraishi, A.Hishinuma, Y.Katano and T.Taoka: J. Phys.  
Soc. Japan 30 (1971) 295.
- 19) K.Shiraishi, A.Hishinuma, Y.Katano and T.Taoka: J. Phys.  
Soc. Japan 32 (1972) 964.

- 20) K.Urban: *phys. stat. sol. (a)*4 (1971) 761.
- 21) D.L.R.Norris: *Phil. Mag.* 20 (1969) 1273.
- 22) D.L.R.Norris: *Phil. Mag.* 23 (1971) 135.
- 23) L.M.Howe: *Phil. Mag.* 22 (1970) 965.
- 24) M.J.Makin: *Phil. Mag.* 20 (1969) 1132.
- 25) J.A.Ytterhus and R.W.Balluffi: *Phil. Mag.* 11 (1965) 707.
- 26) L.E.Thomas and R.W.Balluffi: *Phil. Mag.* 15 (1967) 1137.
- 27) H.Bilger, V.Hivert, J.Verdone, J.L.Leveque and J.C.Soulie:  
*Jul. Con. 2* (vol. II) 1968.
- 28) M.Kiritani, H.Murakami, A.Yoshinaka, A.Sato and S.Yoshida:  
*J. Phys. Soc. Japan* 29 (1970) 1494.
- 29) W.Bauer, A.I.Anderman and A.Sosin: *Phys. Rev.* 185 (1969) 870.
- 30) P.G.Lucasson and R.M.Walker: *Phys. Rev.* 127 (1962) 485.
- 31) G.W.Iseler, H.I.Dawson, A.S.Mehner and J.W.Kauffman: *Phys. Rev.* 146 (1966) 468.
- 32) H.M.Neely and W.Baner: *Phys. Rev.* 149 (1966) 535.
- 33) W.Bauer and A.Sosin: *Phys. Rev.* 135 (1964) A 255, 136 (1964) A 474.
- 34) J.W.Corbett, R.B.Smith and R.M.Walker: *Phys. Rev.* 144  
(1959) 1452 and 1460.
- 35) C.J.Meehan and J.A.Brinkman: *Phys. Rev.* 103 (1959) 33 and 1193.
- 36) A.Sosin and L.H.Rachal: *Phys. Rev.* 130 (1963) 2238.
- 37) K.R.Garr and A.Sosin: *Phys. Rev.* 162 (1967) 669.
- 38) K.R.Garr and A.Sosin: *Phys. Rev.* 162 (1967) 681.
- 39) Y.N.Lwin, M.Doyama and J.S.Koehler: *Phys.Rev.* 165 (1968)  
787.

## Figure Captions

- Fig. 1 The maximum energy transferred,  $T_m$ , to an atomic nucleus by an electron in a head-on elastic collision vs the electron energy for several elements<sup>7)</sup>.
- Fig. 2 Primary and total displacement cross sections for gold computed using the Mott series for different threshold energies vs the electron energy<sup>7)</sup>.
- Fig. 3 A high voltage electron microscope HU-2000 installed in Osaka University in 1972. "A" is the accelerator tank, "B" the microscope column and "C" the vibration free support.
- Fig. 4 Dislocation loops formed in electron irradiated gold. Irradiated for (a) 110 seconds and (b) 240 seconds with 2.5 MeV electrons of the intensity of  $6.4 \times 10^{18}$  electrons/cm<sup>2</sup>sec. Hexagonal loops with stacking fault are denoted by H.
- Fig. 5 Stacking fault fringe contrast inside a dislocation loop.
- Fig. 6 Progress of the formation of dislocation loops for two different intensities at the area with the same thickness and orientation. (a)  $8.4 \times 10^{18}$  electrons/cm<sup>2</sup>sec, and (b)  $2.6 \times 10^{19}$  electrons/cm<sup>2</sup>sec with 2.5 MeV electrons. Integrated dose (electrons/cm<sup>2</sup>) is shown for each micrograph.
- Fig. 7 Variation of number of dislocation loops with the irradiation time in the specimen irradiated with 2.0 MeV electrons of  $4.3 \times 10^{18}$  electrons/cm<sup>2</sup>sec.
- Fig. 8 Variation of the observed number of dislocation loops with the specimen thickness for three different irradiation intensities.  $\circ$  :  $15.5 \times 10^{18}$ ,  $\times$  :  $5.7 \times 10^{18}$  and  $\bullet$  :  $0.8 \times 10^{18}$  electrons/cm<sup>2</sup>sec, all with 2.5 MeV electrons.

Fig. 9 Irradiation intensity dependence of the dislocation loop density compared at the same dose of  $3 \times 10^{20}$  electrons/cm<sup>2</sup>.

Fig. 10 Denuded zone of dislocation loops along a grain boundary. Irradiated with 2.0 MeV electrons.

Fig. 11 Suppression of the formation of dislocation loops by tangled dislocations. Irradiated for 155 seconds with 2.0 MeV electrons of  $3.2 \times 10^{19}$  electrons/cm<sup>2</sup>sec.

Fig. 12 Growth behaviours of dislocation loops. The diameter of the loops A and B increase proportionally to the cube root of the irradiation time.

Fig. 13 Variation of the growth and shrinkage behaviours of loops with the specimen thickness. Thickness increases from right to left in the figure on the top. The location of the enlarged micrographs are indicated by A, B, C and D. Irradiated by 2.0 MeV electrons. The times indicated in the figures are the irradiation time.

Fig. 14 Growth and shrinkage behaviours of black spot defects during and after the irradiation. Formation and growth of dislocation loops and black spot defects during the irradiation, (a), (b) and (c). Rapid growth of the black spot defects after irradiation with the simultaneous shrinkage of loops, (d) and (e). Shrinkage of the black spot defects and the growth of the loops by resuming irradiation, (f). Irradiated at 2.0 MV with intensity of  $1.6 \times 10^{19}$  electrons/cm<sup>2</sup>sec and the specimen thickness was about 800 Å.

Fig. 15 Variations of (a) diameter of dislocation loops in Fig. 14, (b) density and (c) average diameter of black

spot defects near the loops during irradiation and aging.

Fig. 16 Concentration of vacancies during aging estimated from the size and the density of the black spot defects in Fig.15.

Fig. 17 A pair of a stereoscopic micrographs which show the three dimensional distribution of black spot defects appeared after irradiation.

Fig. 18 Progress of the formation of black spot defects in a dislocation forest. Enhanced formation of the black spot defects are observed in the high density regions of dislocations. Formation of a helical dislocation denoted by H and movement of dislocations are also observed.  
2.0 MV,  $3.2 \times 10^{19}$  electrons/cm<sup>2</sup>sec. 30% deformed gold.

Fig. 19 Variation of the areal density of black spot defects with irradiation time in the high and low density regions of dislocations in Fig. 18.

Fig. 20 Formation of black spot defects by a strong irradiation. Enhanced formation of black spot defects are observed inside the large irradiation loops. 2.0.MV,  $3.2 \times 10^{19}$  electrons/cm<sup>2</sup>sec.

Fig. 21 Variation of areal density of black spot defects around a dislocation loop shown in Fig. 20.

Fig. 22 Stacking fault tetrahedra denoted by T in (a) converted into dislocation loops, L, in (b) and shrank in (c).  
Irradiated with 2.0 MeV electrons of  $5.1 \times 10^{17}$  electrons/cm<sup>2</sup>sec.

Fig. 23 Dislocation loops converted from stacking fault tetrahedra shrank by irradiation with 2.0 MeV electrons.

Fig. 24 Computer calculated concentrations of vacancies and interstitials during the constant irradiation with the production rate of  $1 \times 10^{-4}$ /sec for "on clustering case". Numerical values of the parameters used in the calculations are shown in the figure.

Fig. 25 Variation of  $C_V$  and  $C_I$  in the "clustering case" during a constant irradiation, which were obtained by analytical approximation.

Fig. 26 Behaviours of computer calculated concentration of vacancies and interstitials in the "clustering case". This figure corresponds to the analytical approximation in Fig. 25.

Fig. 27 The comparison of the concentration of interstitial clusters in a thin foil obtained by the numerical calculation (—) and analytical approximation (-----).

Fig. 28 Results of the computer simulation of concentrations of vacancies, interstitials, and interstitial clusters for various irradiation intensities. The values used for each parameter are shown in the figure.

Fig. 29 Irradiation intensity dependence of the concentration of interstitial clusters at  $10^{-3}$ ,  $10^{-2}$  and  $10^{-1}$  second in the computer simulated results of Fig. 28.

Fig. 30 The critical temperature for the formation of the vacancy clusters for various vacancy concentrations.

Fig. 31 Progress of the formation of defect clusters in iron. Elimination of equal thickness fringes is observed in the heavily irradiated area.

Fig. 32 Comparison of the defect formation in iron at the same total dose of  $1.5 \times 10^{21}$  electrons/cm<sup>2</sup> for three different irradiation intensities. (a)  $0.5 \times 10^{18}$ , (b)  $1.7 \times 10^{18}$  and (c)  $4.7 \times 10^{18}$  electrons/cm<sup>2</sup>sec, with 2.0 MeV electrons.

Fig. 33 Variation of concentration of defect clusters with total dose for three different irradiation intensities corresponding to the micrographs in Fig. 32.

Fig. 34 Irradiation intensity dependence of saturated density of defect clusters in iron.

Fig. 35 Formation of loops of high density in aluminum, and shrinkage of large vacancy type dislocation loops introduced by quenching.

Fig. 36 Variations of diameters of loops inside a quenched-in large loop and in the matrix during constant irradiation with 2.5 MeV electrons of  $1.0 \times 10^{19}$  electrons/cm<sup>2</sup>sec.

Fig. 37 Preferential nucleation of loops on the dislocation loops introduced by quenching. 2.5MV,  $1.0 \times 10^{19}$  electrons/cm<sup>2</sup>sec.

Fig. 38 Shrinkage of large vacancy type dislocation loops introduced by quenching.

Fig. 39 Electron irradiation of quenched Al-6.5 at.%Zn. Growth of helical dislocations and formation of new loops are observed. Development of a new helical dislocation is seen at the top right of the successive figures. 2.5 MV,  $2.0 \times 10^{19}$  electrons/cm<sup>2</sup>sec.

Fig. 40 Growth of helical dislocation, quenched-in dislocation loops and newly appeared loops by irradiation with 2.0 MeV electrons of  $2.0 \times 10^{19}$  electrons/cm<sup>2</sup>sec.

Table I.

Experimentally determined threshold energy  $T_d$  and corresponding minimum energy  $E_d$  of an electron to make the displacement

element	$T_d$ (eV)	$E_d$ (keV)	References
Au	36	13.8	(29)
Cu	22	4.5	(30)
Al	16	1.7	(31)
	19	2.0	(32)
Fe	24	4.3	(30)

Table II

Recovery stages in Au, Cu and Al after electron irradiation

	Stage I			Stage II			Stage III		
	Au	Cu	Al	Au	Cu	Al	Au	Cu	Al
Approx. temp(K)	45	16~55	14~50	45~240	absent	70~140	240~330	250~350	200~280
Percentage of recovery	28	90	85	36	0	5	36	9	10
Activation energy	0.02 ~0.15	0.05 ~0.12				0.22 ~0.33	0.80* 0.85**	0.60	0.60** 0.62**
Order of reaction	1,?	1~3	1,2				2	2	2
References	(9) (33)	(34)	(36)	(33)	(34)	(37)	(33)* (10)**	(35)	(38)** (39)**

Table III.

	Experimental	Kinetics Analysis	
		Di-interstitial case	Tri-interstitial case
Interstitial Cluster Density ( $\text{cm}^{-3}$ )	$10^{15}$	$1.2 \times 10^{15}$	$8.4 \times 10^{11} \sim 4.1 \times 10^{13}^{**}$ ( $B = 0 \sim 0.1 \text{eV}$ )
P-Dependence of Inter. Cluster Density	$P^{1/2}$	$P^{1/2}$	$P^{3/4}$
Dislocation Loop Diameter ( $\text{\AA}$ )	$90 t^{1/3}$	$100 t^{1/3}$	$2000 t^{1/3}$

\* Interstitial cluster densities are compared at  $P=10^{-4}$ /sec and the mobility of an interstitial is assumed to be  $3 \times 10^{10}$  jumps/sec in the kinetics analysis.

\*\* The density of interstitial clusters alters with binding energy of an di-interstitial.

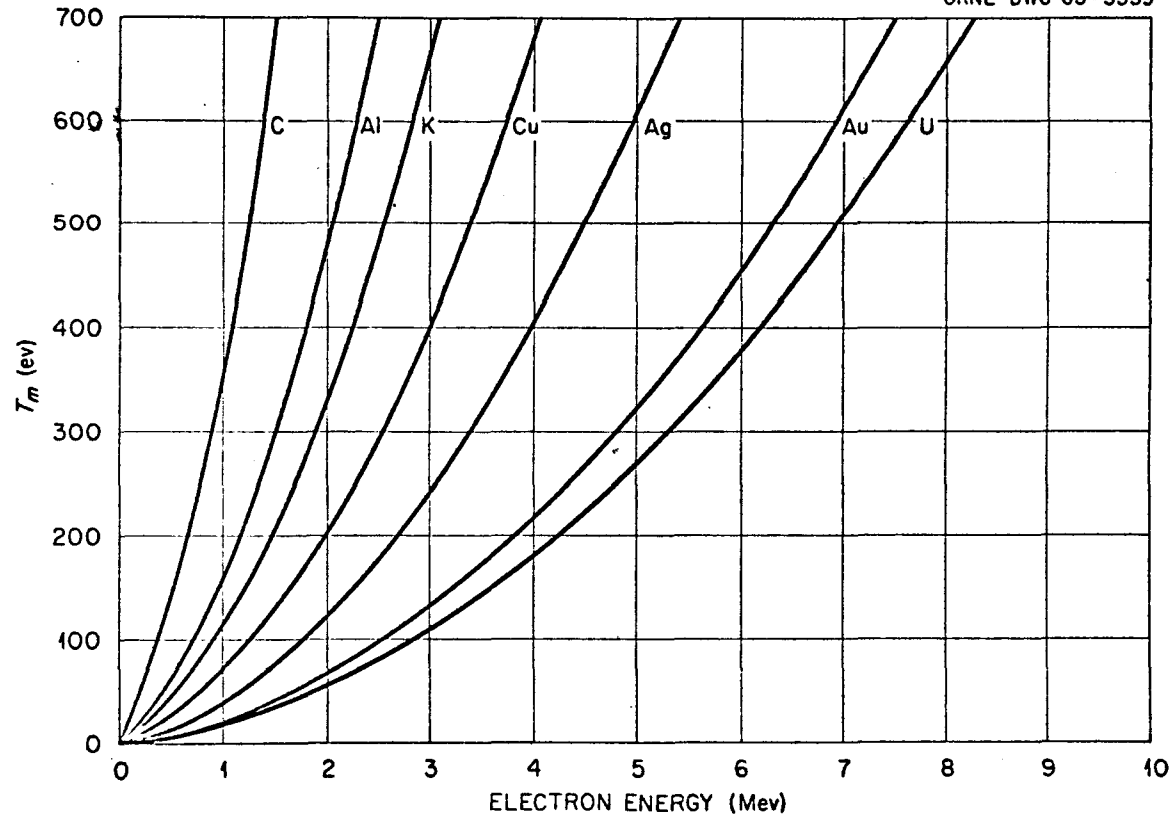


Fig. 1

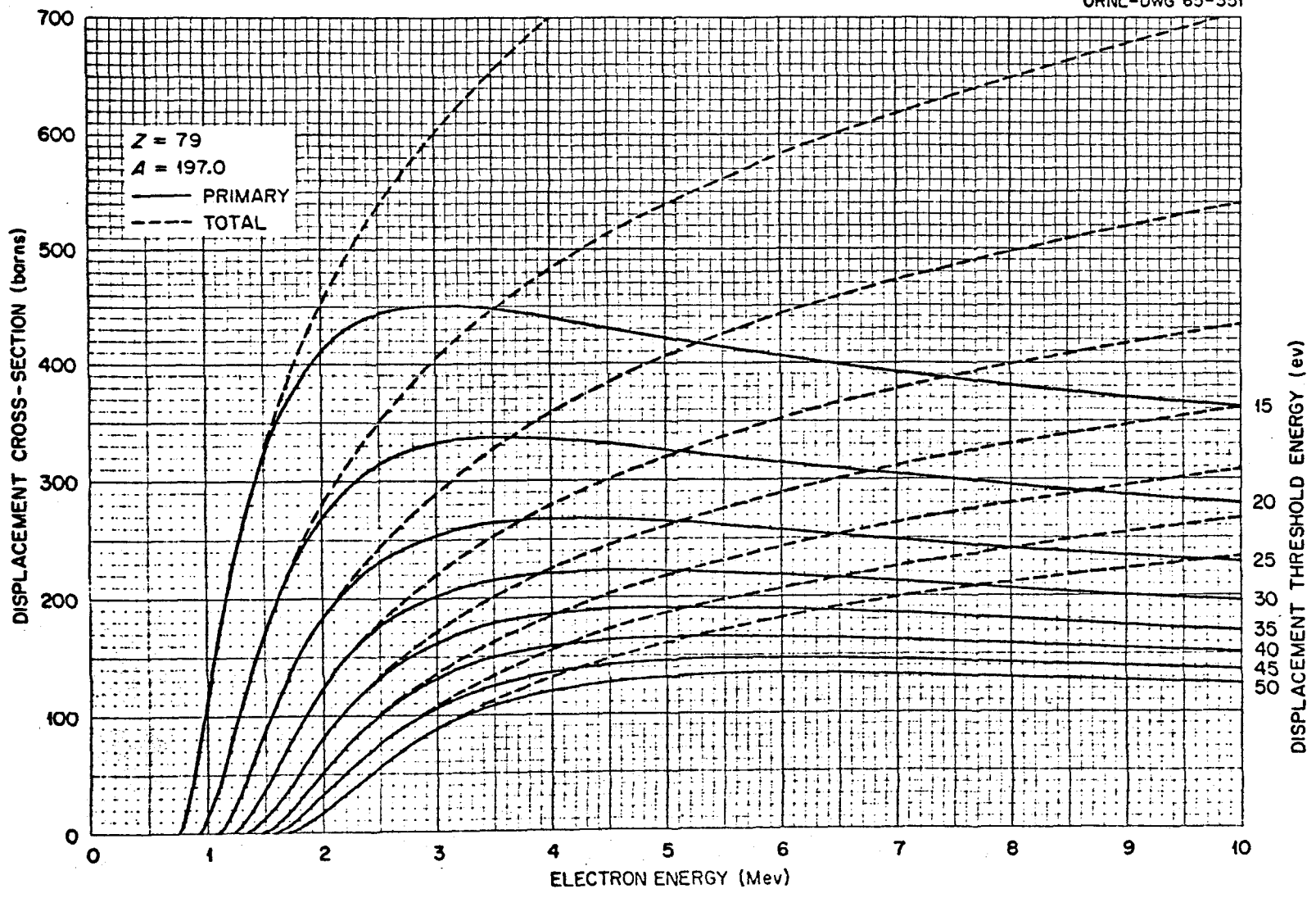


Fig. 2



Fig. 3

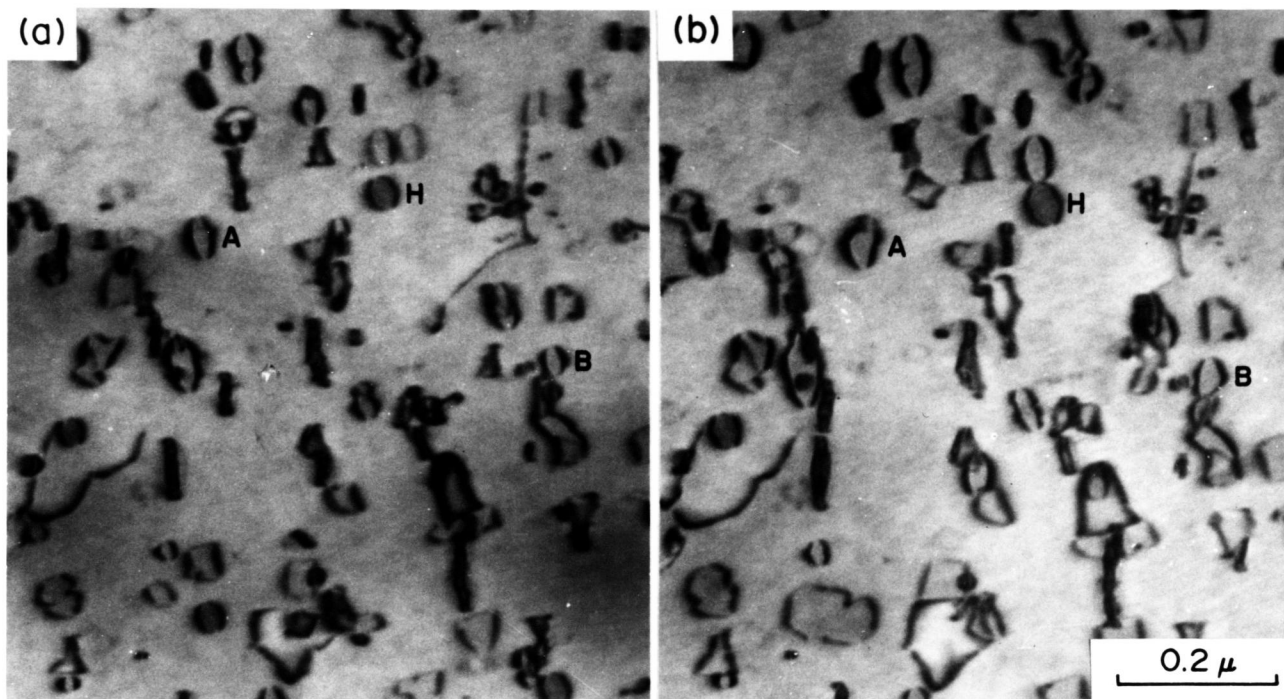


Fig. 4

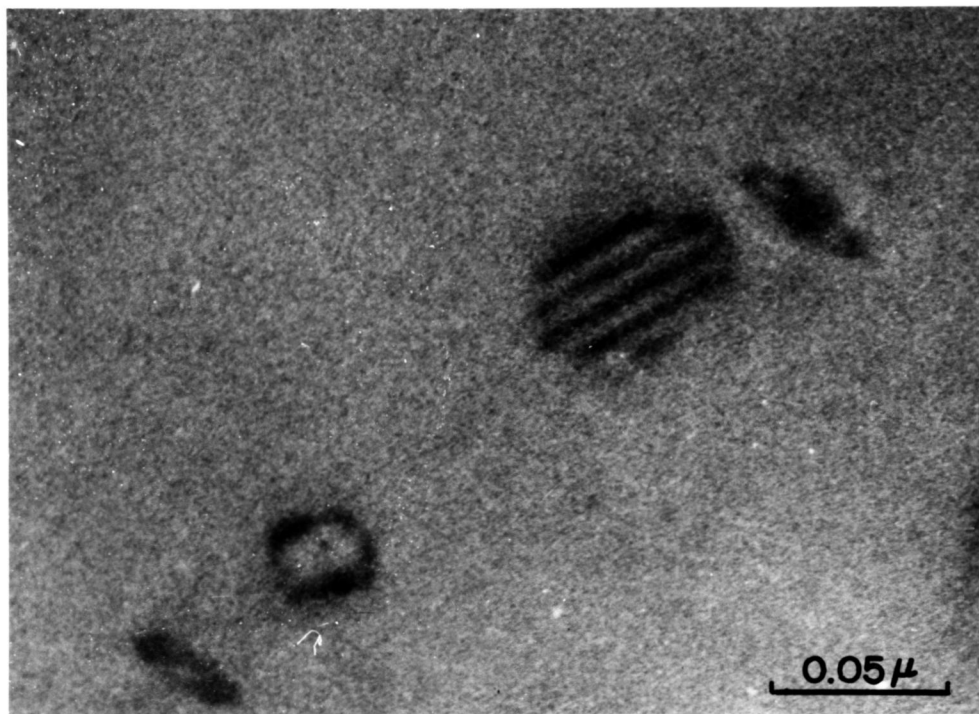


Fig. 5

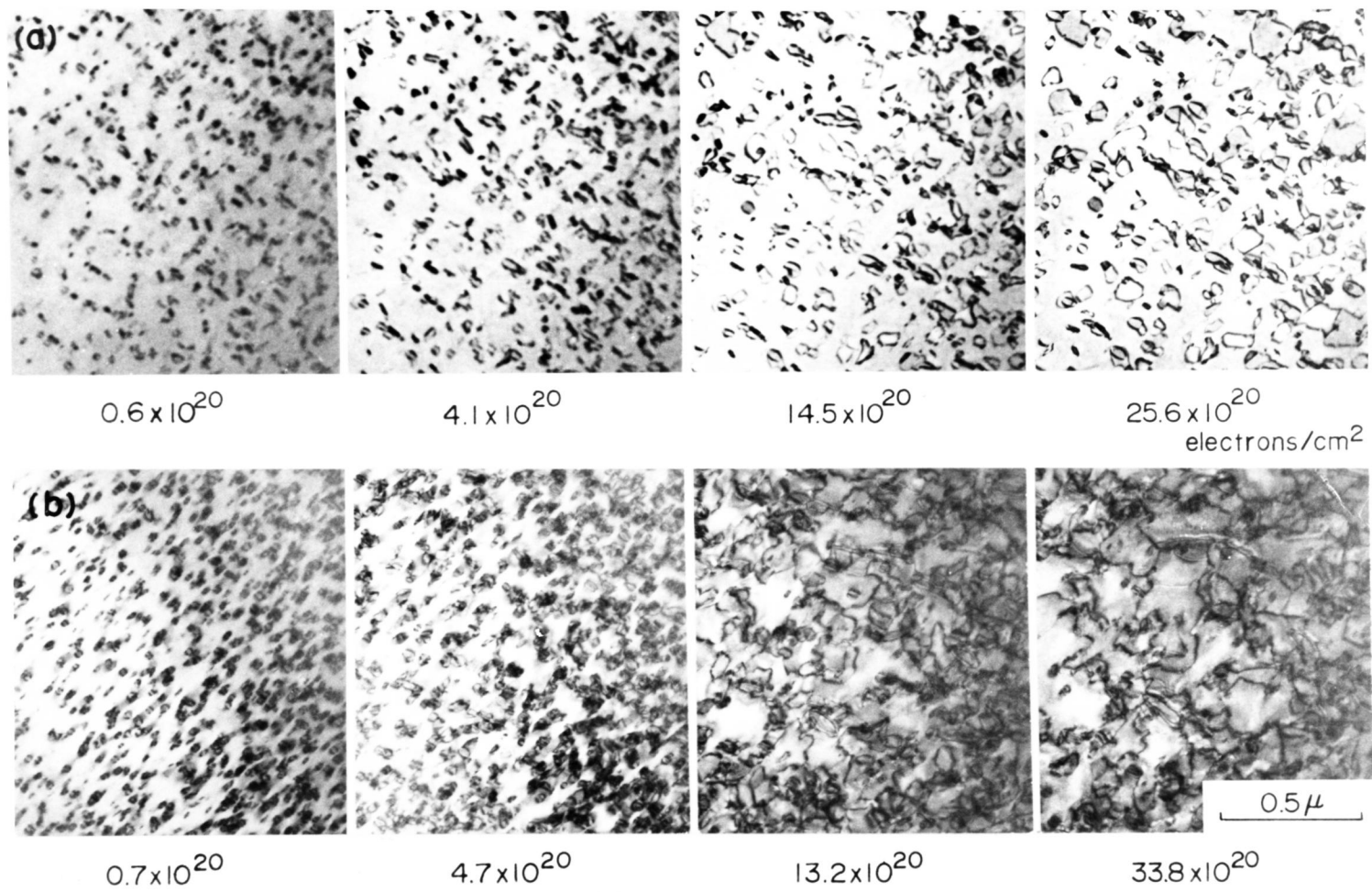


Fig. 6

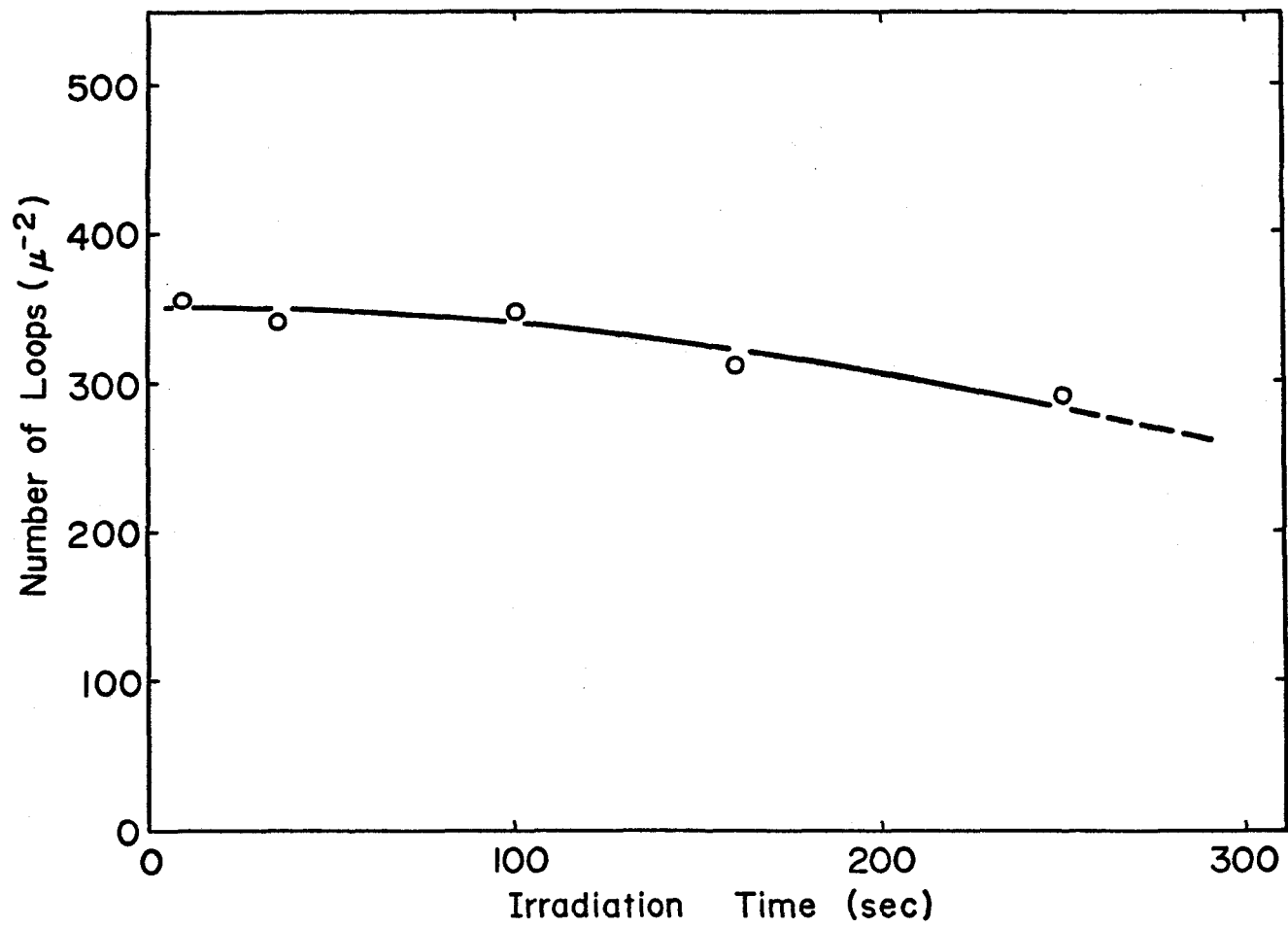


Fig. 7

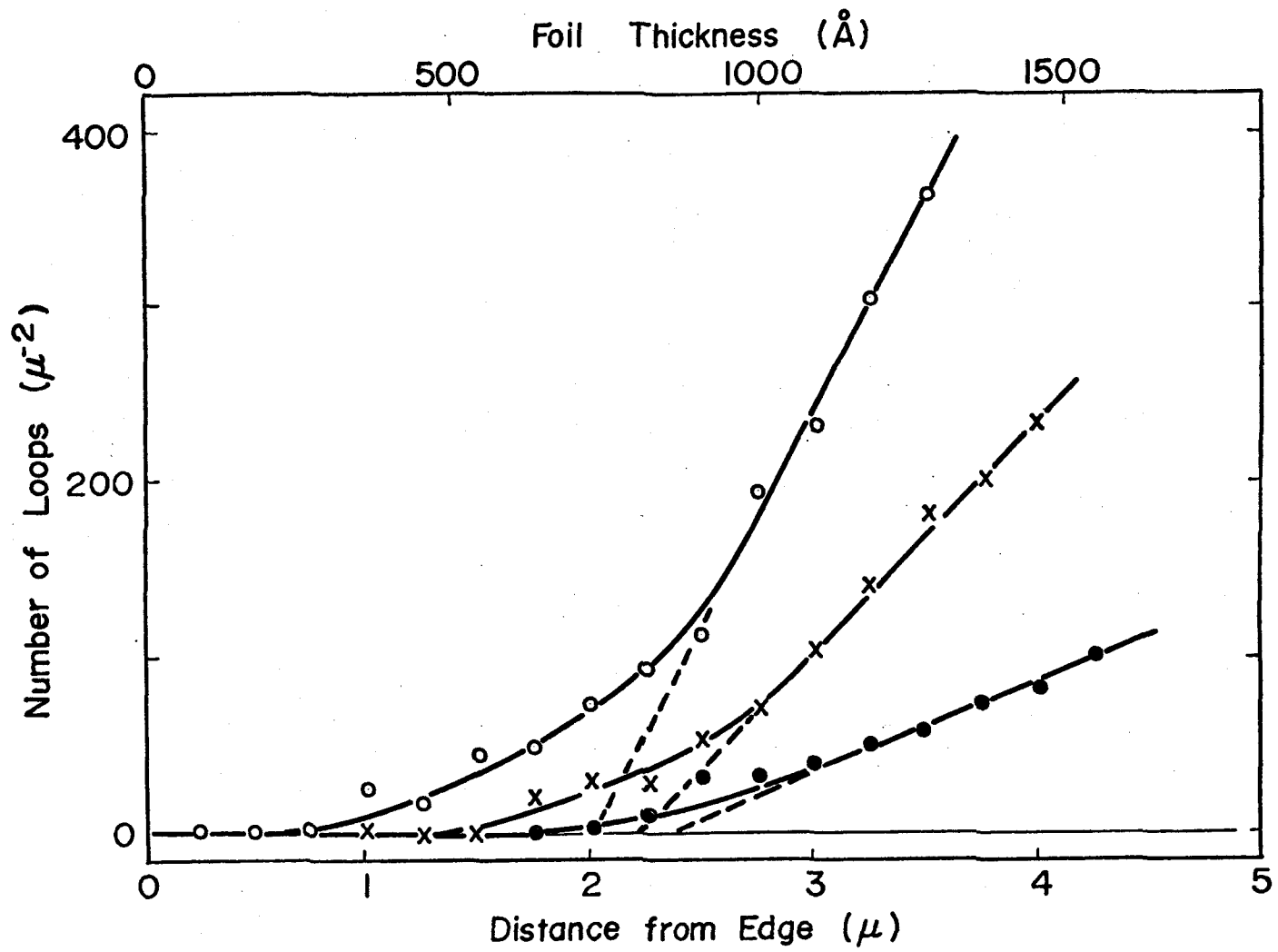


Fig. 8

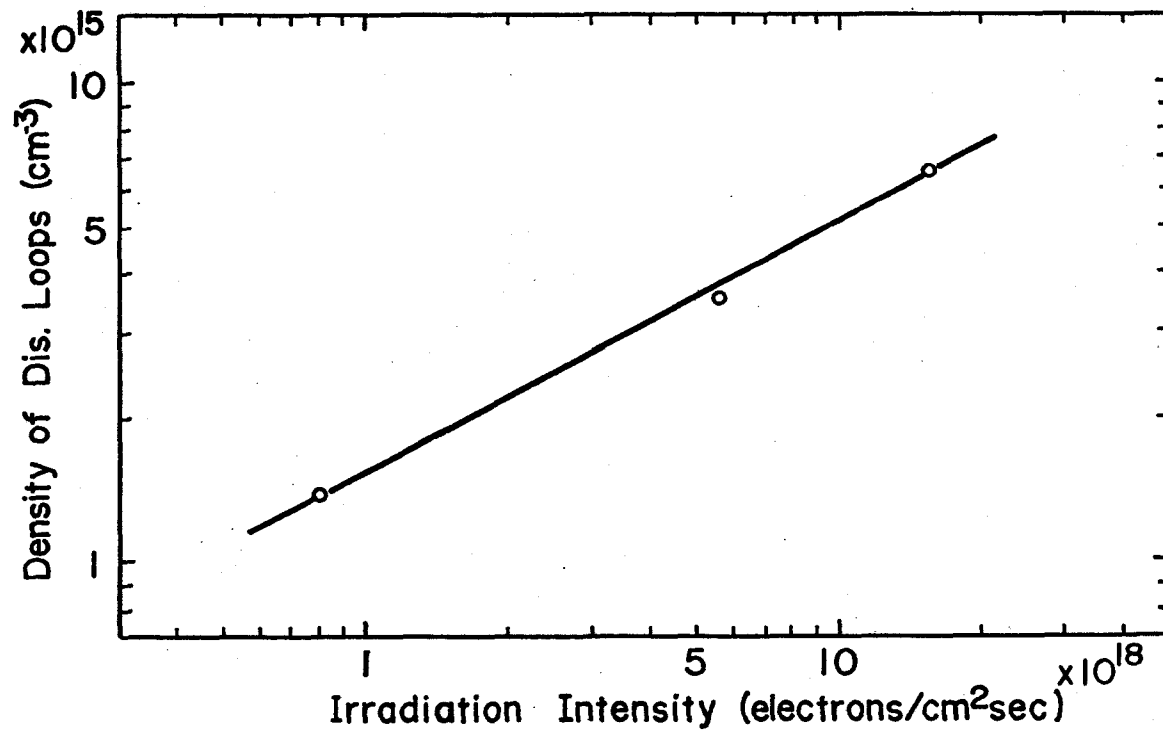


Fig. 9

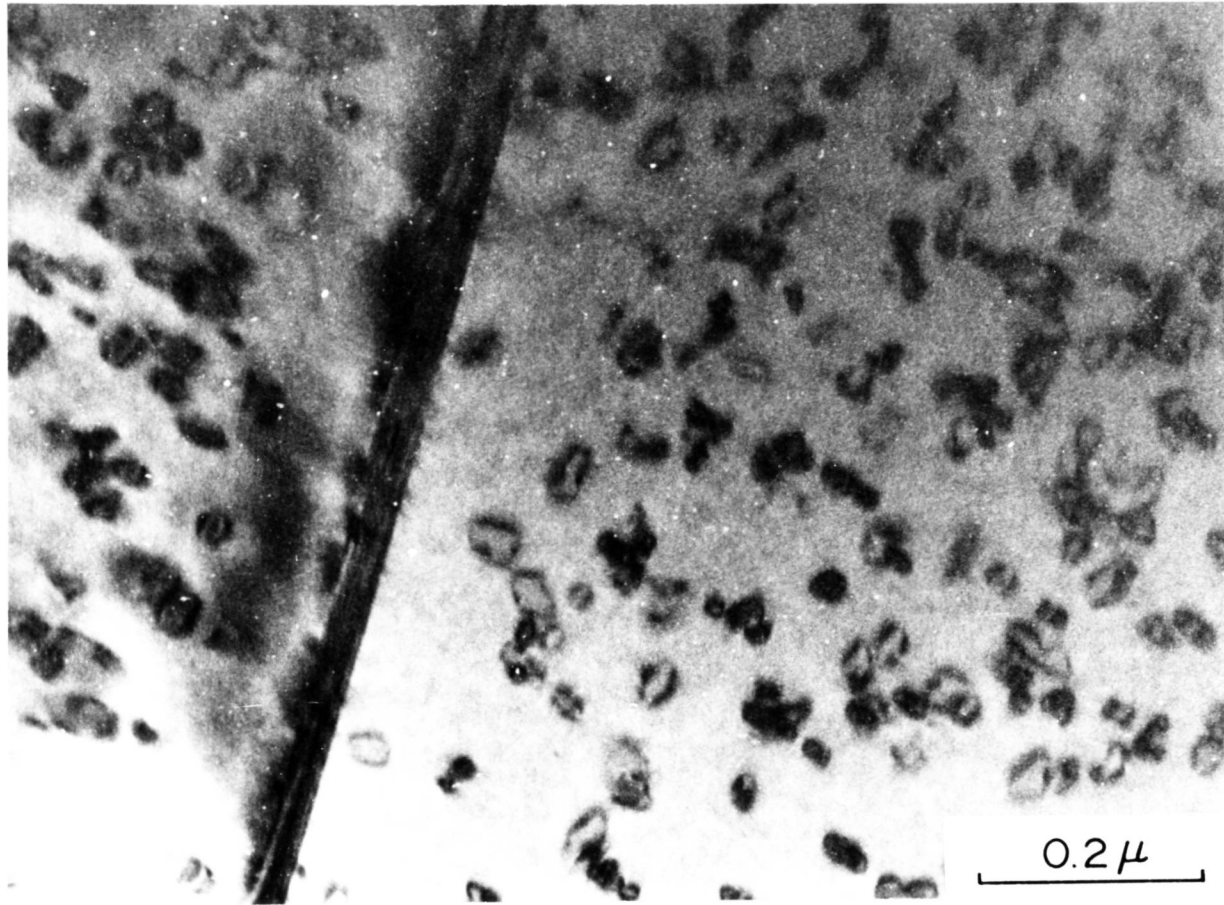


Fig. 10

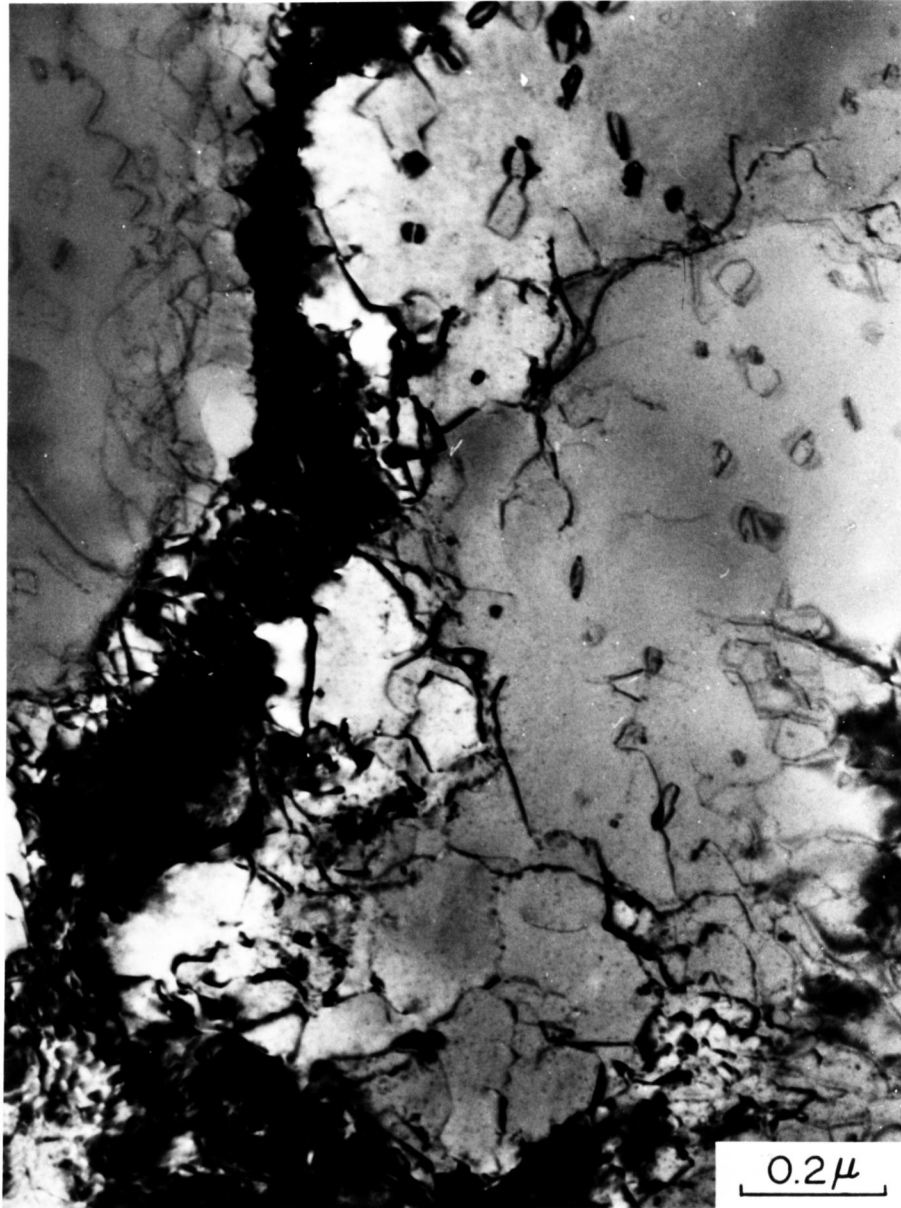


Fig. 11

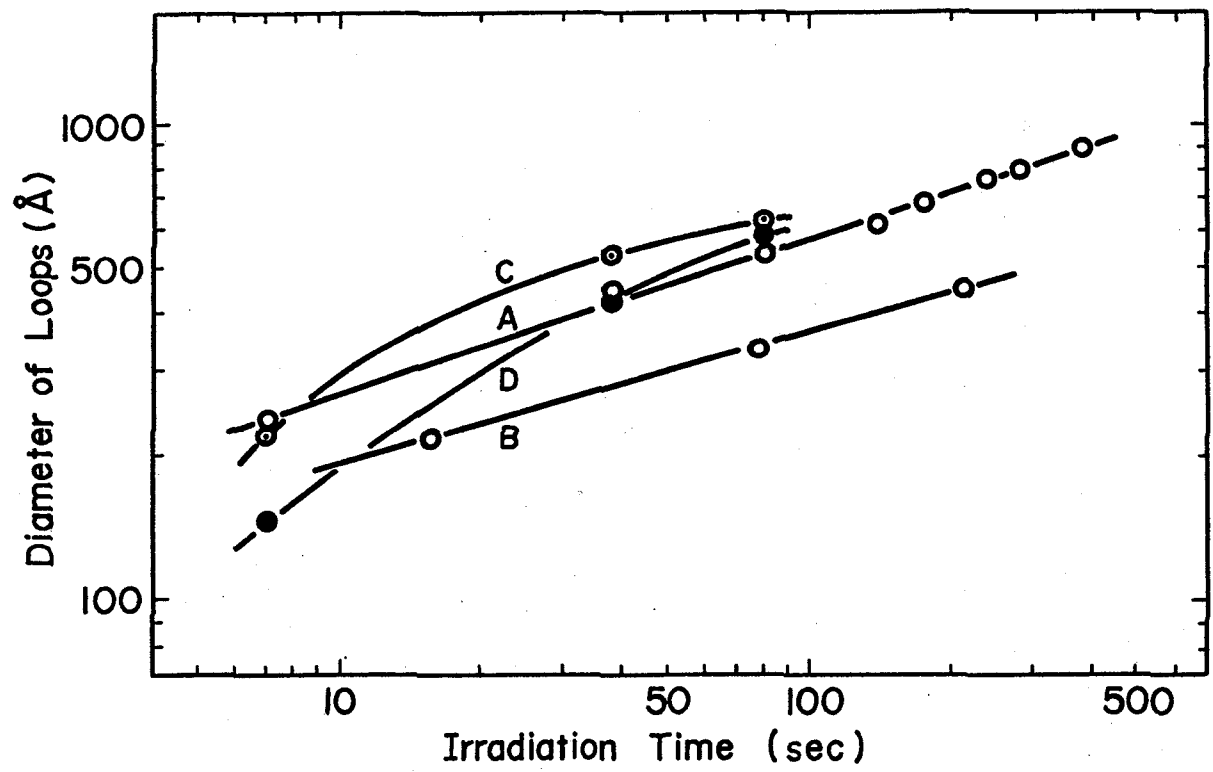


Fig. 12

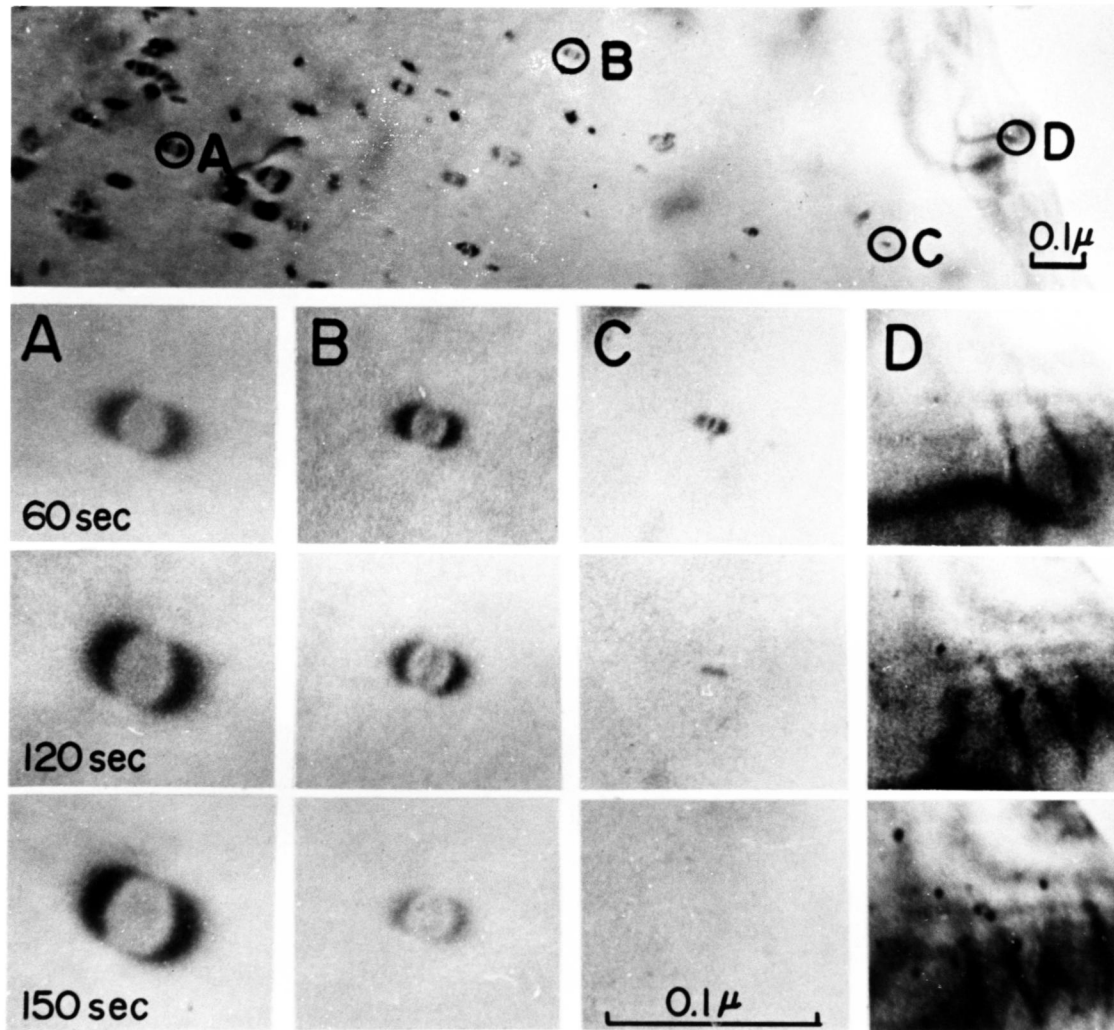


Fig. 13

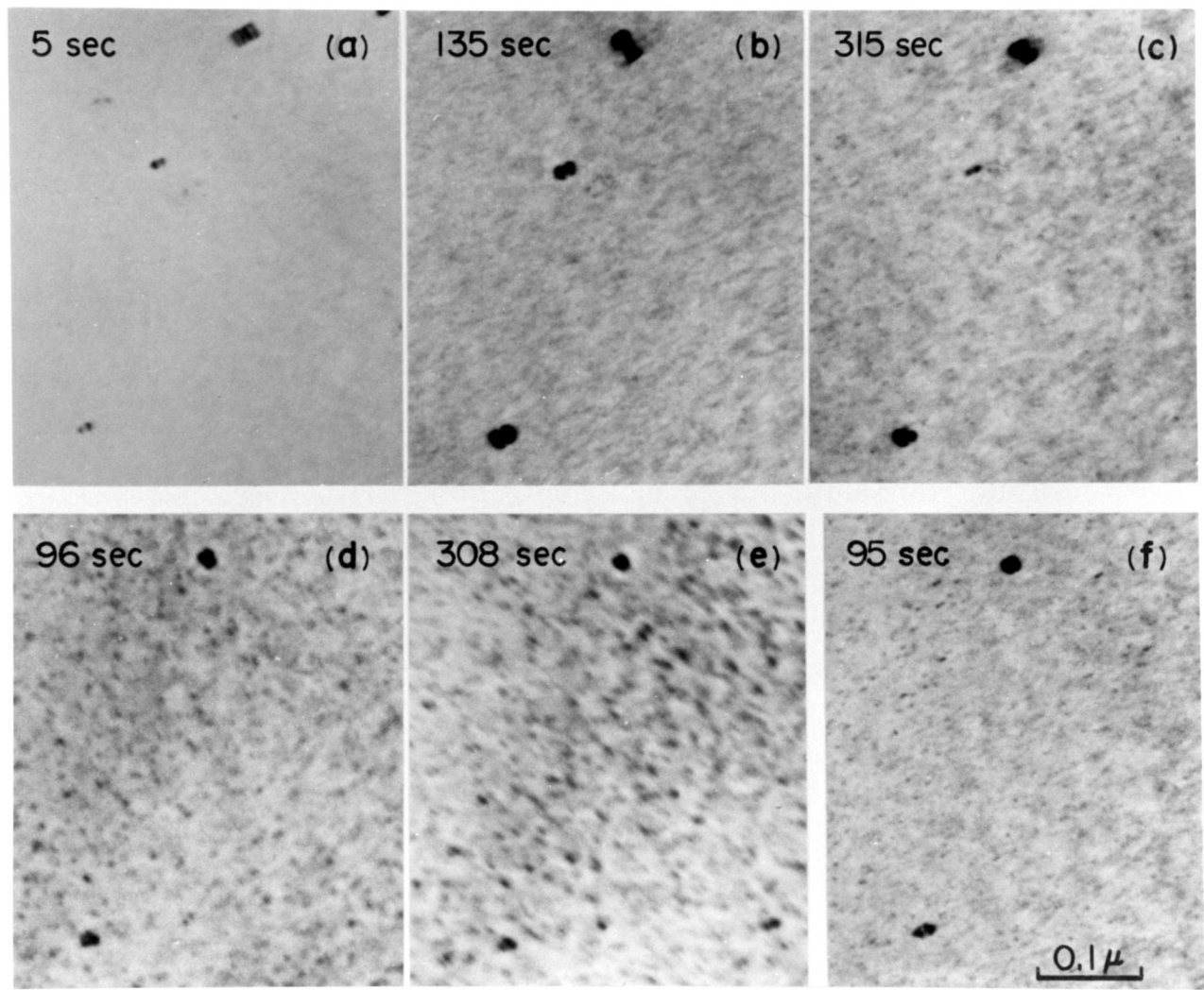


Fig. 14

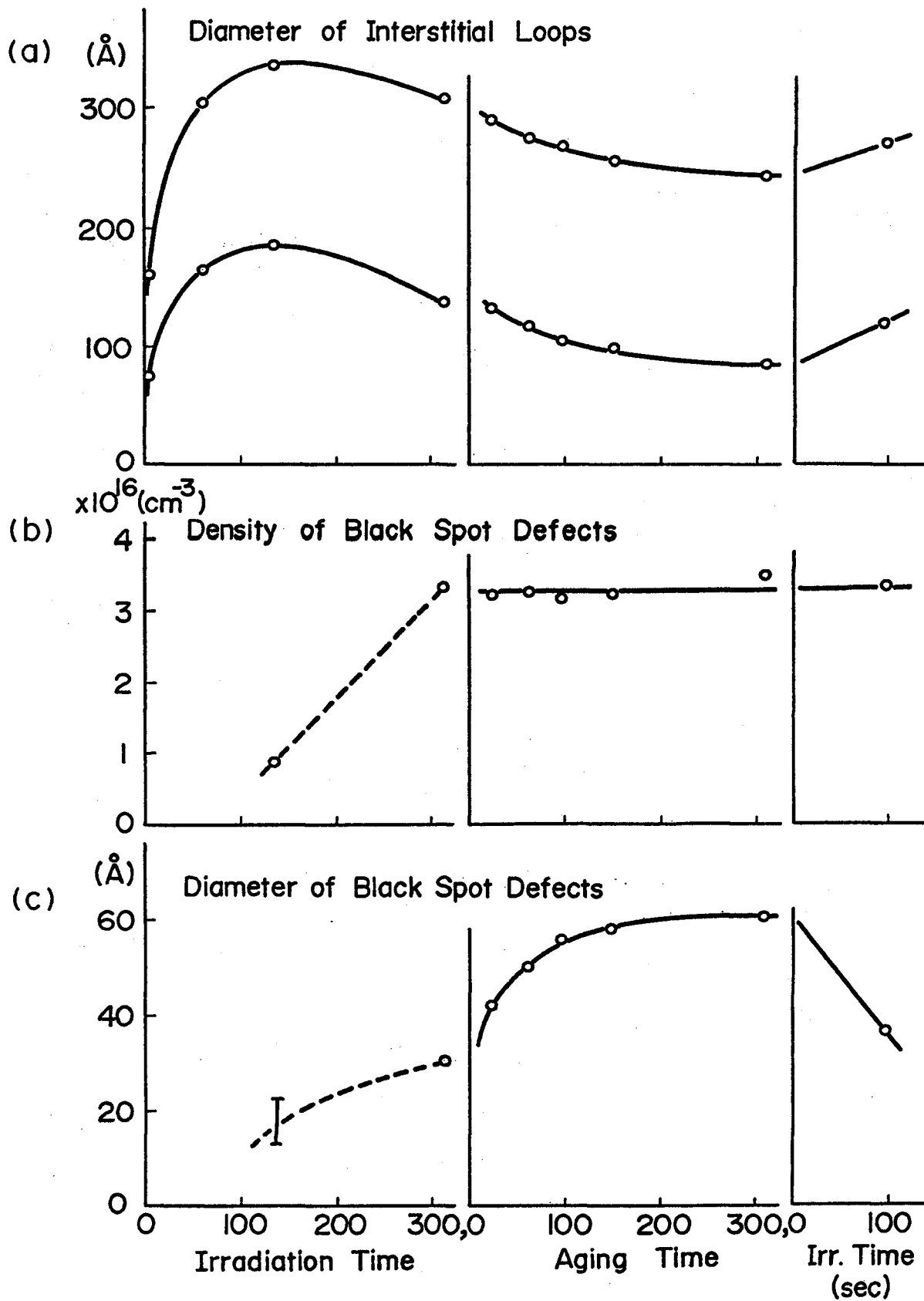


Fig. 15

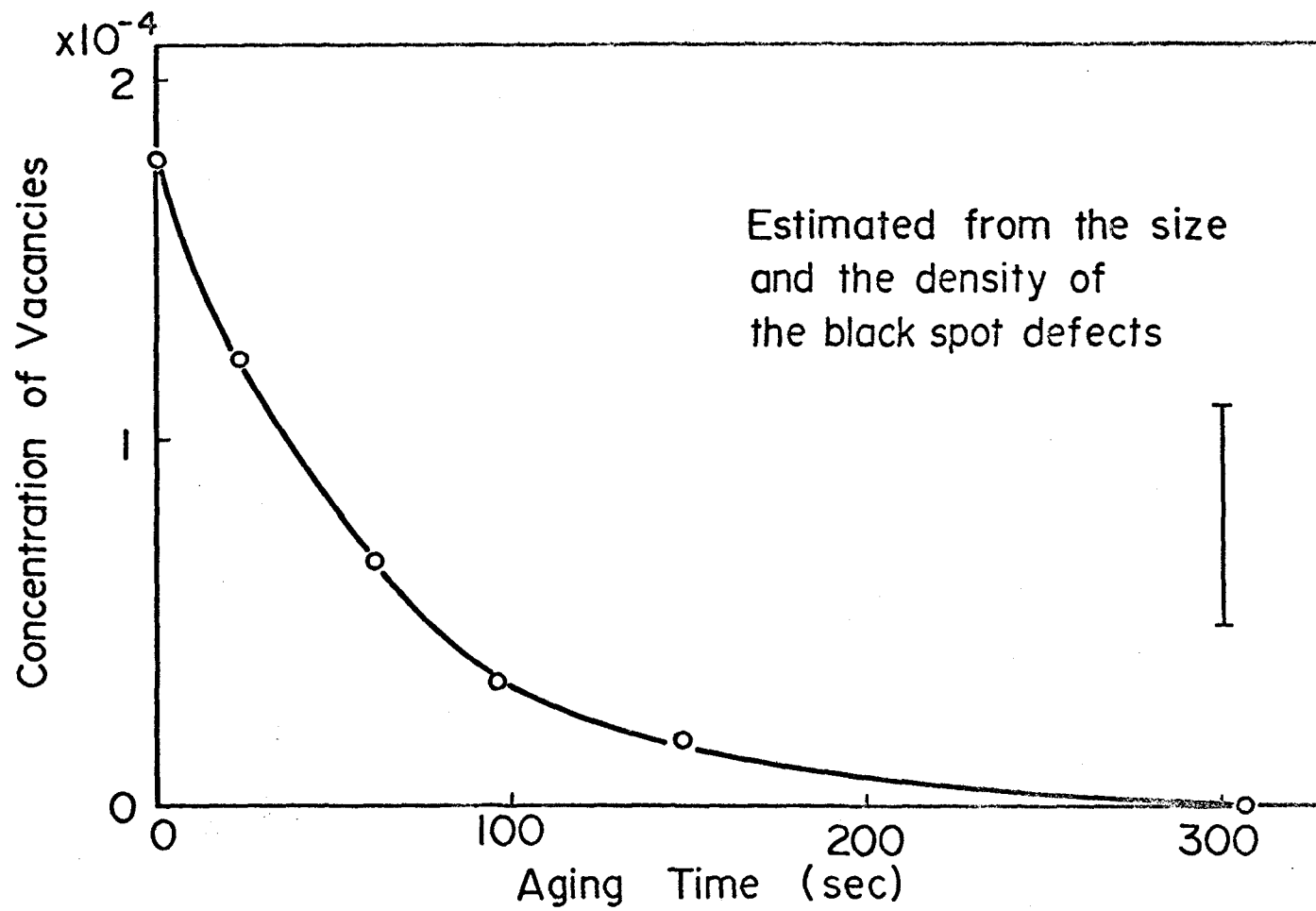


Fig. 16

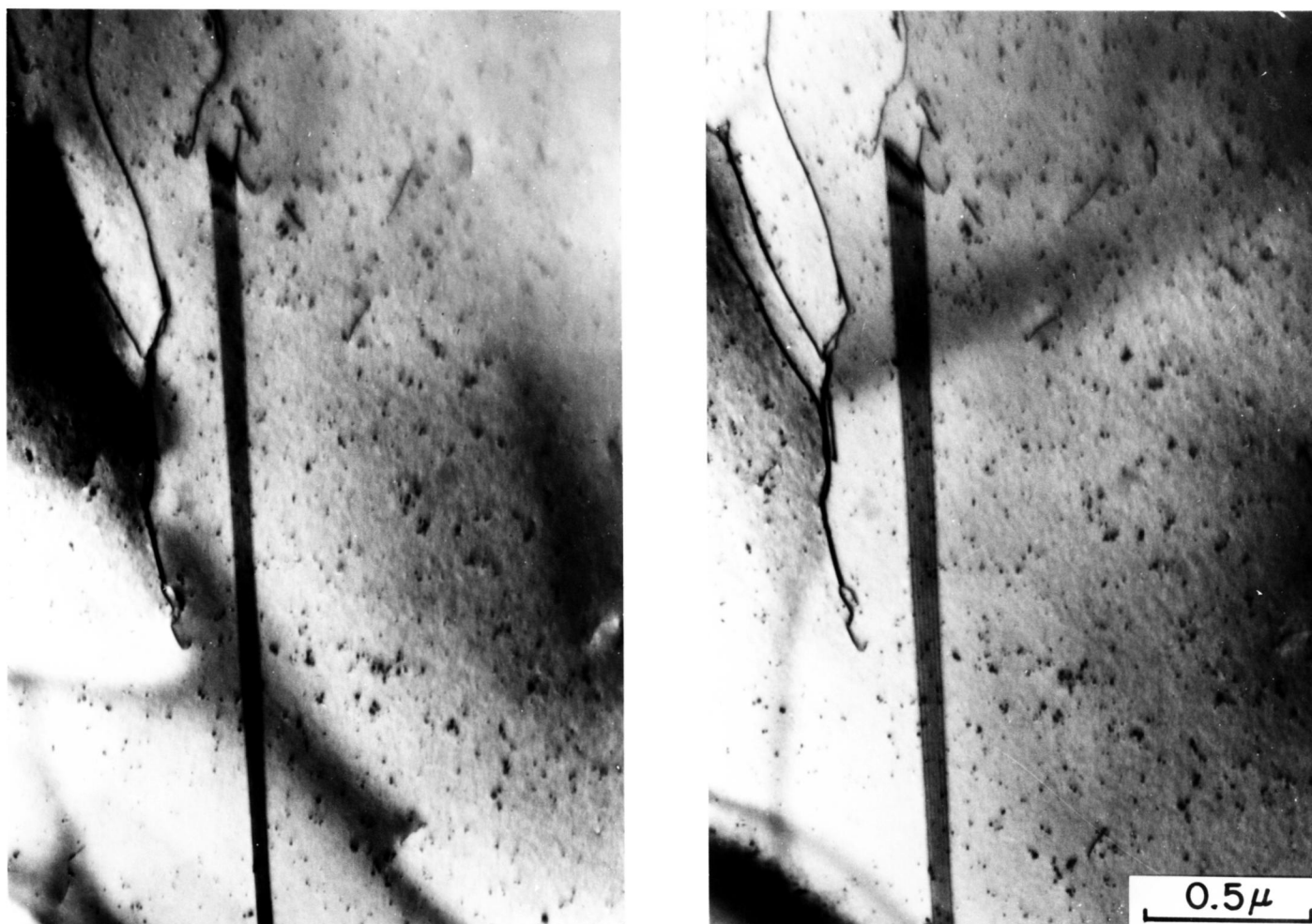


Fig. 17

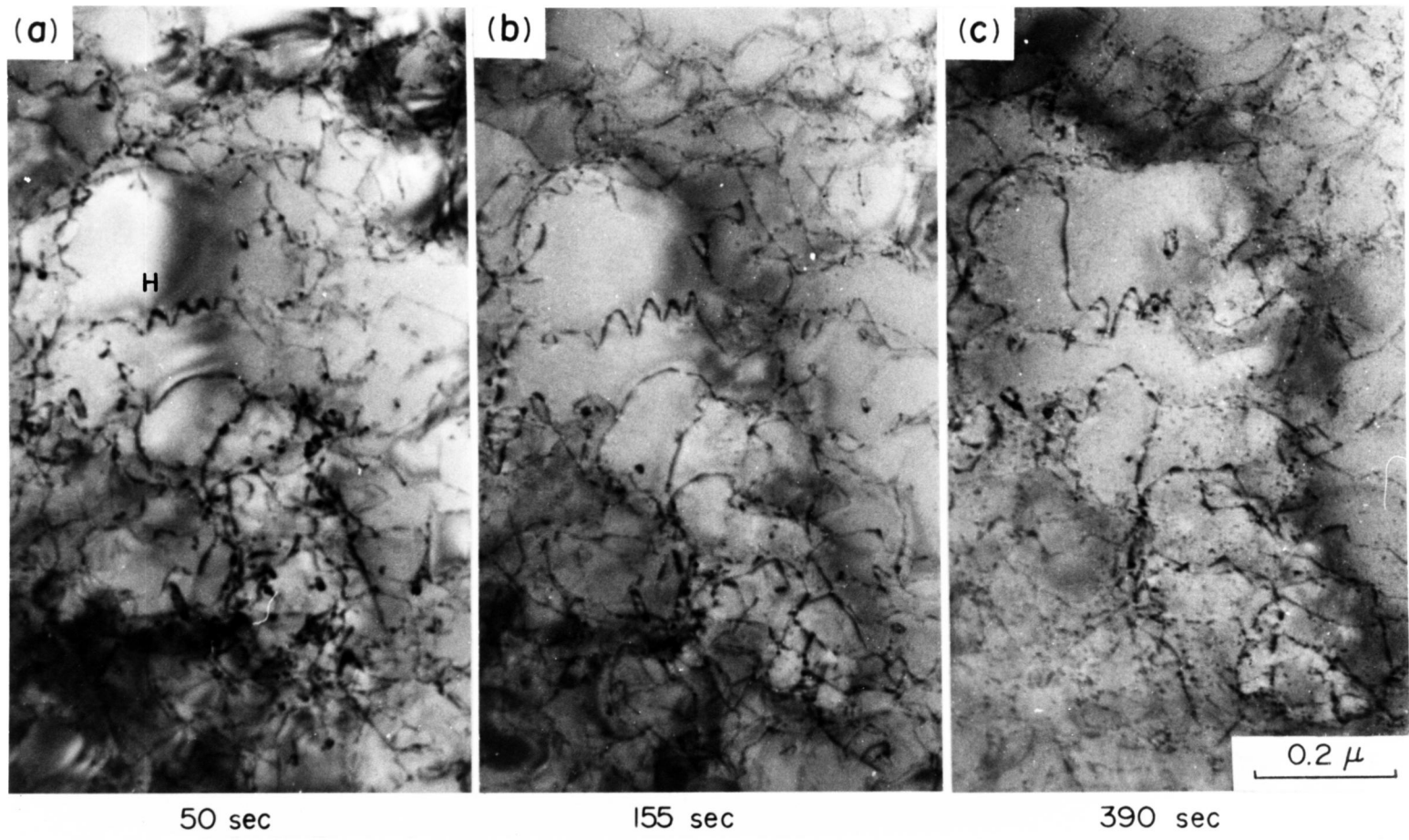


Fig. 18

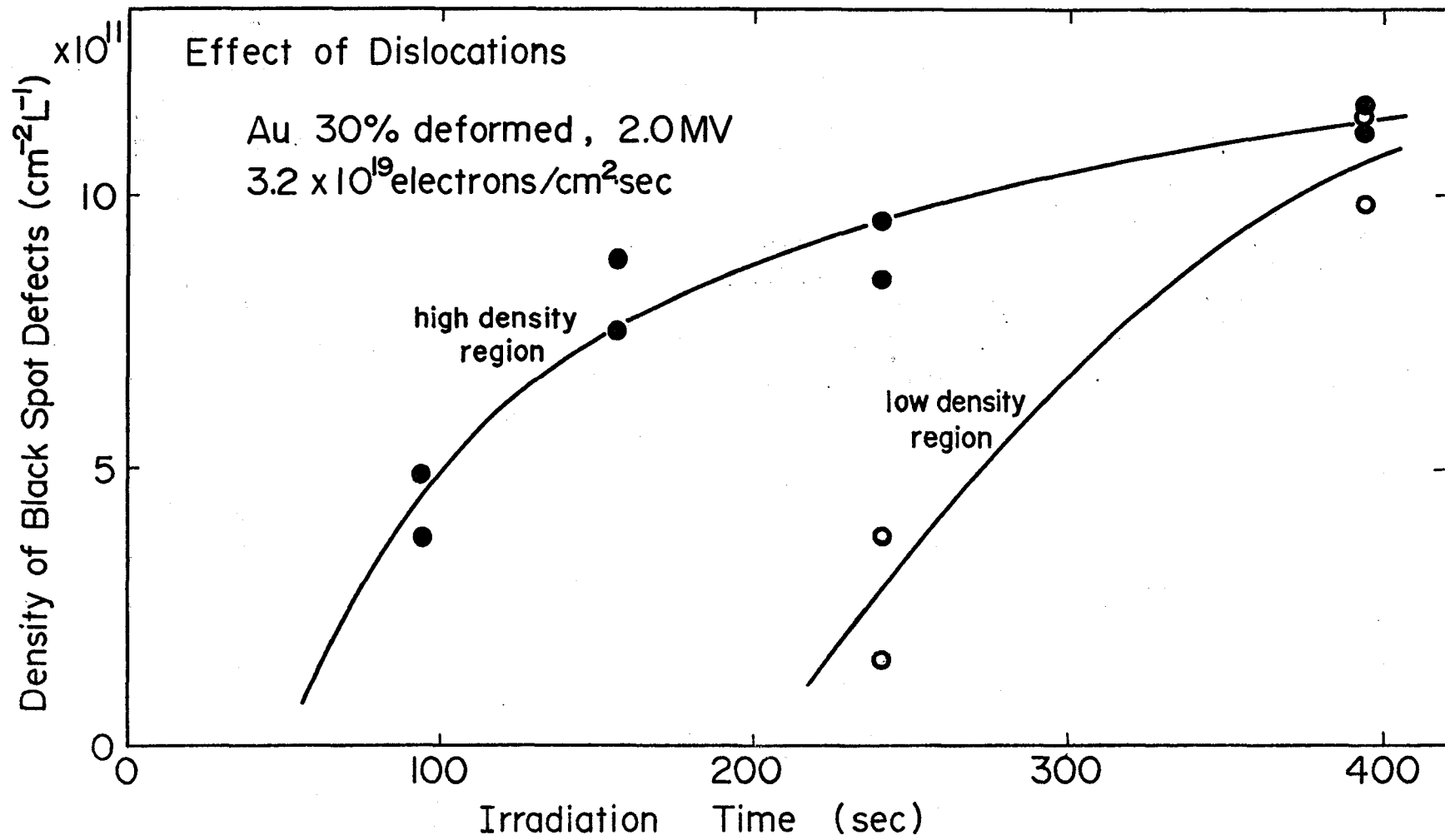


Fig. 19

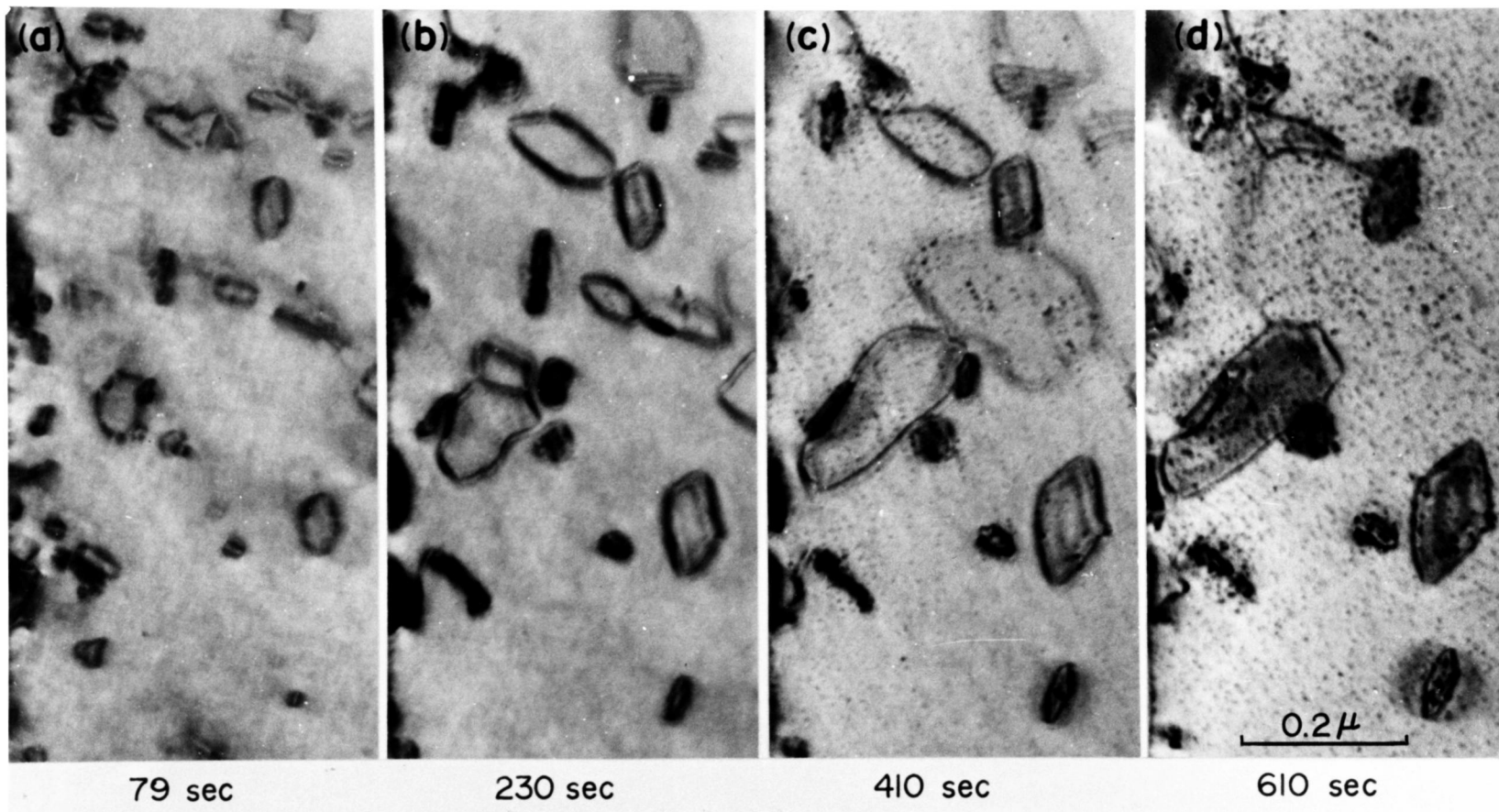


Fig. 20

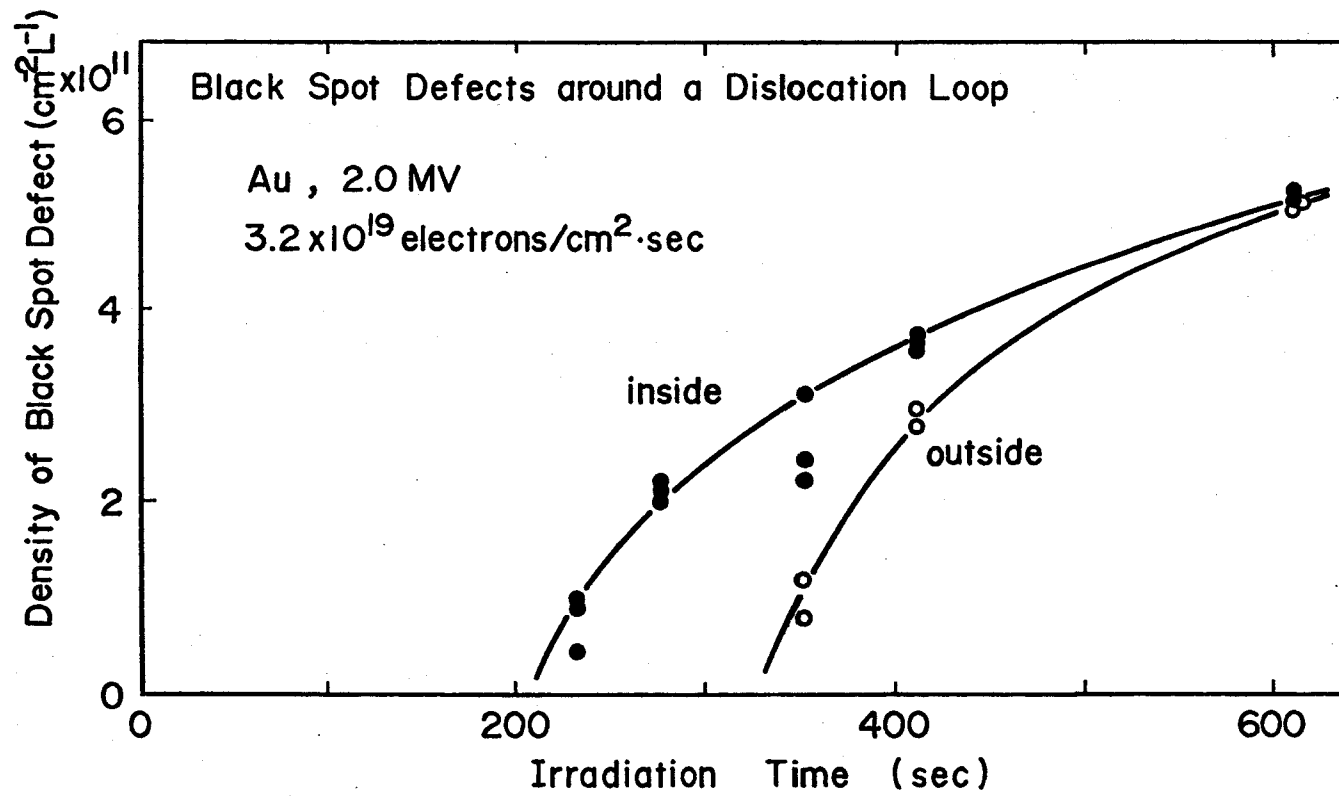


Fig. 21

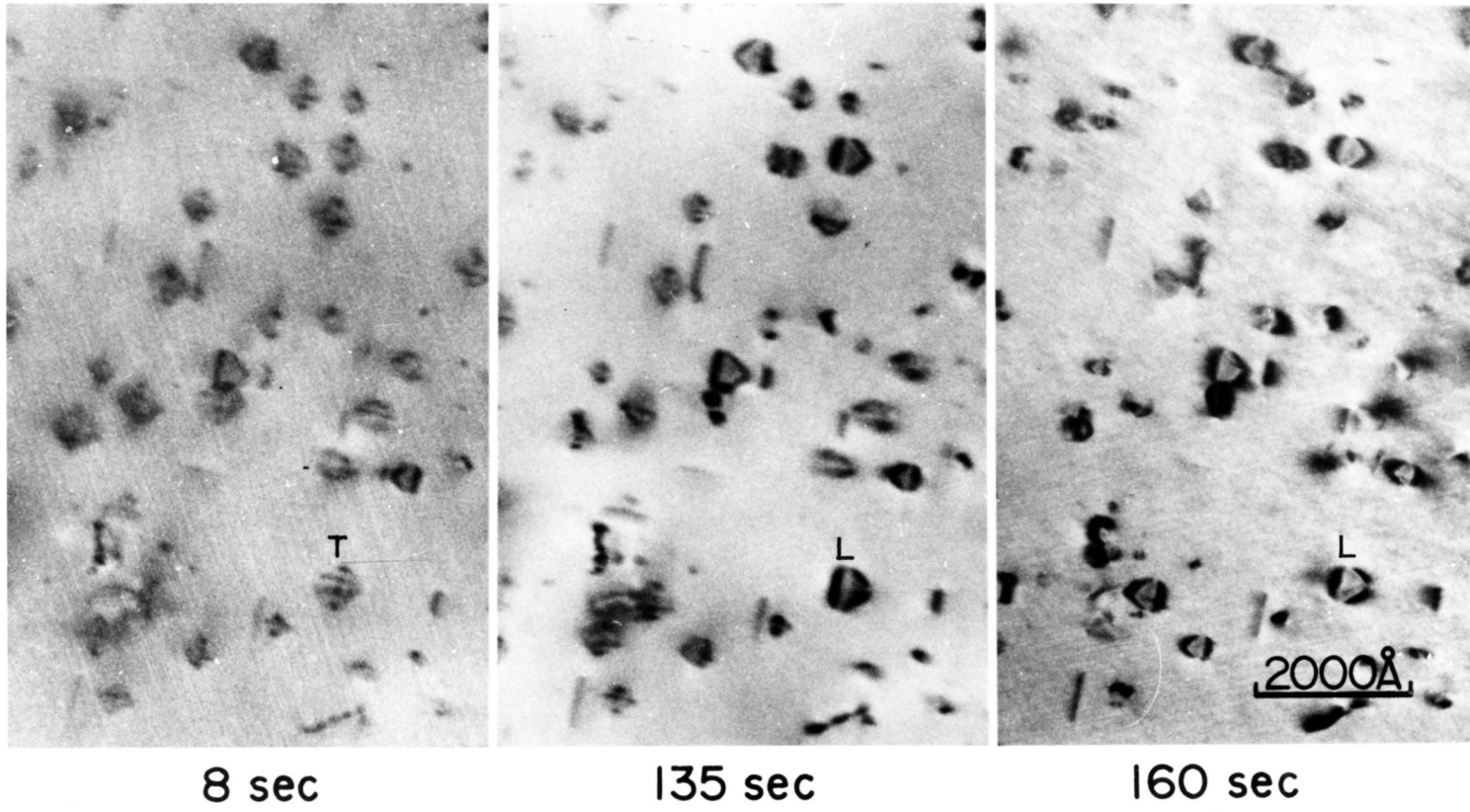


Fig. 22

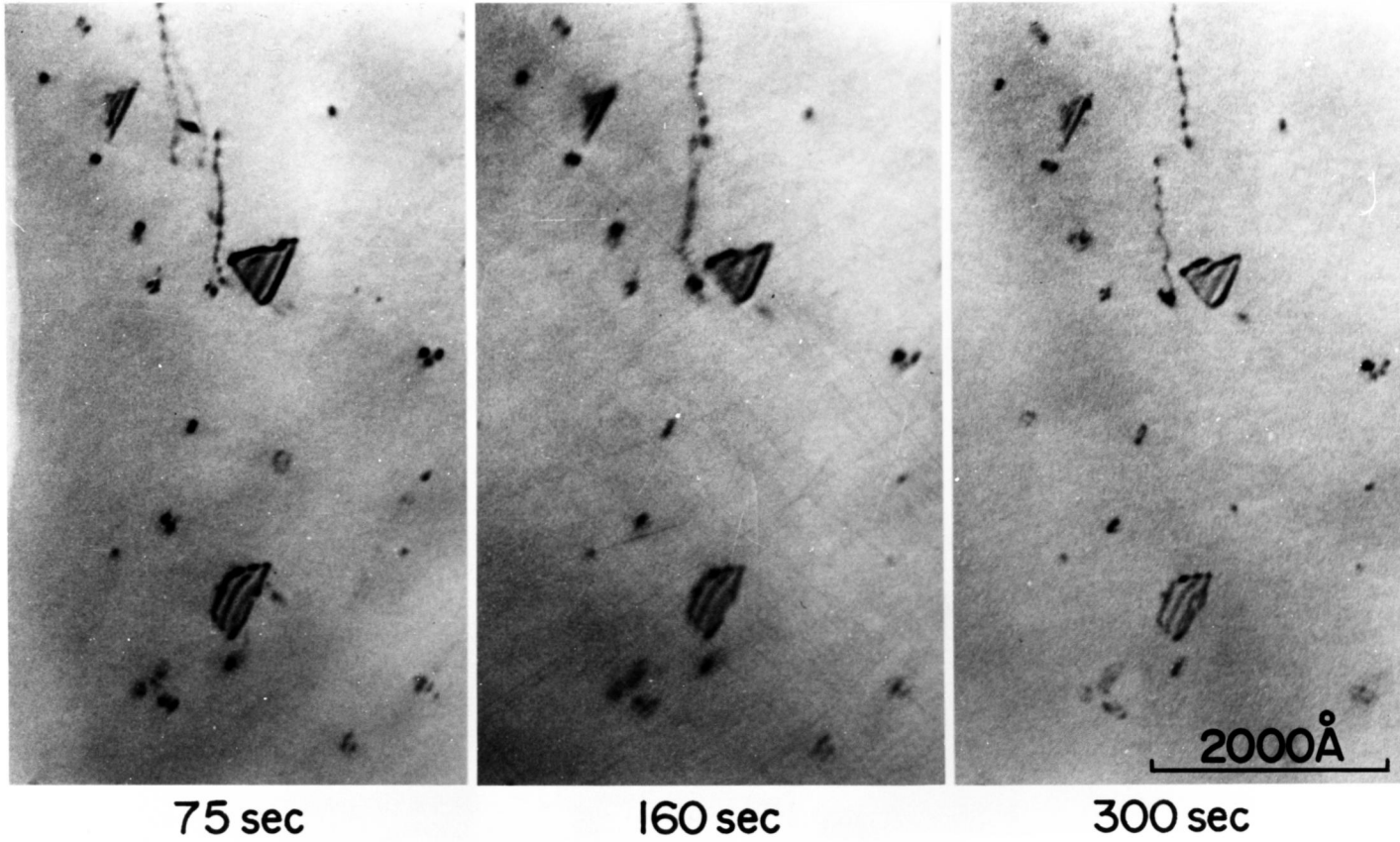


Fig. 23

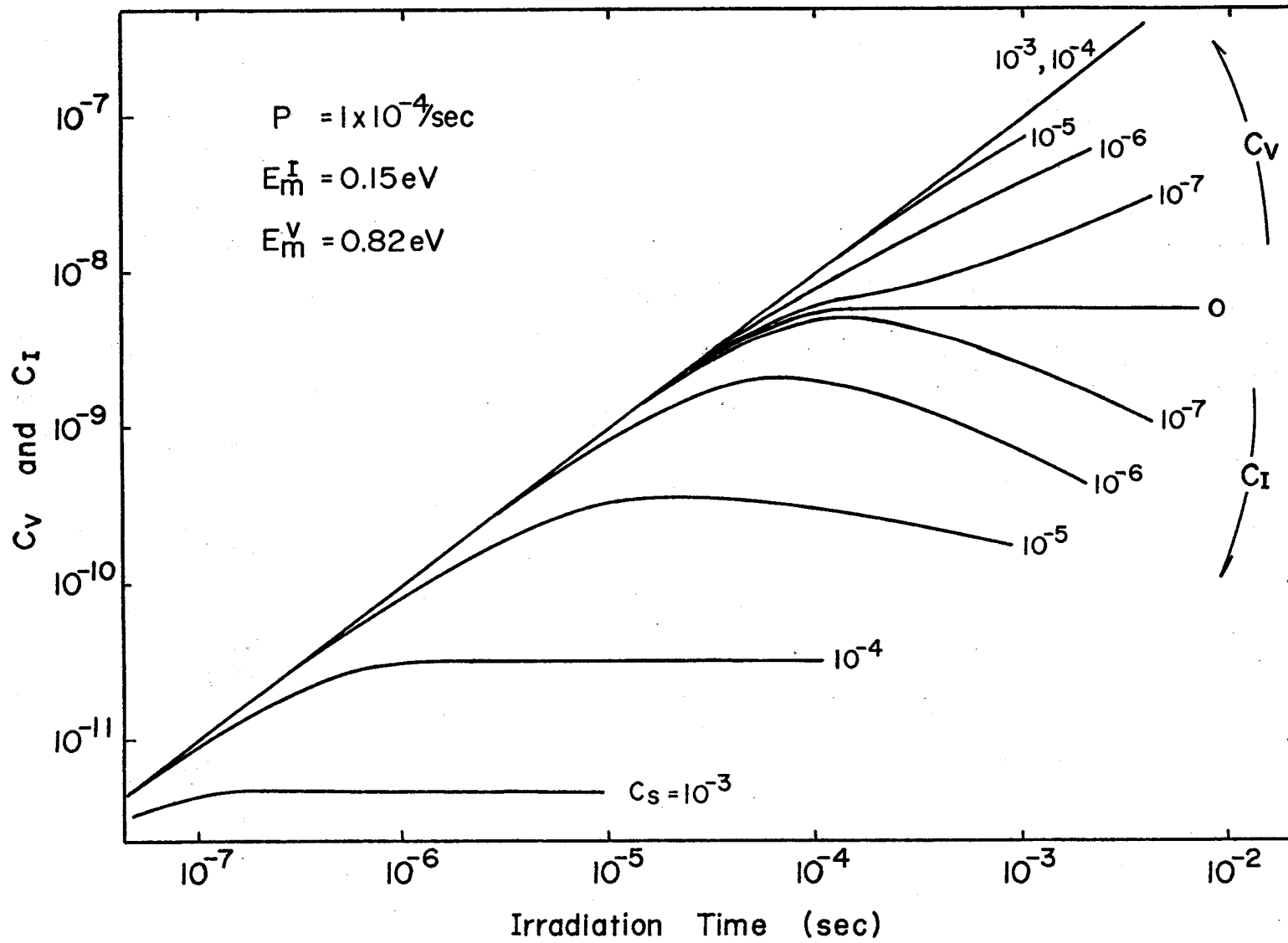
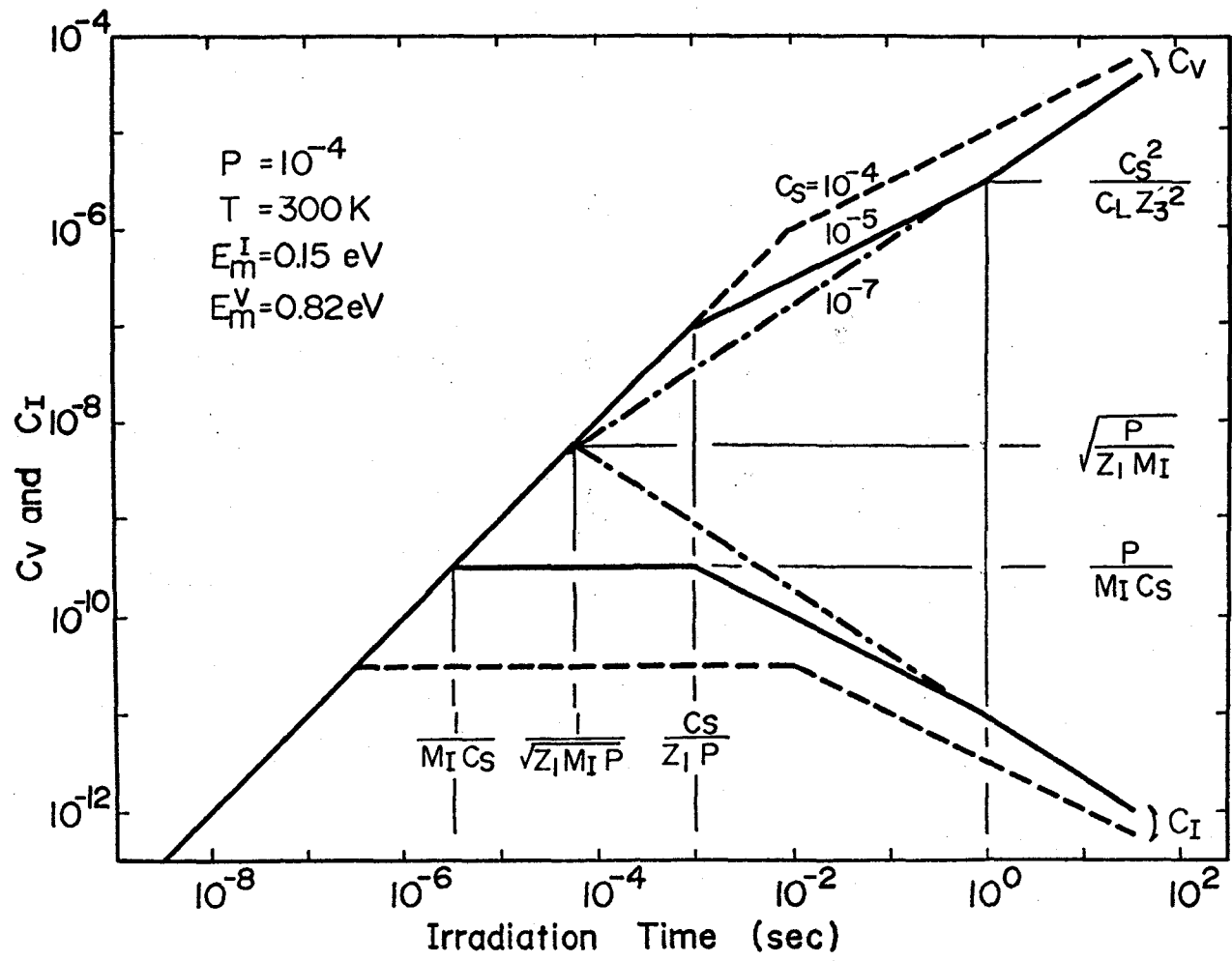


Fig. 24



$C_V \propto t$	$t$	$t^{1/2}$	$t^{2/3}$
$C_I \propto t$	const.	$t^{-1/2}$	$t^{-2/3}$

Fig. 25

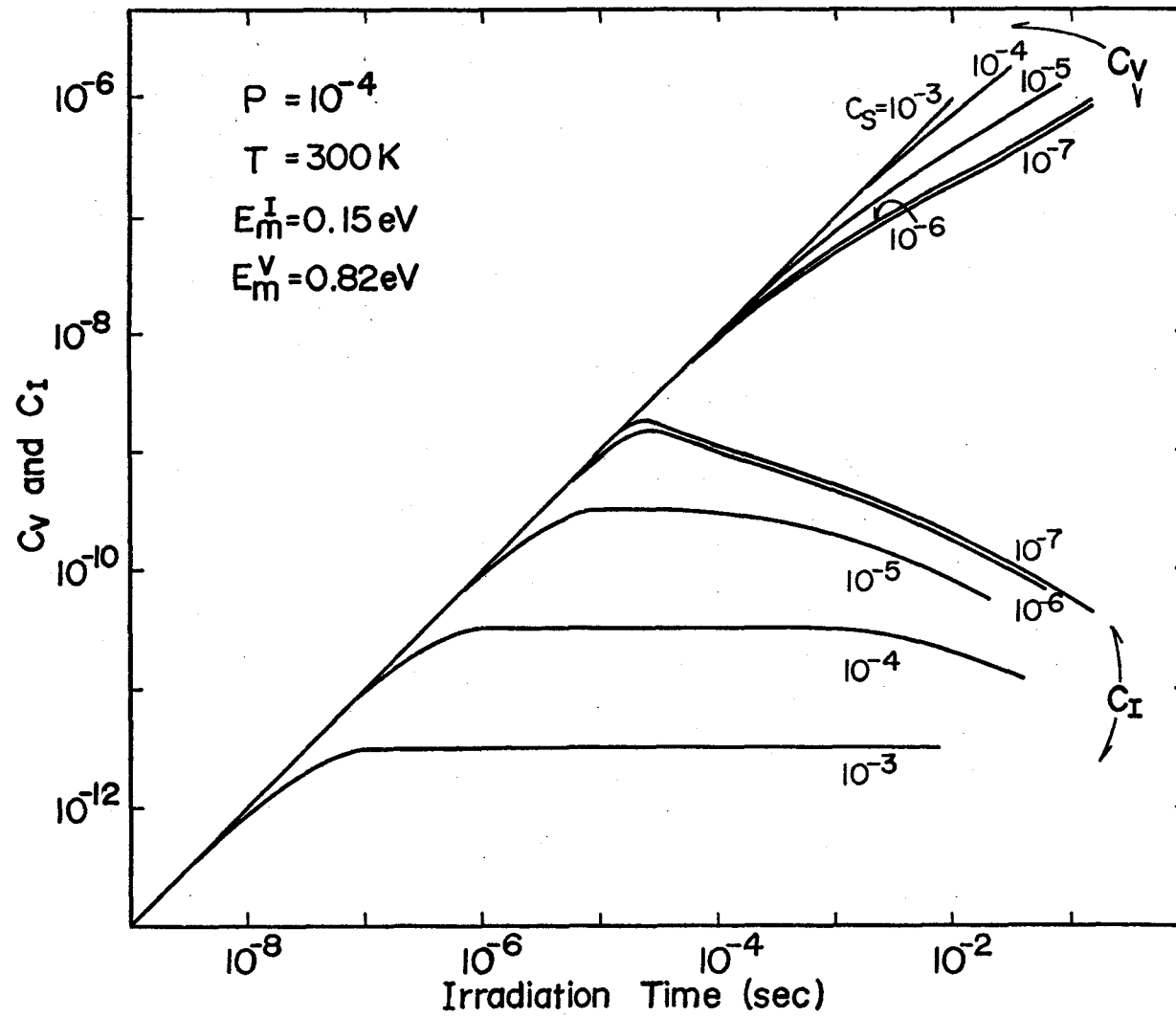


Fig. 26

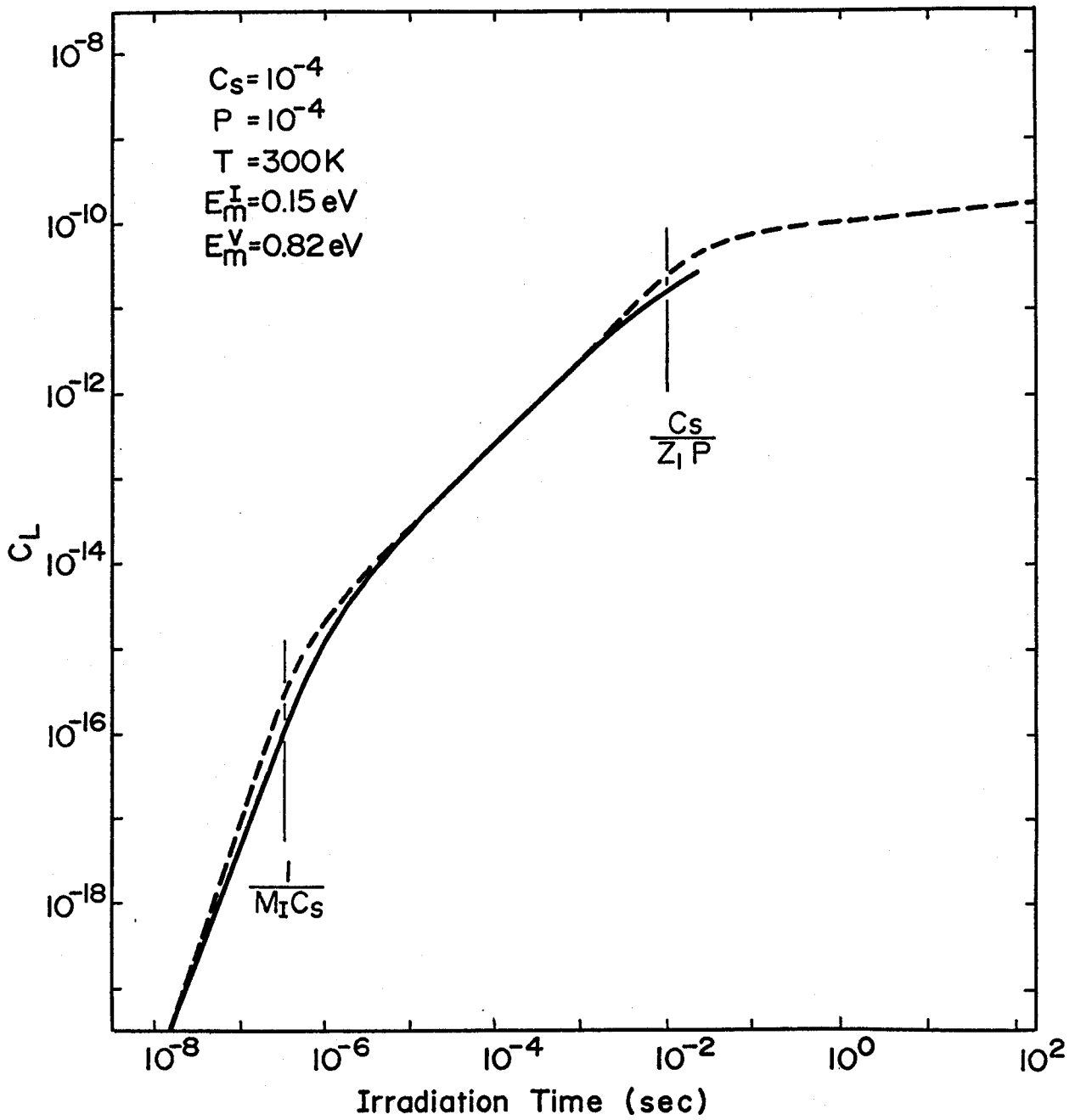


Fig. 27

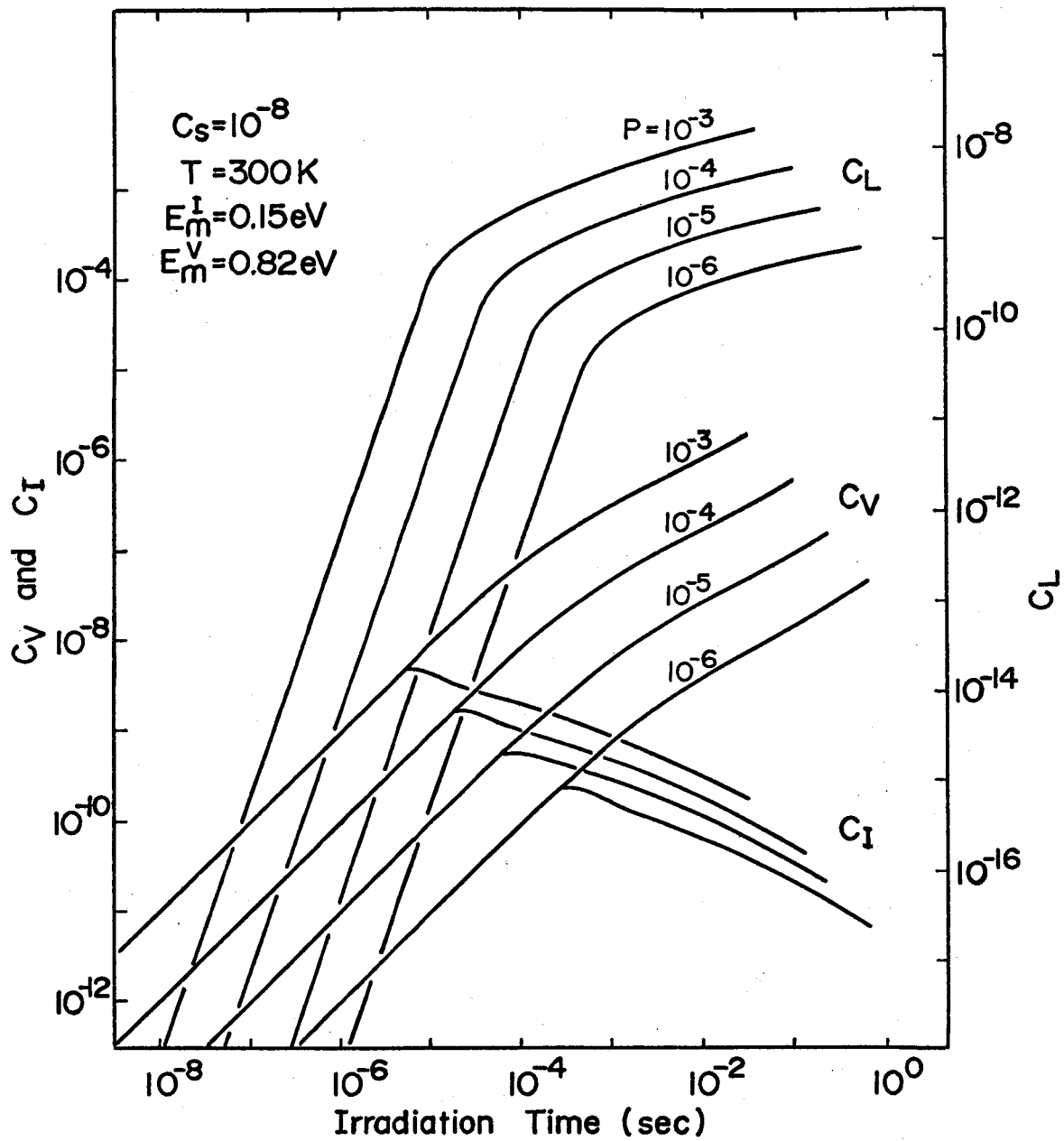


Fig. 28

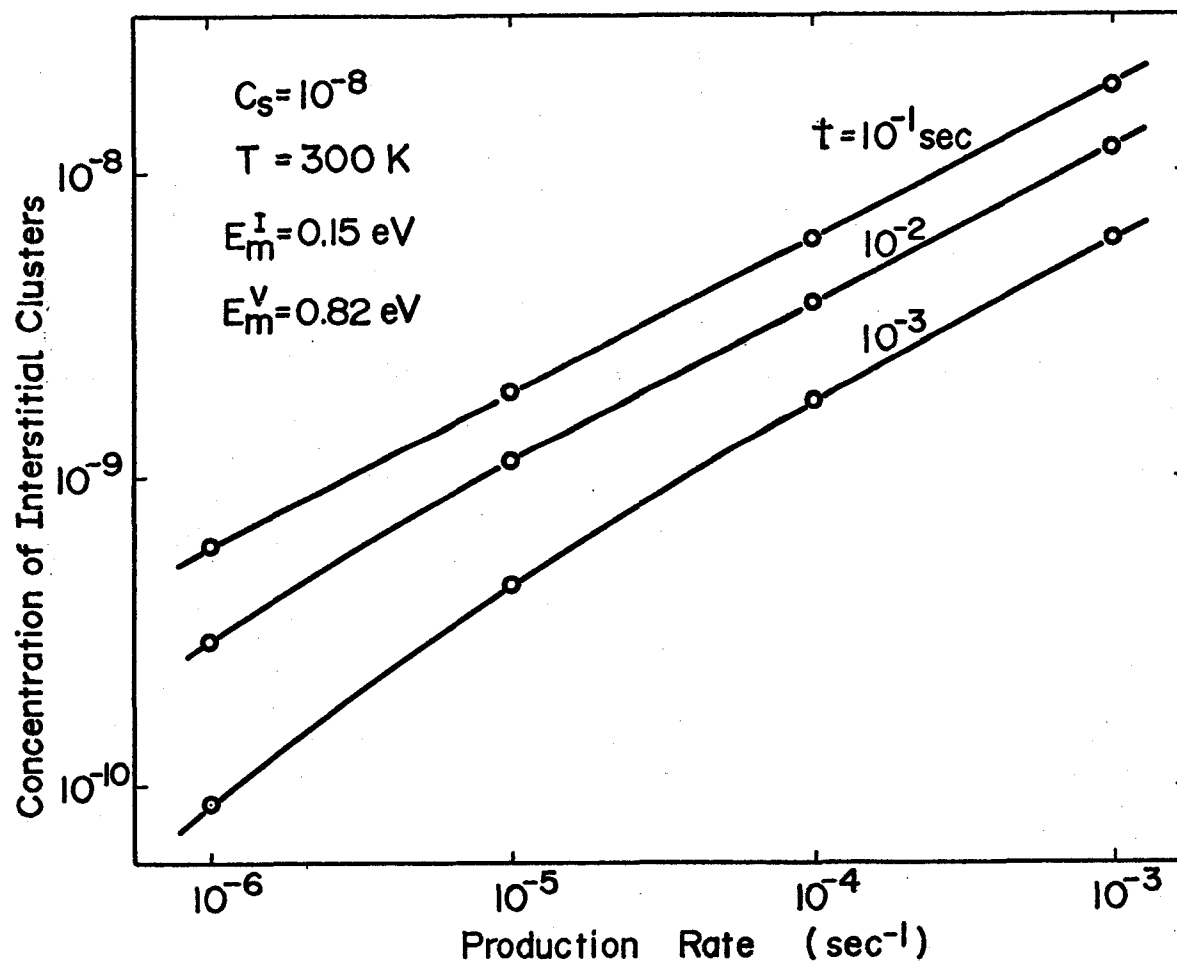


Fig. 29

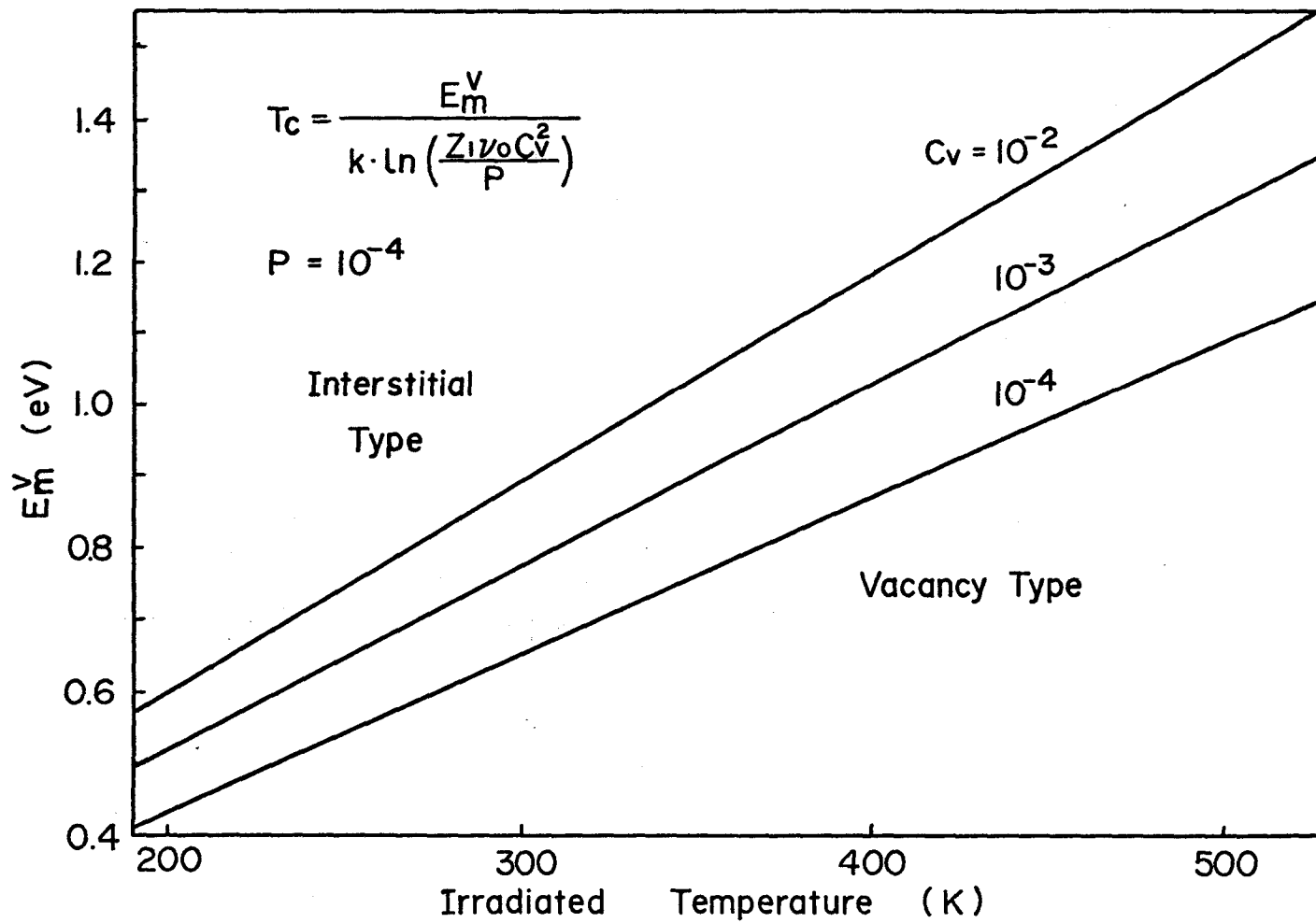


Fig. 30

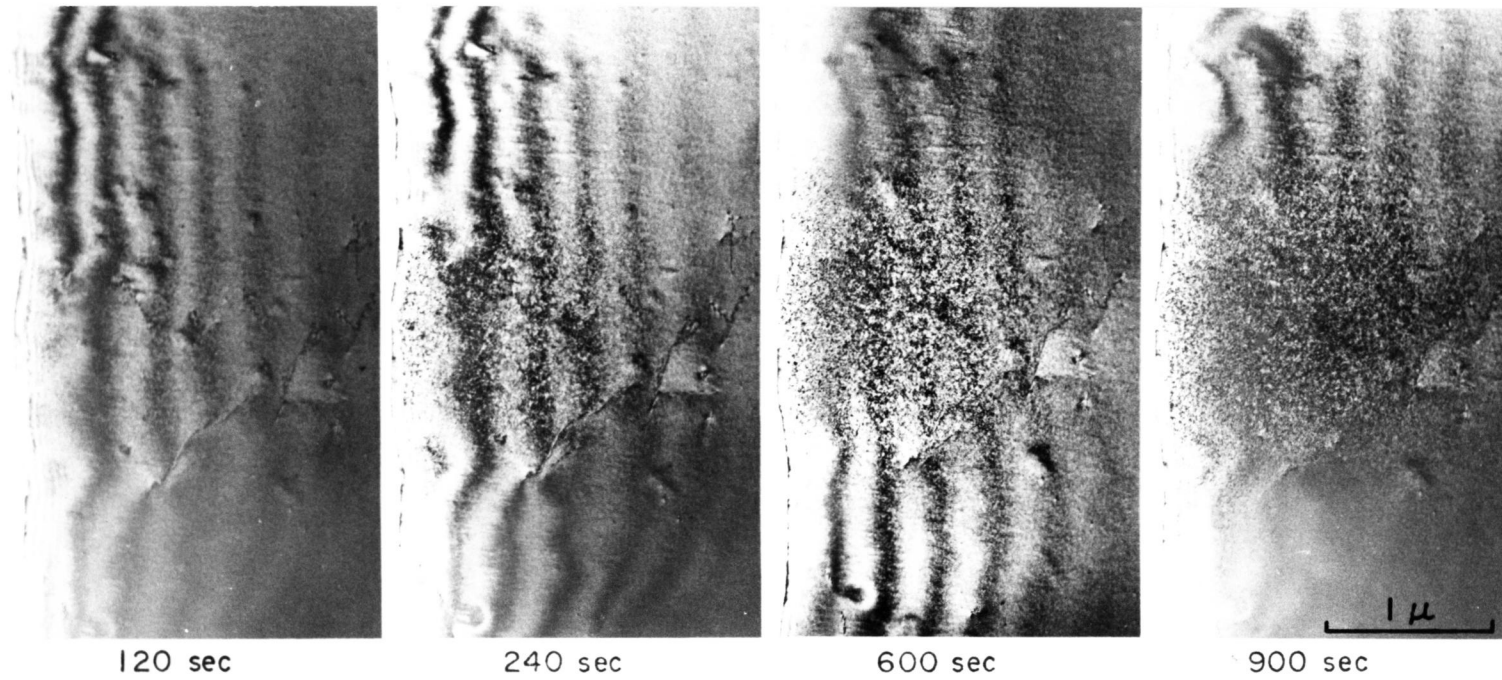


Fig. 31

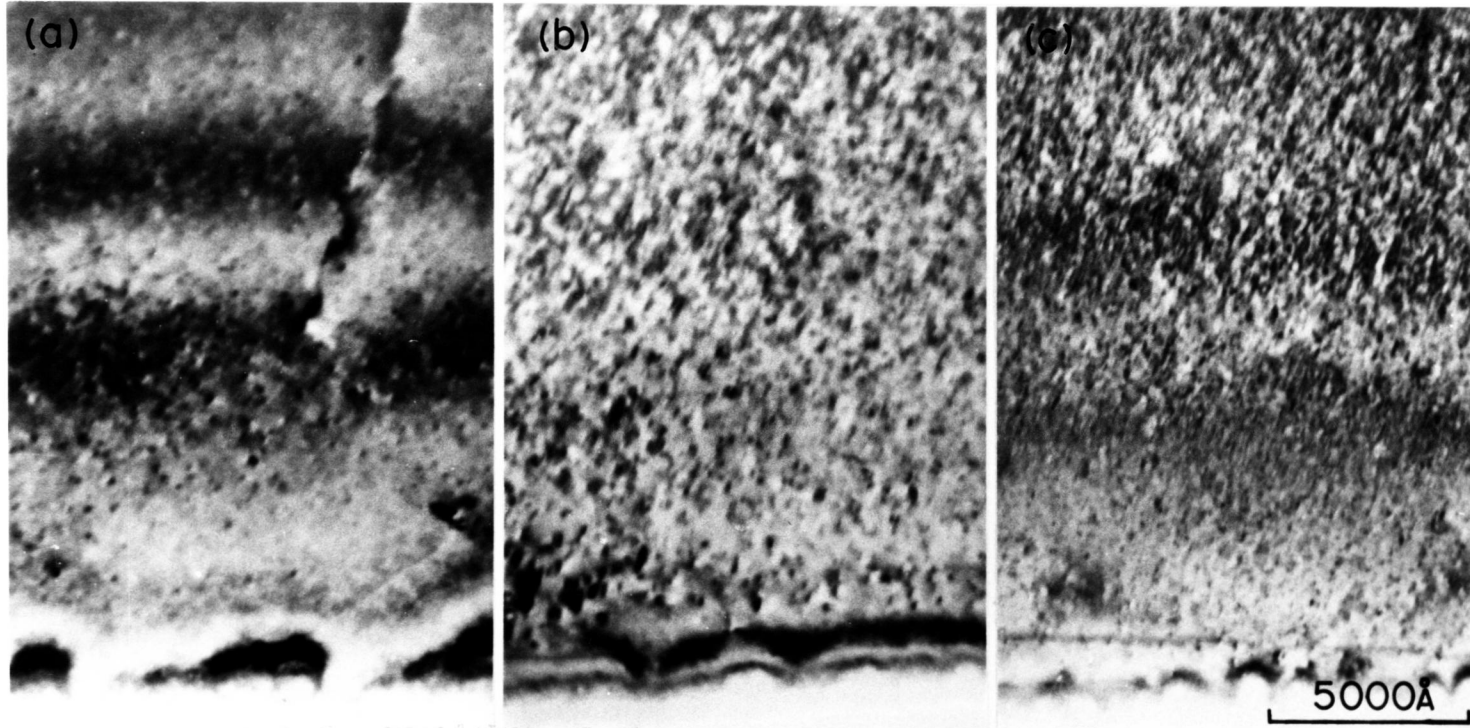


Fig. 32

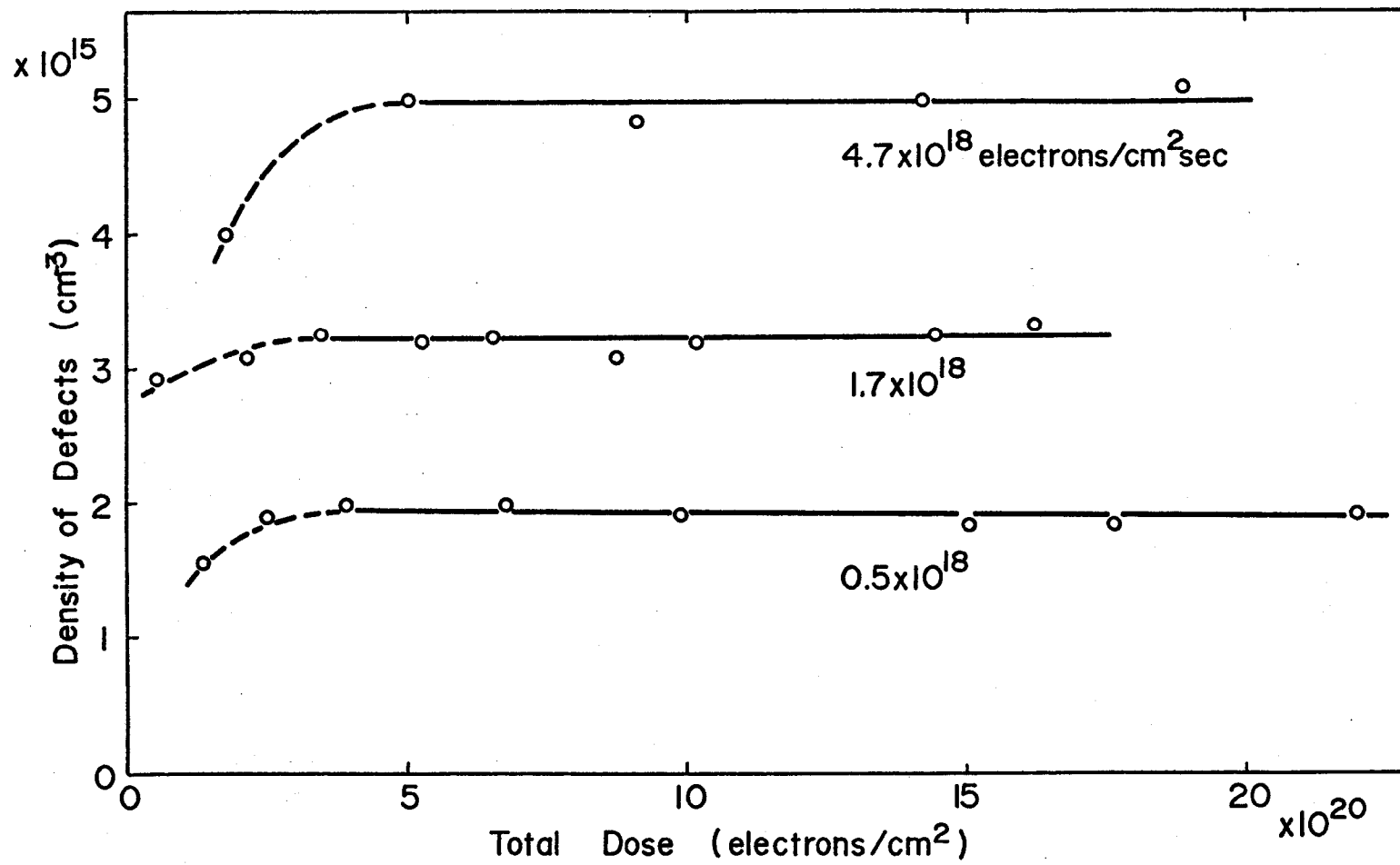


Fig. 33

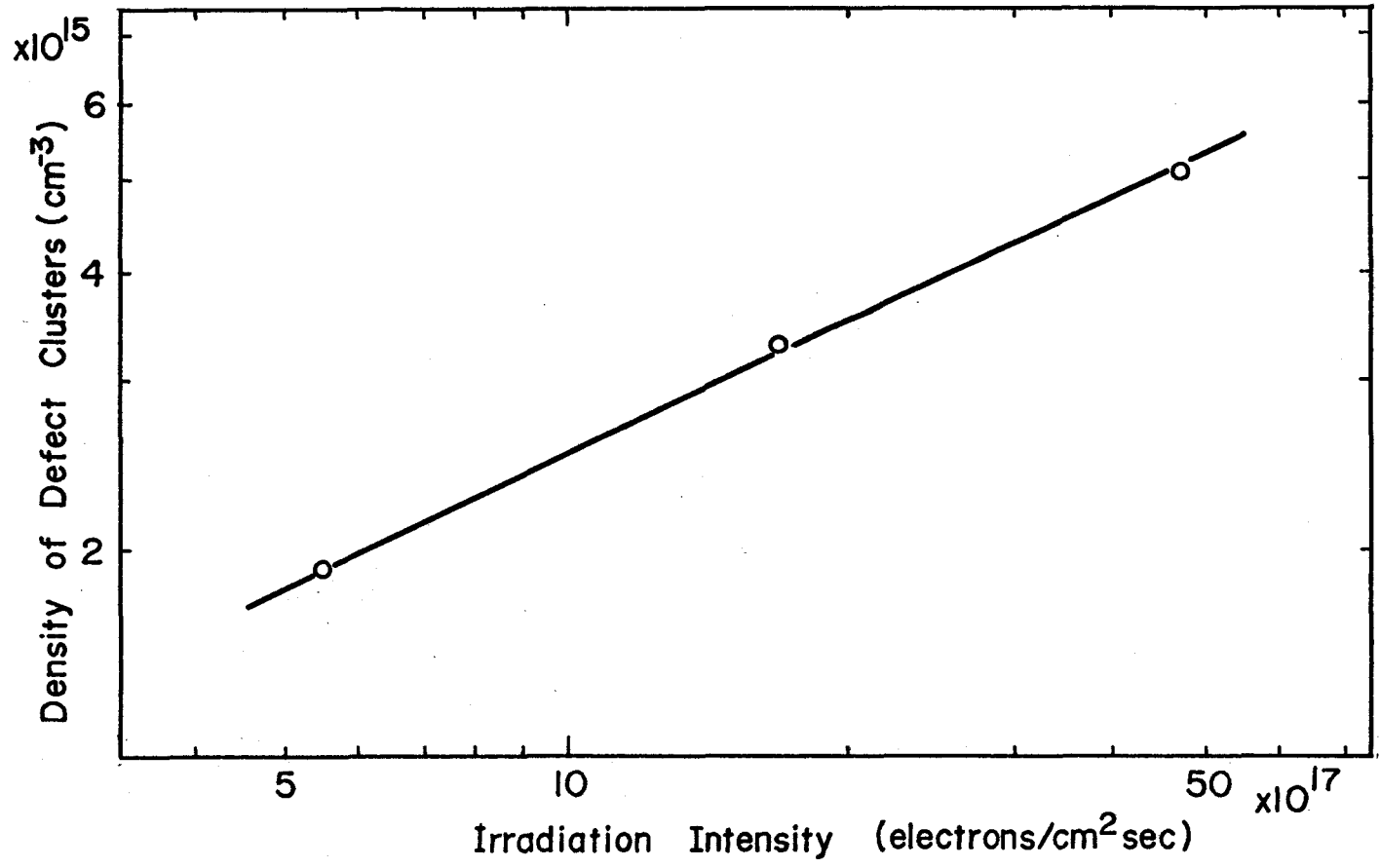


Fig. 34

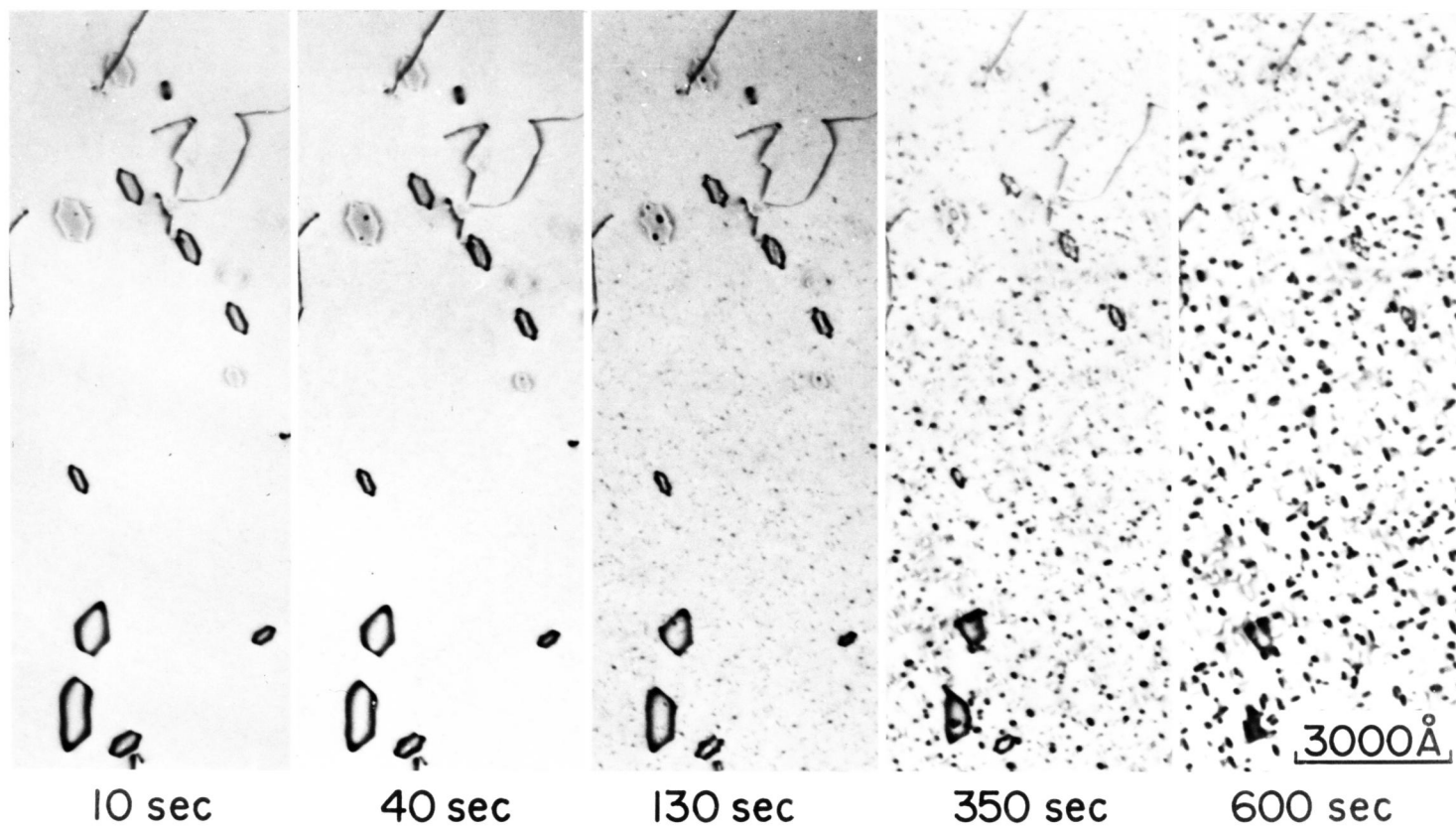


Fig. 35

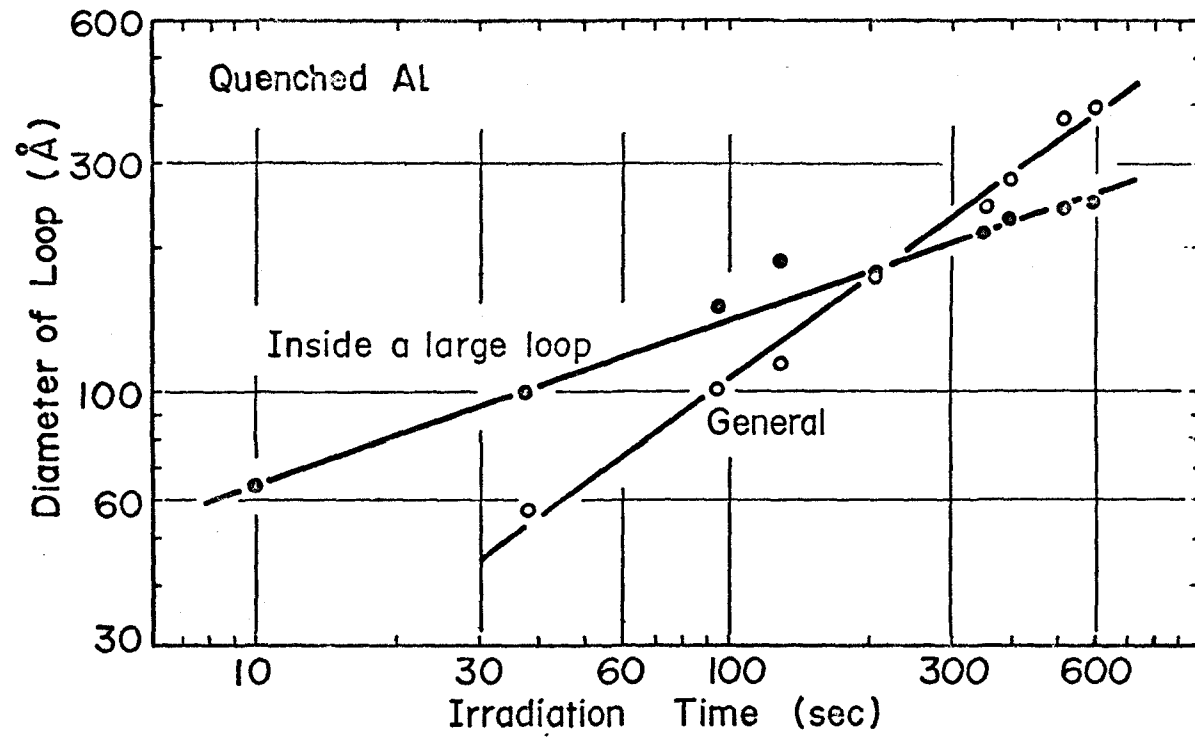


Fig. 36

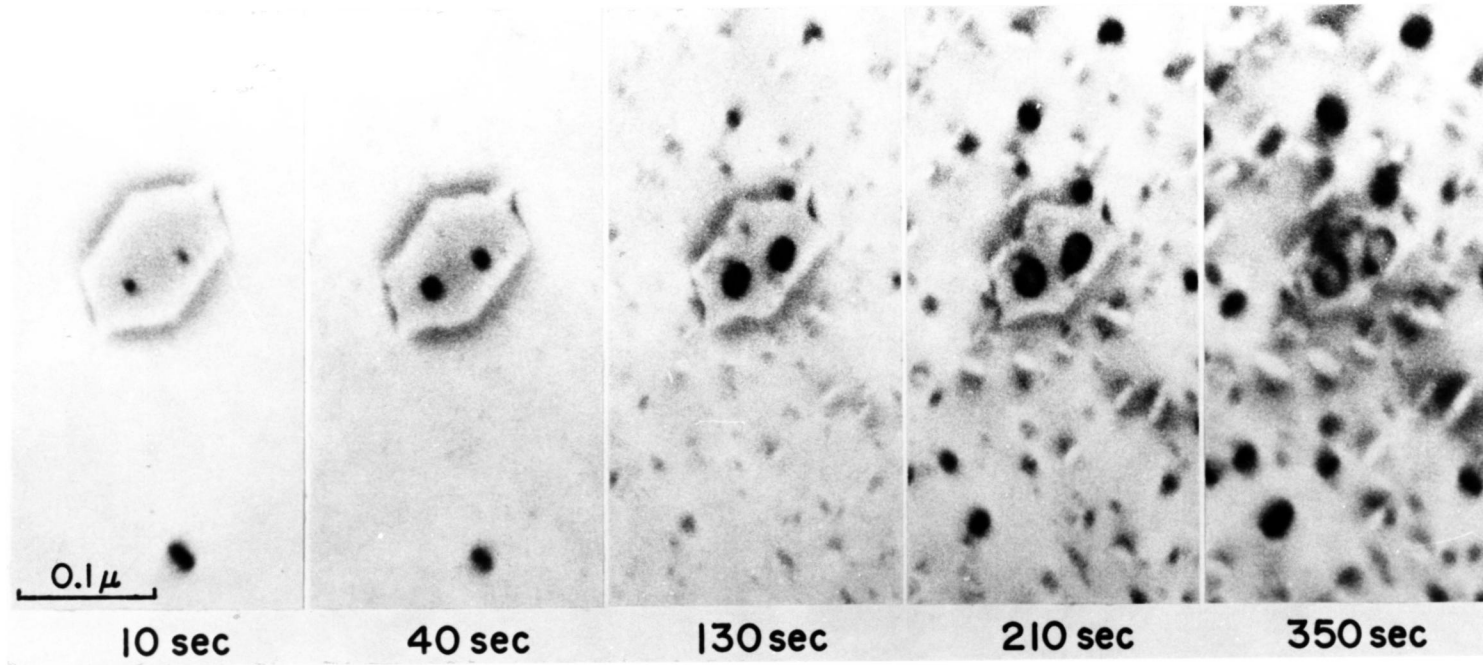


Fig. 37

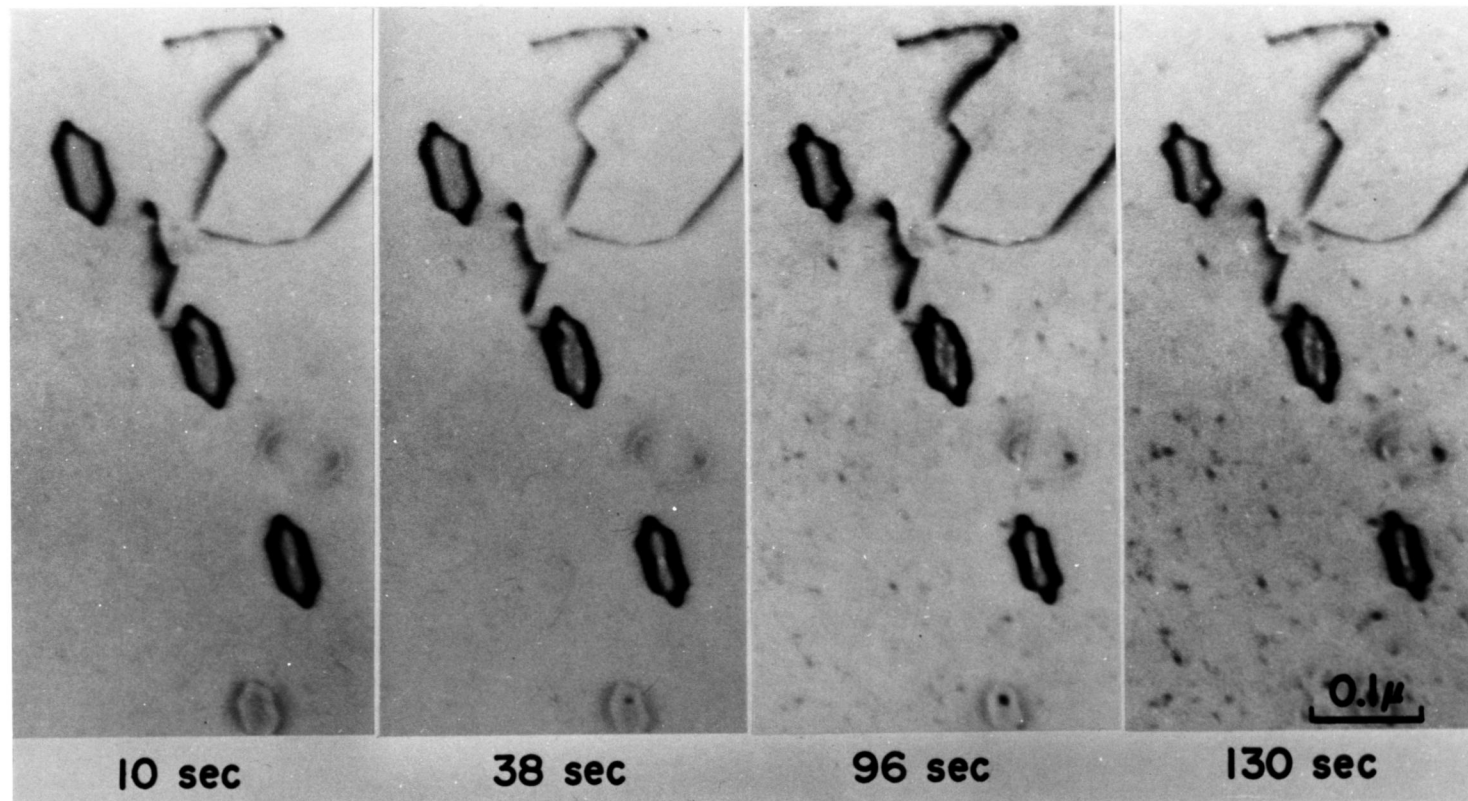


Fig. 38

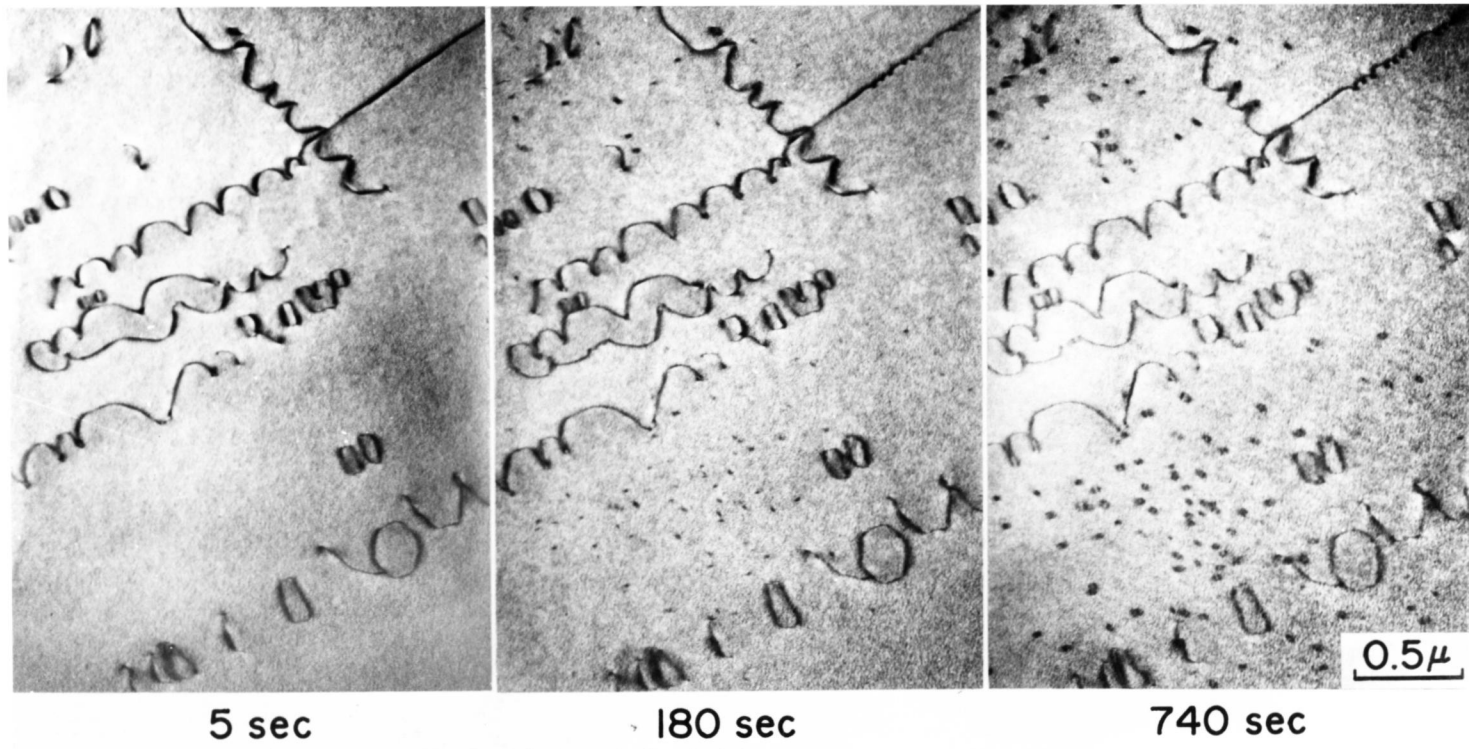


Fig. 39

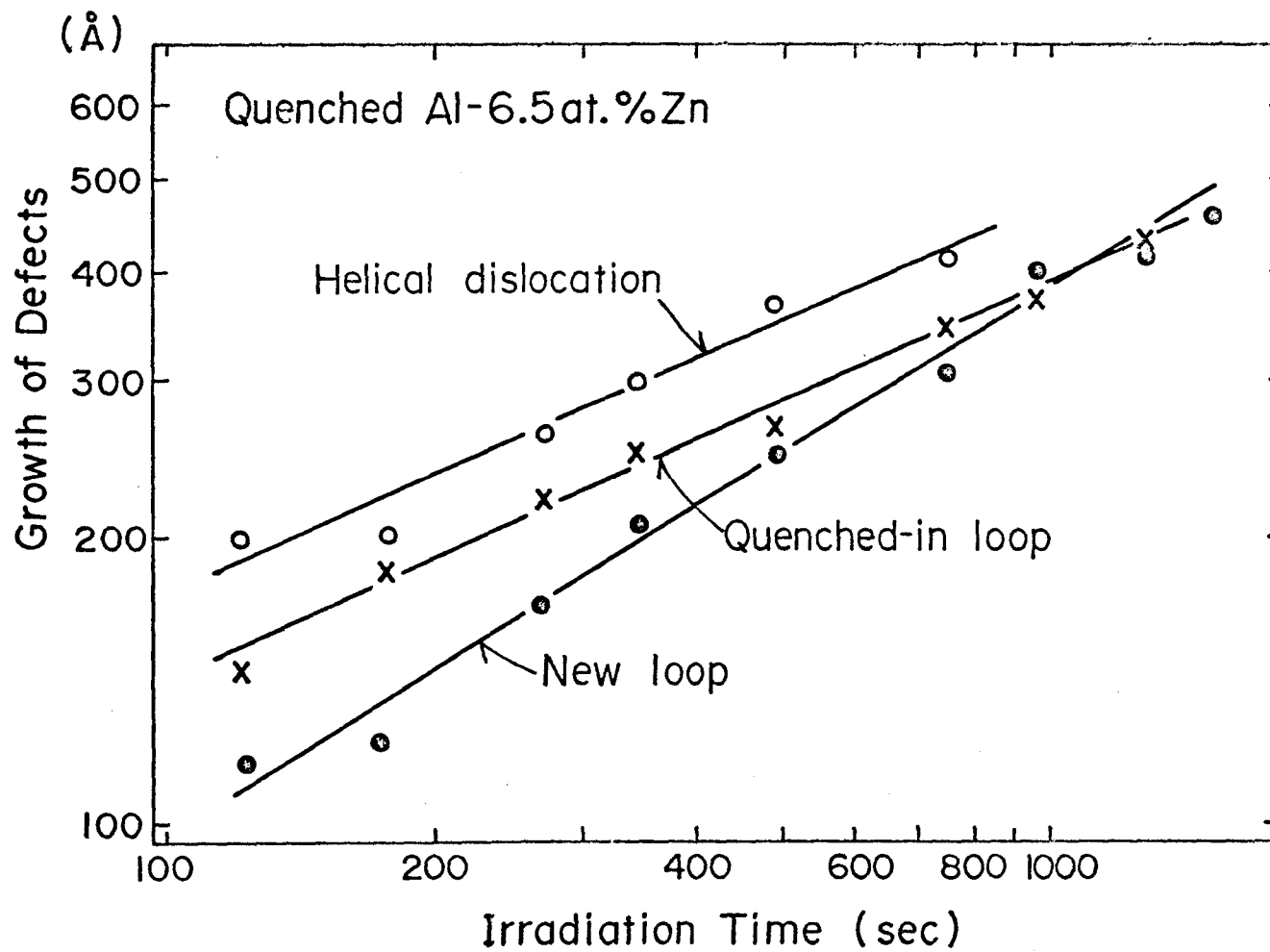


Fig. 40